



Observation of photon-induced W^+W^- production in pp collisions at $\sqrt{s} = 13$ TeV using the ATLAS detector



The ATLAS Collaboration*

ARTICLE INFO

Article history:

Received 9 October 2020
 Received in revised form 1 March 2021
 Accepted 2 March 2021
 Available online 4 March 2021
 Editor: M. Doser

ABSTRACT

This letter reports the observation of photon-induced production of W -boson pairs, $\gamma\gamma \rightarrow WW$. The analysis uses 139 fb^{-1} of LHC proton–proton collision data taken at $\sqrt{s} = 13$ TeV recorded by the ATLAS experiment during the years 2015–2018. The measurement is performed selecting one electron and one muon, corresponding to the decay of the diboson system as $WW \rightarrow e^\pm\nu\mu^\mp\nu$ final state. The background-only hypothesis is rejected with a significance of well above 5 standard deviations consistent with the expectation from Monte Carlo simulation. A cross section for the $\gamma\gamma \rightarrow WW$ process of $3.13 \pm 0.31(\text{stat.}) \pm 0.28(\text{syst.}) \text{ fb}$ is measured in a fiducial volume close to the acceptance of the detector, by requiring an electron and a muon of opposite signs with large dilepton transverse momentum and exactly zero additional charged particles. This is found to be in agreement with the Standard Model prediction.

© 2021 The Author(s). Published by Elsevier B.V. This is an open access article under the CC BY license (<http://creativecommons.org/licenses/by/4.0/>). Funded by SCOAP³.

Contents

1. Introduction	1
2. ATLAS detector	2
3. Data and simulated event samples	2
4. Event reconstruction and selection	3
5. Modelling of signal and backgrounds	4
5.1. Modelling of additional pp interactions	4
5.2. Modelling of the underlying event	5
5.3. Signal modelling	6
6. Event categories and background estimation	7
7. Systematic uncertainties	7
8. Results	8
9. Conclusion	10
Declaration of competing interest	10
Acknowledgements	11
References	11
The ATLAS Collaboration	12

1. Introduction

The study of W -boson pair production from the interaction of incoming photons ($\gamma\gamma \rightarrow WW$) in proton–proton (pp) collisions offers a unique window to a wide range of physical phenomena. In the Standard Model (SM), the $\gamma\gamma \rightarrow WW$ process proceeds

through trilinear and quartic gauge-boson interactions. This process is unique in that, at leading order, it only involves diagrams with self-couplings of the electroweak gauge bosons, as shown in Fig. 1. Hence, a cross-section measurement directly tests the $SU(2) \times U(1)$ gauge structure of the SM. At the same time, as a process driven only by electroweak boson self-interactions, it is sensitive to anomalous gauge-boson interactions [1] as parameterised in effective field theory (EFT) with additional dimension-6 and dimension-8 operators [2,3]. Thus, cross-section measurements of

* E-mail address: atlas.publications@cern.ch.

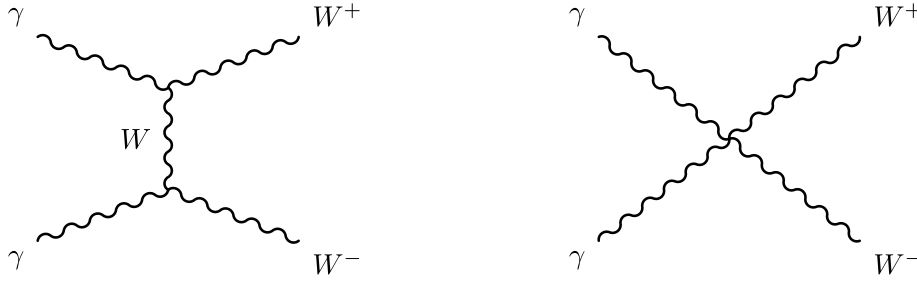


Fig. 1. The leading-order Feynman diagrams contributing to the $\gamma\gamma \rightarrow WW$ process are the t-channel diagram (left) proceeding via the exchange of a W boson between two γWW vertices and a diagram with a quartic $\gamma\gamma WW$ coupling (right). In addition, a u-channel diagram exists (not shown), which also proceeds via two γWW vertices.

$\gamma\gamma \rightarrow WW$ can in future provide valuable input for the global EFT fits.

This letter presents a measurement in the $W^+W^- \rightarrow e^\pm\nu\mu^\mp\nu$ channel that results in the observation of photon-induced WW production. Previously, the ATLAS and CMS Collaborations found only evidence for $\gamma\gamma \rightarrow WW$ production with the Run-1 data, ATLAS by using 8 TeV pp collisions [4] and CMS by combining their 7 TeV and 8 TeV pp collision data [5,6].

The signal process proceeds through the $pp(\gamma\gamma) \rightarrow p^{(*)}W^+W^-p^{(*)}$ reaction, where $p^{(*)}$ indicates that the final-state proton either stays intact or fragments after emitting a photon. Whilst the former occurs through a coherent photon radiation off the whole proton without disintegration, for the latter at least one of the photons can be considered as being radiated off a parton in the proton. These contributions are classified as elastic, single-dissociative, and double-dissociative WW production. Elastic $\gamma\gamma \rightarrow WW$ production with leptonic decays of the W bosons results in a final state containing two charged leptons and no additional charged-particle activity. Even in the case of dissociative photon-induced production, the charged particles from the proton remnants often fall outside the acceptance of the tracking detector.

The suppressed activity in the central region of the detector in the $\gamma\gamma \rightarrow WW$ signal gives the means to control and significantly reduce background from quark- and gluon-induced WW production or top-quark production where the leptonic final state is typically produced in association with a substantial amount of hadronic activity. The analysis therefore selects events that have no additional charged-particle tracks reconstructed in the vicinity of the selected interaction vertex. The modelling of the hadronic activity in quark- and gluon-induced processes, as well as uncorrelated activity from additional pp interactions, is constrained using same-flavour ee and $\mu\mu$ Drell-Yan, $DY(\rightarrow ee/\mu\mu)$, events in data, reducing the associated uncertainties by a significant amount. Background from other photon-induced processes, mainly dilepton production $\gamma\gamma \rightarrow \ell\ell$, is reduced by selecting only different-flavour lepton pairs, $e\mu$, leaving a smaller contribution from $\gamma\gamma \rightarrow \tau\tau$ production with leptonic τ decays. Since the contribution from the $\gamma\gamma \rightarrow \tau\tau$ process falls off rapidly with increasing transverse momentum of the dilepton system, $p_T^{e\mu}$, it can be further suppressed by placing requirements on $p_T^{e\mu}$. A fiducial cross section for the $pp(\gamma\gamma) \rightarrow p^{(*)}W^+W^-p^{(*)}$ process through the decay channel $W^+W^- \rightarrow e^\pm\nu\mu^\mp\nu$ is measured in a fit to the number of events in several kinematic regions with different signal and background contributions.

2. ATLAS detector

The ATLAS detector [7] at the Large Hadron Collider (LHC) is a multipurpose detector with a forward-backward symmetric cylin-

drical geometry and nearly 4π coverage in solid angle.¹ It consists of an inner tracking detector surrounded by a thin superconducting solenoid providing a 2 T axial magnetic field, electromagnetic and hadron calorimeters, and a muon spectrometer.

The inner tracking detector (ID) covers the pseudorapidity range $|\eta| < 2.5$ and is composed of three subdetectors. The high-granularity silicon pixel detector covers the vertex region and typically provides four measurements per track, the first hit normally being in the insertable B-layer [8,9]. It is followed by the silicon microstrip tracker (SCT), which usually provides eight measurements per charged-particle track. These silicon detectors are complemented by the transition radiation tracker, which enables radially extended track reconstruction up to $|\eta| = 2.0$ and provides electron identification information. The resolution of the z-coordinate of tracks at the point of closest approach to the beam line is about 0.170 mm for tracks with $p_T = 500$ MeV and improves with higher track momentum [10]. For tracks with $p_T < 1$ GeV, the dominant contribution to the z-resolution is due to multiple scattering.

Lead/liquid-argon (LAr) sampling calorimeters provide electromagnetic (EM) energy measurements with high granularity. A steel/scintillator-tile hadron calorimeter covers the central pseudorapidity range ($|\eta| < 1.7$). The endcap and forward regions are instrumented with LAr calorimeters for EM and hadronic energy measurements up to $|\eta| = 4.9$. The muon spectrometer (MS) surrounds the calorimeters and is based on three large air-core toroidal superconducting magnets with eight coils each. The muon spectrometer includes a system of precision tracking chambers ($|\eta| < 2.7$) and fast detectors for triggering ($|\eta| < 2.4$). A two-level trigger system [11] selects the events used in the analysis.

3. Data and simulated event samples

The analysis uses proton-proton collision data recorded with the ATLAS detector during the Run-2 data-taking period (2015–2018) at $\sqrt{s} = 13$ TeV with the number of interactions, μ_{int} , per bunch crossing (also referred to as pile-up) ranging from about 10 to 60 with an average of 33.7 [12].

The size of the region where the collisions occur, the so-called beam spot, is a result of the operating parameters of the LHC. Of specific importance for this analysis is its width along the z-direction, which determines the density of pp interactions. The width is determined by fitting the distribution of the z positions of the reconstructed vertices to Gaussian functions using an unbinned

¹ ATLAS uses a right-handed coordinate system with its origin at the nominal interaction point in the centre of the detector and the z-axis coinciding with the axis of the beam pipe. The x-axis points from the interaction point to the centre of the LHC ring, and the y-axis points upward. The pseudorapidity is defined in terms of the polar angle θ as $\eta = -\text{In}(\tan(\theta/2))$, and ϕ is the azimuthal angle around the beam pipe relative to the x-axis. The angular distance is defined as $\Delta R = \sqrt{(\Delta\eta)^2 + (\Delta\phi)^2}$.

likelihood fit. It varied between 30 and 50 mm during the Run-2 data-taking period [13]. The data correspond to an integrated luminosity of $\mathcal{L} = 139.0 \pm 2.4 \text{ fb}^{-1}$ after data quality requirements [14] have been applied. This value is derived from the calibration of the luminosity scale with the method explained in Ref. [12], using the LUCID-2 detector [15] for the primary luminosity measurement.

Signal and background processes were modelled using Monte Carlo (MC) event generators to study kinematic distributions, to evaluate background contamination in the signal region and to interpret the results. To simulate the detector response, the generated events were passed through a detailed simulation of the ATLAS detector [16] based on GEANT4 [17] or on a combination of GEANT4 and a parameterised calorimeter simulation [18]. The present measurement relies only on tracking information from charged hadrons, muons and electrons, which is simulated by GEANT4 in either case, as well as the modelling of the calorimetric response of electrons which can be reliably parametrized. Multiple pp interactions occurring in the same or adjacent bunch crossings are included in the simulation by overlaying several inelastic pp collisions matching the average number of interactions per bunch crossing. The inelastic pp collisions were generated with PYTHIA 8.186 [19] using a set of tuned parameters called the A3 tune [20] and the NNPDF2.3LO [21] set of parton distribution functions (PDF). All MC samples are corrected to the beam conditions of the data as described in Section 5.1. In all samples using PYTHIA8 or HERWIG7 to simulate the parton showering, underlying event and hadronisation, the decays of bottom and charm hadrons were performed with EvtGen 1.2.0 [22].

The elastic component of the $\gamma\gamma \rightarrow WW$ signal process was modelled at leading order (LO) using HERWIG 7.1.5 [23,24] interfaced with the BudnevQED photon flux [25] through THEPEG software [26]. This sample is used to model the photon-induced processes in the fiducial region of the measurement as it uses a photon flux, which is differential in both x and virtuality Q^2 . It is corrected to match the cross section, including the dissociative as well as non-perturbative components, using a data-driven method described in Section 5.3. This data-driven approach is validated using elastic and dissociative $\gamma\gamma \rightarrow WW$ samples produced using MG5_AMC@NLO 2.6.7 [27] interfaced to PYTHIA 8.243. The default photon flux in MG5_AMC@NLO and the CT14QED [28] PDF were used to model the photon radiation from protons and quarks, respectively. The parametrized detector simulation was used in the generation of the MG5_AMC@NLO samples. They are used whenever regions with reconstructed track multiplicities larger than zero are studied.

The production of $\gamma\gamma \rightarrow \ell\ell$, with $\ell = e, \mu, \tau$, was modelled in the same way as for the $\gamma\gamma \rightarrow WW$ signal process. Additional generators were used to validate the modelling of the $\gamma\gamma \rightarrow \ell\ell$ dissociative events. The single-dissociative processes were modelled using LPAIR 4.0 [29]. Alternative $\gamma\gamma \rightarrow \ell\ell$ double-dissociative samples were produced with PYTHIA 8.240 using the NNPDF3.1NLOluxQED PDF set [30]. Diffractive QCD-processes and $\gamma\gamma \rightarrow 4\ell$ production were produced using PYTHIA 8.244 and MG5_AMC@NLO 2.6.7 interfaced to PYTHIA 8.243 and studied using particle-level information only. The contribution of these processes was found to be negligible in the signal region of the measurement.

The dominant background from quark-induced WW production, also referred to as $q\bar{q} \rightarrow WW$, was modelled at next-to-leading-order (NLO) accuracy using the POWHEG-Box v2 [31–35] generator interfaced to PYTHIA8 and alternatively to HERWIG7. The POWHEG-Box v2 sample employs the CT10 [36] PDF for the matrix element calculation and is interfaced to PYTHIA 8.212 for parton showering and hadronisation employing the parameter values of the AZNLO tune [37] and the CTEQ6L1 [38] PDF. Samples using a set of variations in the tune parameters (eigentune variations)

sensitive to initial- and final-state radiation, as well as further variations related to multiple parton interactions and colour reconnection, were produced to study the description of the parton showers and hadronisation. HERWIG 7.1.6 was used as an alternative parton shower, using the H7UE tune [24] and the MMHT2014LO PDF set [39] for events generated with the POWHEG-Box v2 generator. An alternative sample for quark-induced WW production was generated using the SHERPA [40,41] event generator in order to evaluate modelling uncertainties. The SHERPA 2.2.2 sample uses matrix elements at NLO accuracy in QCD for up to one additional parton and at LO accuracy for up to three additional parton emissions. The matrix element calculations were matched and merged with the SHERPA parton shower based on Catani-Seymour dipole factorisation [42,43] using the MEPS@NLO prescription [40,44–46]. The virtual QCD corrections were provided by the OPENLOOPS1 library [47–49]. The sample was generated using the NNPDF3.0NNLO set [50], along with the dedicated set of tuned parton-shower parameters developed by the SHERPA authors.

DY production, $pp \rightarrow Z/\gamma^* \rightarrow \ell\ell$ with $\ell = e, \mu, \tau$, was modelled using the same settings for SHERPA, POWHEG+PYTHIA8 and POWHEG+HERWIG7 as for the quark-induced WW event generation described above. $DY(Z/\gamma^* \rightarrow \tau\tau)$ was modelled with POWHEG interfaced to PYTHIA 8.186 using the NNPDF3.0NLO PDF set [50] and the AZNLO tune together with the CTEQ6L1 PDF set for parton showering and hadronisation.

The WZ and ZZ background processes were modelled at NLO using SHERPA as well as POWHEG-Box v2 interfaced to PYTHIA 8.212 with the same settings as employed for the WW event generation. $W\gamma$ production, gluon-induced WW production including resonant and non-resonant contributions and $WWjj$ production in vector-boson scattering were simulated using the SHERPA 2.2.2 generator with the NNPDF3.0NNLO PDF set. These samples use matrix elements at NLO QCD accuracy for up to one additional parton and LO accuracy for up to three additional parton emissions for $W\gamma$ and gluon-induced WW production and LO-accurate matrix elements for $WWjj$ production in vector-boson scattering.

The $t\bar{t}$ and Wt processes were simulated with the POWHEG-Box [31–33,51,52] v2 generator at NLO with the NNPDF3.0NLO PDF interfaced to PYTHIA 8.230 using the A14 tune [53] and the NNPDF2.3LO set of PDFs. For the Wt process, the diagram removal scheme [54] was applied to remove interference and overlap with $t\bar{t}$ production.

4. Event reconstruction and selection

Candidate events from $\gamma\gamma \rightarrow WW$ production are identified by the presence of an electron and a muon with high transverse momentum and the absence of additional reconstructed charged-particle tracks associated with the interaction vertex.

Tracks are reconstructed from position measurements (hits) in the ID caused by the passage of charged particles [55,56]. The track reconstruction consists of an iterative track-finding algorithm seeded by combinations of at least three silicon-detector hits followed by a combinatorial Kalman filter [57] to build track candidates based on hits compatible with the extrapolated trajectory. Ambiguities between the track candidates are then resolved and quality criteria are applied to suppress combinations of hits unlikely to originate from a single charged particle. At least one hit in the two innermost layers is required if the extrapolated track crosses the sensitive region of an active sensor module. The number of silicon hits in the pixel and SCT detectors must be larger than 9 for $|\eta| \leq 1.65$ or larger than 11 for $|\eta| > 1.65$, with no more than two missing SCT hits on a track if the respective SCT modules are operational. Additionally, a selection is imposed on the transverse impact parameter, $|d_0| < 1 \text{ mm}$, to reject tracks from secondary interactions. Tracks are required to have $p_T > 500 \text{ MeV}$

and be within $|\eta| < 2.5$. These selection criteria result in an efficiency of 75–80% depending on the track p_T . The largest source of inefficiency is hadronic interactions with the detector material. In simulated events, reconstructed tracks can be classified as originating from the hard scatter or from additional pp collisions by matching the hits that contributed to the track fit to the energy deposited by the charged particle in the GEANT4 simulation. The respective tracks are counted as $n_{\text{trk}}^{\text{HS}}$ and $n_{\text{trk}}^{\text{PU}}$.

Electrons are reconstructed from energy clusters in the electromagnetic calorimeter that are matched to tracks reconstructed in the ID [58,59]. The best-matching track is selected using as criteria track–cluster spatial distance and the number of hits in the silicon detectors [59]. Further tracks may be assigned to the electron candidate if they are likely to originate from interactions with detector material. The pseudorapidity of electrons is required to be within the range of $|\eta| < 2.47$, excluding the transition region between the barrel and endcaps in the LAr calorimeter ($1.37 < |\eta| < 1.52$). Electron candidates are required to have transverse momenta $p_T > 20$ GeV.

Muons are built from tracks reconstructed using MS hits matched to ID tracks. A global fit using the hits from both sub-detectors is performed [60]. Each muon candidate is matched uniquely to exactly one ID track and is required to satisfy $|\eta| < 2.4$ and $p_T > 20$ GeV.

Identification and isolation criteria are applied to electron and muon candidates to suppress non-prompt leptons from hadron decays. Identification criteria are based on shower shapes and track parameters for the electrons, and on track parameters for the muons. The isolation criteria use information about ID tracks and calorimeter energy deposits in a fixed cone of $\Delta R = 0.2$ around each lepton. Electrons must satisfy the ‘medium’ identification criteria as well as the loose isolation criteria described in Ref. [59], which have a combined efficiency of 75–85% depending on the electron p_T . Muon candidates are required to satisfy the ‘medium’ identification and loose isolation criteria introduced in Ref. [60], which have an efficiency of about 95%. The significance of the transverse impact parameter, defined as the absolute value of d_0 , divided by its uncertainty, σ_{d_0} , must satisfy $|d_0|/\sigma_{d_0} < 3$ for muons and $|d_0|/\sigma_{d_0} < 5$ for electrons.

The decision on whether or not to record the event was made by single-electron or single-muon triggers with requirements on lepton identification and isolation similar to those applied offline. The transverse momentum thresholds for these triggers were 24 GeV for electrons [61] and 20 GeV for muons [62] in 2015, whilst during the 2016–2018 data-taking period the thresholds were both raised to 26 GeV and requirements on lepton identification and isolation were tightened. Complementary triggers with higher p_T thresholds and no isolation or looser identification criteria were used to increase the trigger efficiency.

Events are required to contain exactly two leptons of opposite electric charge that satisfy the above criteria. One of the leptons must have transverse momentum exceeding 27 GeV and be matched to an object that provided one of the triggers used for the read-out and storage of the event. The invariant mass of the two selected leptons must exceed $m_{\ell\ell} = 20$ GeV. Both same-flavour ($ee/\mu\mu$) and different-flavour ($e\mu$) events are accepted either for auxiliary measurements or for the signal extraction, respectively.

The interaction vertex is reconstructed from the two leptons in the event, ℓ_1 and ℓ_2 , as the weighted average z -position of the tracks extrapolated to the beam line:

$$z_{\text{vtx}}^{\ell\ell} = \frac{z_{\ell_1} \sin^2 \theta_{\ell_1} + z_{\ell_2} \sin^2 \theta_{\ell_2}}{\sin^2 \theta_{\ell_1} + \sin^2 \theta_{\ell_2}},$$

where $\sin^2 \theta_{\ell}$ approximately parameterises the resolution of the z -position [10]. This definition of the interaction vertex is not bi-

ased by the presence of additional tracks from hadronic activity in association with the dilepton pair production or by additional tracks from nearby pile-up interactions. It results in a 30% higher efficiency than a primary vertex selection based on the sum of squared track transverse momenta [63]. Requirements are placed on each lepton to fulfil $|(z_{\ell} - z_{\text{vtx}}^{\ell\ell}) \sin \theta| < 0.5$ mm.

A window of $\Delta z = \pm 1$ mm around $z_{\text{vtx}}^{\ell\ell}$ defines the region in which ID tracks are matched to the interaction vertex. The number of tracks in this window, excluding those used in the reconstruction of leptons, is counted as n_{trk} . Signal $\gamma\gamma \rightarrow WW$ event candidates are selected using the exclusivity requirement that $n_{\text{trk}} = 0$. Events with low track multiplicities, $1 \leq n_{\text{trk}} \leq 4$, are used to evaluate backgrounds. The modelling of n_{trk} is therefore vital to the extraction of the $\gamma\gamma \rightarrow WW$ signal, and this is discussed further in the following section.

5. Modelling of signal and backgrounds

Corrections are applied to the simulated signal and background event samples to adjust the lepton trigger, reconstruction, identification and isolation efficiencies, as well as the energy and momentum resolutions, to those observed in data. The muon momentum scale is corrected in the MC simulation, whilst the electron energy scale is corrected in data [59–62]. Accurate modelling of the transverse momenta of the bosons is important because of its correlation with the expected charged-particle multiplicity from hadronic activity. The p_T^{WW} distribution in the MC samples for quark-induced WW production is reweighted to the theoretical calculation at next-to-next-to-leading-order (NNLO) accuracy in perturbative quantum chromodynamics with resummation of soft gluon emissions up to next-to-next-to-next-to-leading-logarithm ($N^3\text{LL}$) accuracy using MATRIX+RadISH [48,49,64–72]. A correction for the transverse momentum distribution of dilepton pairs from the DY process is derived from data using ee and $\mu\mu$ final states with an invariant mass within 15 GeV of the nominal Z boson mass corrected for background, and is applied to all DY samples as a function of the generator-level p_T^Z . Additional data-driven corrections are needed for this analysis to account for (i) mismodelling of the additional pp interactions produced in the same bunch crossing, (ii) mismodelling of the charged-particle multiplicity in the $qq \rightarrow WW$ background process, and (iii) second scatterings and the dissociative contribution to the $\gamma\gamma \rightarrow WW$ signal process.

5.1. Modelling of additional pp interactions

Tracks from nearby additional pp interactions can be matched to the interaction vertex and, thus, lower the efficiency of the exclusivity requirement. Their number depends on the density of additional pp interactions and the number of tracks originating from these interactions. Data-driven techniques are used to derive corrections to the simulated events to further improve their description of the data, targeting the density of pp interactions and the number of tracks per interaction separately.

The simulated events are reweighted such that the distribution of the average number of pp interactions per bunch crossing reproduces the one measured in the data. The longitudinal width of the beam spot, σ^{BS} , determines the average density, along z , of additional pp interactions near the interaction vertex. The average longitudinal width of the beam spot varied throughout the data-collection period due to changes in the LHC beam optics. It was about 44 mm in 2015 and between 34 and 38 mm in 2016–2018 compared to 42 mm in MC simulation. The photon-induced MC samples were produced with both, the nominal conditions in MC simulation and also with a beam spot width of 35 mm to study the impact of these settings. Only the latter samples were used in the final analysis. To account for the different densities of additional

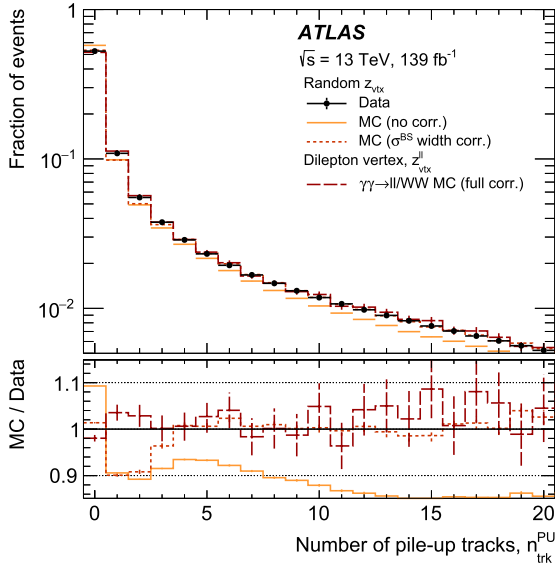


Fig. 2. The normalised distribution of tracks from additional pp interactions, $n_{\text{trk}}^{\text{PU}}$, associated with the interaction vertex, in data and signal simulated with a beam spot width of $\sigma_{\text{MC}}^{\text{BS}} = 42$ mm. For data, $n_{\text{trk}}^{\text{PU}}$ is determined using a random z -position along the beam axis away from the interaction vertex. The same quantity is shown for simulated $\gamma\gamma \rightarrow WW$ events before and after correcting the beam spot width to the one observed in data. The inverse ratio of the beam-spot-corrected simulation to data corresponds to the correction applied to $n_{\text{trk}}^{\text{PU}}$ in the simulation using the GEANT4-based classification. To demonstrate the closure of the correction, the number of tracks reconstructed in elastic $\gamma\gamma \rightarrow WW$ signal MC samples is shown after applying the full set of corrections, namely the σ^{BS} correction and the $n_{\text{trk}}^{\text{PU}}$ correction. The shown uncertainties are statistical only.

pp interactions in data and simulation, the beam spot width is effectively corrected by modifying the matching of tracks to the interaction vertex in simulation: tracks classified as originating from a pile-up interaction are counted in n_{trk} if they have a longitudinal impact parameter z within $1 \text{ mm} \times \sigma_{\text{MC}}^{\text{BS}}/\sigma_{\text{Data}}^{\text{BS}}$ of $z_{\text{vtx}}^{\text{ll}}$. The values for $\sigma_{\text{Data}}^{\text{BS}}$ are sampled from the LHC run conditions during Run 2 according to the luminosity taken at a given value of $\sigma_{\text{Data}}^{\text{BS}}$.

An ancillary data measurement is used to determine the correction for the number of tracks from additional pp interactions randomly matched to the interaction vertex, $n_{\text{trk}}^{\text{PU}}$. In same-flavour $Z \rightarrow \ell\ell$ events, this correction is obtained by counting the number of tracks satisfying the nominal selection criteria relative to a random position in z that is well separated from the interaction vertex, $|z_{\text{vtx}}^{\text{ll}} - z| > 10$ mm. Each event is sampled multiple times using non-overlapping regions in z . This procedure optimises the statistical power, but does not consider the actual distribution of $z_{\text{vtx}}^{\text{ll}}$ along z . To correct for the resulting bias, $n_{\text{trk}}^{\text{PU}}$ is extracted as a function of the z -coordinate and weighted with the normalised beam spot distribution.

This method is tested using simulated events and found to reproduce the $n_{\text{trk}}^{\text{PU}}$ distribution in data within 0.1–3.5% for low track multiplicities, with larger disagreement for larger n_{trk} . Fig. 2 shows the probability distribution of $n_{\text{trk}}^{\text{PU}}$ associated with $z_{\text{vtx}}^{\text{ll}}$, extracted in data and simulation before and after the corrections for the beam spot width. The bottom panel shows the ratio to data. The inverse ratio of the beam-spot-corrected simulation to data corresponds to the correction applied as a function of $n_{\text{trk}}^{\text{PU}}$ in the simulation. The distributions of the number of $n_{\text{trk}}^{\text{PU}}$ in $\gamma\gamma \rightarrow \ell\ell$ and $\gamma\gamma \rightarrow WW$ MC events are shown after the beam spot and the pile-up corrections. Before any corrections, the disagreement can be up to 15% depending on the beam spot conditions in the simulation. After the σ^{BS} correction, for low track multiplicities disagreements of about 10% persists because the σ^{BS} correction only improves the modelling of the density of the pile-up vertices but not of their track

multiplicity. This is corrected using the $n_{\text{trk}}^{\text{PU}}$ correction. The full set of corrections is applied to all MC samples used in the analysis.

The presence of the additional tracks from pile-up will randomly lead to the rejection of signal events and therefore the distribution of $n_{\text{trk}}^{\text{PU}}$ can be used to extract the signal efficiency of the exclusivity requirement ($n_{\text{trk}} = 0$). This exclusive efficiency depends strongly on the number of interactions per bunch crossing and the general beam conditions. The average efficiency for the 2015–2018 dataset with an average μ_{int} of 33.7 is 52.6%. It drops from 60% at $\mu_{\text{int}} = 20$ to about 30% at $\mu_{\text{int}} = 60$. When comparing the data-driven efficiency with that obtained directly from signal MC samples, the results agree to better than 0.2%.

The full effect of the data-driven correction for tracks from additional pp interactions is assigned as a systematic uncertainty, resulting in 1% and 3% uncertainty in the efficiency to select events without any additional associated tracks ($n_{\text{trk}} = 0$) for signal and background, respectively. The uncertainty of having a low number of tracks associated with the vertex ($1 \leq n_{\text{trk}} \leq 4$) is 2% for photon-induced processes and 10% for quark- and gluon-induced processes.

5.2. Modelling of the underlying event

For quark-induced diboson production, additional charged particles can be produced from initial-state radiation or secondary partonic scatters in the same pp collision, also called the underlying event. However, for low values of the number of charged particles, the n_{ch} distribution was found to be not well modelled by many of the phenomenological models implemented in the generators [73–76]. The underlying event can be assumed to be similar for quark-induced production of different colourless final states if the transverse momenta of these final states are comparable [76]. Therefore, the charged-particle multiplicity in $qq \rightarrow WW$ events can be constrained using data measurements of DY production of $\ell\ell$ pairs in pp collisions. Specifically, the charged-particle multiplicity is measured for $Z \rightarrow \ell\ell$ produced in slices of $p_{\text{T}}^{\ell\ell}$. This two-dimensional measurement is then used to correct the DY and diboson simulation. The general validity of this approach has been tested using DY and diboson samples generated with POWHEG+PYTHIA8, SHERPA and POWHEG+HERWIG7. The multiplicity spectra of charged particles are found to be very different in the different MC samples, yet relatively similar between the respective DY and diboson processes at a constant value of the boson or diboson p_{T} with the agreement being of the order to 10–20%.

The $Z \rightarrow \ell\ell$ events are selected using the criteria described in Section 4 with an additional requirement on the dilepton mass ($70 \text{ GeV} < m_{\ell\ell} < 105 \text{ GeV}$) to suppress contributions from background processes. The contribution of pile-up tracks is estimated from data by sampling random z -positions well separated from the dilepton vertex as discussed in Section 5.1. The background at low track multiplicities is dominated by $\gamma\gamma \rightarrow \ell\ell$ events, which have a different $p_{\text{T}}^{\ell\ell}$ dependence than DY events and amount to about 5% of the total events selected with $70 \text{ GeV} < m_{\ell\ell} < 105 \text{ GeV}$ and $n_{\text{trk}} = 0$ while their contribution is 0.5% or smaller for higher track multiplicities. The relative normalisations for the elastic, single-dissociative and double-dissociative $\gamma\gamma \rightarrow \ell\ell$ as well as the DY process are determined in a fit to the measured $p_{\text{T}}^{\ell\ell}$ distribution in a $m_{\ell\ell} > 105 \text{ GeV}$ sideband, requiring $n_{\text{trk}} = 0$ and using the shapes from MC simulation. In this sideband, the $\gamma\gamma \rightarrow \ell\ell$ process contributes about 60% to the total event sample. The contribution from the $\gamma\gamma \rightarrow WW$ process with a same-flavour final state amounts to less than 1% of the $\gamma\gamma \rightarrow \ell\ell$ processes in this kinematic region and is neglected. The overall normalisations of the different $\gamma\gamma \rightarrow \ell\ell$ contributions relative to the prediction are compatible within the statistical uncertainty with those from earlier ATLAS studies [77].

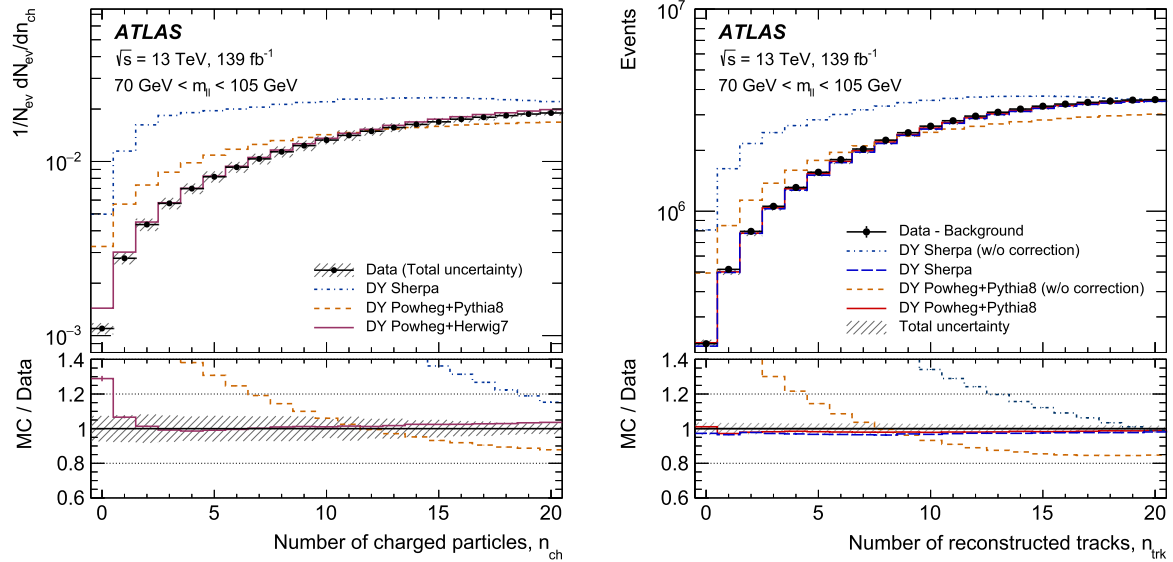


Fig. 3. On the left, the normalised number of events with a given number of charged particles, $1/N_{\text{ev}} dN_{\text{ev}}/dn_{\text{ch}}$, predicted by SHERPA, POWHEG+PYTHIA8, and POWHEG+HERWIG7 is compared with the unfolded data. The ratio on the bottom is the inverse of the weights that are applied at particle level as a function of the number of charged particles. The effect of the correction for the underlying event is illustrated for the number of reconstructed tracks on the right. SHERPA and POWHEG+PYTHIA8 are shown before and after the correction and compared with data. The total uncertainty of the correction is shown for POWHEG+PYTHIA8 in the upper panel, and as a band around unity for the lower panel. The total uncertainties for SHERPA and POWHEG+PYTHIA8 are very similar.

After the $\gamma\gamma \rightarrow \ell\ell$ and pile-up contributions are subtracted as backgrounds, D'Agostini unfolding [78,79] is used to unfold the distribution of the reconstructed track multiplicity, n_{trk} , to that of the number of charged particles, n_{ch} , using four iterations.² The charged-particle multiplicity is extracted as a function of the p_{T} of the dilepton system, which corresponds to the transverse momentum of the recoil, using 5-GeV-wide intervals of p_{T} . The largest sources of uncertainty are the contributions from pile-up tracks and uncertainties in the distribution used as the prior, assessed by comparing POWHEG+PYTHIA8 and SHERPA. Other uncertainties originate from the event selection and the $\gamma\gamma \rightarrow \ell\ell$ background subtraction, assessed by varying the kinematic selection and the normalisation of the photon-induced background within the uncertainties of the fit in the $m_{\ell\ell}$ sideband. Fig. 3 (left) compares the unfolded charged-particle multiplicity distribution for different MC models and data. For low values of n_{ch} , the charged-particle multiplicity distribution is mismodelled by a factor of 2.5 in POWHEG+PYTHIA8 and by a factor of 4 in SHERPA, whilst good agreement with the POWHEG+HERWIG7 model is found except at $n_{\text{ch}} = 0$ where the POWHEG+HERWIG7 prediction exceeds the data yield by about 30%.

The charged-particle multiplicity in simulated DY events is corrected using per-event weights determined as the ratio of the unfolded data to the unfolded MC simulation as a function of the charged-particle multiplicity, and of the particle-level p_{T} of the decay products of the Z boson. The impact of the charged-particle multiplicity correction is shown in Fig. 3 (right) for DY events. The simulation is shown both before and after the correction for pile-up modelling and underlying-event modelling in $Z \rightarrow \ell\ell$ events satisfying $70 \text{ GeV} < m_{\ell\ell} < 105 \text{ GeV}$. The corrections bring the MC simulation into agreement with data within the systematic uncertainty of the charged-particle measurement. The correction for the underlying-event modelling is applied to WW, WZ and ZZ processes as a function of the charged-particle multiplicity, and of the particle-level p_{T} of the decay products of the diboson system.

5.3. Signal modelling

After the initial $\gamma\gamma \rightarrow WW$ process, the protons can undergo a second inelastic interaction. These additional rescatterings do not change the kinematics of the $\gamma\gamma \rightarrow WW$ process, but lead to the production of particles such that the cross section of $\gamma\gamma \rightarrow WW$ production without associated tracks is reduced. This effect is not included in the modelling of the signal. The probability that no such additional particles are produced is commonly referred to as the survival factor. In addition, the $\gamma\gamma \rightarrow WW$ signal when applying the exclusivity requirement is modelled by HERWIG7, which includes only the elastic component. To obtain a better estimate of the expected signal yield including the dissociative components and to correct for effects from the rescattering of protons, a correction factor is obtained from a $\gamma\gamma \rightarrow \ell\ell$ control sample in data, following a procedure similar to that applied in Refs. [4,6] using same-flavour lepton final states. To enhance the purity in $\gamma\gamma \rightarrow \ell\ell$ production and to mimic the kinematic threshold of $\gamma\gamma \rightarrow WW$ production, the dilepton mass is required to be larger than 160 GeV. The exclusivity requirement of $n_{\text{trk}} = 0$ is applied. In the region, where the correction factor is extracted, the predicted event yield from the $\gamma\gamma \rightarrow WW$ process with same-flavour final states is approximately 1.5% of the $\gamma\gamma \rightarrow \ell\ell$ yield so that the derived correction factor is essentially independent of the $\gamma\gamma \rightarrow WW$ signal process.

The background, dominated by DY production, is estimated using a data-driven technique. The shape of the $m_{\ell\ell}$ distribution for background events is estimated using events with $n_{\text{trk}} = 5$, which is a compromise between small signal contamination and closeness to the signal region. This template is normalised to the $n_{\text{trk}} = 0$ selection using a narrow window around the nominal Z boson mass ($83.5 \text{ GeV} < m_{\ell\ell} < 98.5 \text{ GeV}$) where the contribution from photon-induced processes is small. The $m_{\ell\ell}$ lineshape in simulated DY events is found to be independent of n_{trk} for low multiplicities.

When the exclusivity requirement of $n_{\text{trk}} = 0$ is applied, the ratio of the yield from photon-induced processes in data to the MC prediction for the elastic processes is found to be 3.59 ± 0.15 (tot.). This agrees with the expectation of 3.55 obtained using the MC prediction. It has been verified that the signal modelling correction

² Similarly to Ref. [80], charged particles are defined to be stable if they have a mean lifetime $\tau > 30 \text{ ps}$ and satisfy $p_{\text{T}} > 500 \text{ MeV}$ and $|\eta| < 2.5$.

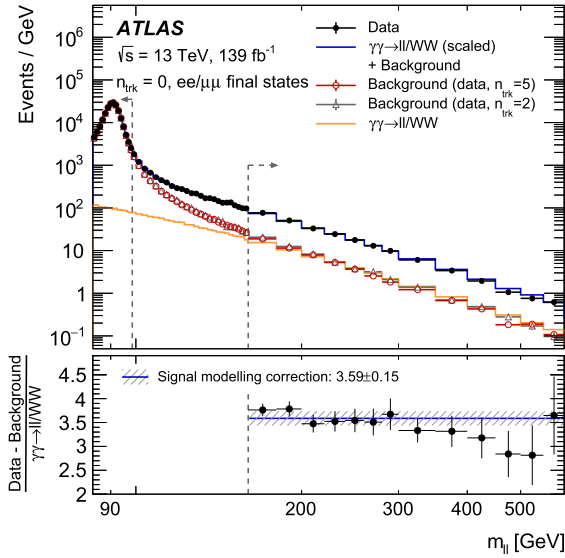


Fig. 4. The distribution of $m_{\ell\ell}$ in the region where the signal modelling correction is extracted as the ratio of the yield of $\gamma\gamma \rightarrow \ell\ell$ and $\gamma\gamma \rightarrow WW$ processes passing the exclusivity requirement of $n_{\text{trk}} = 0$ to the yield of the simulated elastic process only. Shown are the data, where a requirement of $n_{\text{trk}} = 0$ has been applied, and the background templates selected from data using $n_{\text{trk}} = 2$ and $n_{\text{trk}} = 5$. In addition, the $\gamma\gamma \rightarrow \ell\ell$ and $\gamma\gamma \rightarrow WW$ MC predictions are depicted, as well as the sum of the nominal background template ($n_{\text{trk}} = 5$) and the $\gamma\gamma \rightarrow \ell\ell$ and $\gamma\gamma \rightarrow WW$ MC predictions scaled by the signal modelling correction. The normalisation region around the nominal Z boson mass is indicated by a vertical dashed line, as is the region where the signal modelling correction is extracted ($m_{\ell\ell} > 160$ GeV). The excess in data relative to the elastic $\gamma\gamma \rightarrow \ell\ell$ and $\gamma\gamma \rightarrow WW$ prediction is attributed to the dissociative photon-induced processes and used to extract the signal modelling correction that is shown in the lower panel of the plot. The uncertainties shown are statistical only.

does not vary as a function of $p_T^{e\mu}$ within the boundaries used to extract the signal.

Fig. 4 illustrates the extraction of the signal modelling correction from data. The signal modelling correction is only applicable to events with $n_{\text{trk}} = 0$. The simulated HERWIG7 events are used in conjunction with the signal modelling correction for predictions of photon-induced processes in events where the $n_{\text{trk}} = 0$ requirement is applied, while the event samples from MG5_AMC@NLO+PYTHIA8 are used for predictions in regions with larger track multiplicities.

Uncertainties are evaluated by increasing the mass window of the DY background normalisation region to $73.5 \text{ GeV} < m_{\ell\ell} < 108.5 \text{ GeV}$ and by changing the number of tracks used in the selection of the template, using $n_{\text{trk}} = 2$ instead of the nominal value. The resulting uncertainty in the signal modelling correction amounts to 4.2%. When the signal modelling correction is applied to $\gamma\gamma \rightarrow WW$, an additional transfer uncertainty is included to account for potential differences between $\gamma\gamma \rightarrow \ell\ell$ and $\gamma\gamma \rightarrow WW$ events due to the fact that rescattering effects are mass-dependent. It is calculated as the largest variation that arises from placing different lower bounds on the evaluation region; the lower bound on $m_{\ell\ell}$ was varied from $m_{\ell\ell} = 110 \text{ GeV}$ to 400 GeV in intervals of 10 GeV . The resulting uncertainty amounts to 11%. This uncertainty affects only the scaling of the $\gamma\gamma \rightarrow WW$ process and thus the measured signal strength and any cross section prediction derived using the signal correction factor, but cancels out in the measurement of the fiducial cross section.

6. Event categories and background estimation

One signal region and three control regions, enriched in signal and background events respectively, are defined using the dilepton

transverse momentum, $p_T^{e\mu}$, and the number of additional tracks associated with the interaction vertex, n_{trk} . The signal region is defined by selecting $p_T^{e\mu} > 30 \text{ GeV}$ and $n_{\text{trk}} = 0$. It has an expected purity of 57% and an expected background contamination from $qq \rightarrow WW$ production of 33%.

Additional kinematic regions with alternative requirements on $p_T^{e\mu}$ and n_{trk} are used to control the modelling of background processes. The first control region is defined by $p_T^{e\mu} < 30 \text{ GeV}$ and $1 \leq n_{\text{trk}} \leq 4$ and helps to constrain the $DY(Z/\gamma^* \rightarrow \tau\tau)$ normalisation, as this process contributes 75% of the selected events in this region. It also has non-negligible contributions from $qq \rightarrow WW$ events and non-prompt leptons. The second control region is defined by $p_T^{e\mu} > 30 \text{ GeV}$ and $1 \leq n_{\text{trk}} \leq 4$ and is designed to be enriched in $qq \rightarrow WW$ events, with an expected contribution of about 70% from that process and minor contributions from the DY process and non-prompt lepton events. An additional control region is selected with $p_T^{e\mu} < 30 \text{ GeV}$ and $n_{\text{trk}} = 0$. It brings some additional control for the modelling of backgrounds specific to events with no tracks, however has a signal contamination of the order of 10%. The boundaries between these regions are chosen such that good signal-background separation is achieved. In addition, the regions used to control the normalisation of the backgrounds are defined to be topologically very similar to the signal region, which helps to minimise uncertainties in extrapolating the normalisation from the control regions to the signal region.

Background events from non-prompt leptons contribute about 6% of the selected signal candidates in the signal region. The primary source of these backgrounds in dilepton events is W +jets production where one of the leptons is prompt and the other stems from light-hadron or heavy-flavour decays. Background events from non-prompt leptons are estimated from a control region where exactly one of the leptons must fail to satisfy some of the lepton identification criteria of the nominal event selection. All other kinematic selection criteria are the same as for the signal selection. The contribution from non-prompt leptons is then estimated by scaling the number of events in the control region by the ratio of the number of non-prompt leptons passing all identification requirements to those failing some of these requirements. This ratio is measured in data selected with one electron and one muon with the same electric charge, and requiring $1 \leq n_{\text{trk}} \leq 4$. Contributions from prompt leptons are subtracted using MC simulation. For the extrapolation to the event samples selected with $n_{\text{trk}} = 0$ a dedicated uncertainty is assigned.

7. Systematic uncertainties

Uncertainties and their correlations are evaluated in each of the signal and control regions. The uncertainties in the measurement of tracks originate from uncertainties in the inner detector alignment, the reconstruction efficiency, and the probability to incorrectly reconstruct tracks by including hits from noise or from several tracks. The combined uncertainty amounts to 5–7% of the event yields for DY and $qq \rightarrow WW$ production, whilst for photon-induced processes these uncertainties are $< 1\%$ in the regions where these processes contribute significantly.

Systematic uncertainties in the event yields due to electron and muon reconstruction, including effects from the trigger and reconstruction efficiencies, energy/momentum scale and resolution, and pile-up modelling are 0.5% and up to 2% depending on the process, in the signal and control regions, respectively [59–62].

The uncertainty in the background from non-prompt leptons is dominated by the uncertainty in the measurement of the ratio of non-prompt leptons passing all identification requirements to those failing some, in particular the subtraction of contributions from genuine leptons in the numerator of that ratio. The resulting uncertainty on this background estimation ranges between 50%

Table 1

Summary of the data event yields, and the predicted signal and background event yields in the signal region and control regions as obtained after the fit. The uncertainties shown include statistical and systematic components. Because the fit introduces correlations between systematic uncertainties, the uncertainty in the total expected yield is smaller than its components. The leftmost column of values corresponds to the signal region used to measure $\gamma\gamma \rightarrow WW$ in proton–proton collisions. The numbers for $qq \rightarrow WW$ also contain a small contribution from gluon-induced WW and electroweak $WWjj$ production. The event yields for other backgrounds include contributions from WZ and ZZ diboson production, top-quark production and other gluon-induced processes.

n_{trk}	Signal region		Control regions	
	$n_{\text{trk}} = 0$		$1 \leq n_{\text{trk}} \leq 4$	
$p_{\text{T}}^{e\mu}$	> 30 GeV	< 30 GeV	> 30 GeV	< 30 GeV
$\gamma\gamma \rightarrow WW$	174 ± 20	45 ± 6	95 ± 19	24 ± 5
$\gamma\gamma \rightarrow \ell\ell$	5.5 ± 0.3	39.6 ± 1.9	5.6 ± 1.2	32 ± 7
Drell–Yan	4.5 ± 0.9	280 ± 40	106 ± 19	4700 ± 400
$qq \rightarrow WW$ (incl. gg and VBS)	101 ± 17	55 ± 10	1700 ± 270	970 ± 150
Non-prompt	14 ± 14	36 ± 35	220 ± 220	500 ± 400
Other backgrounds	7.1 ± 1.7	1.9 ± 0.4	311 ± 76	81 ± 15
Total	305 ± 18	459 ± 19	2460 ± 60	6320 ± 130
Data	307	449	2458	6332

and 100% depending on the region. The statistical uncertainty in the control region for the estimation of background from misidentified leptons is also a significant source of uncertainty.

The uncertainties in the correction of pile-up modelling and the underlying event as well as the uncertainty in the signal modelling correction are described in Section 5. The correction for the underlying-event modelling in the WW , WZ and ZZ processes is derived in bins of $p_{\text{T}}^{\ell\ell}$, but applied as a function of diboson p_{T} , utilising the fact that there are only relatively small differences in charged-particle multiplicity between the DY and diboson processes. Residual differences are evaluated at the particle level and considered as systematic uncertainties. For the largest source of background, the quark-induced WW process, further studies are made. The predicted event yields are compared for POWHEG+PYTHIA8 and variations of the PYTHIA8 parton-shower tunes, and for POWHEG+HERWIG7 and SHERPA, with each prediction using its dedicated underlying-event correction. The event yields agree well for $1 \leq n_{\text{trk}} \leq 4$, but disagree in the signal region, $n_{\text{trk}} = 0$. The background yield from the quark-induced WW process is estimated as the average of the highest and lowest value of the various predictions, that is the midpoint of the most extreme predictions as no preference for either model can be deduced from the data. The envelope of all predictions is taken as the upper and lower one-standard-deviation boundary, amounting to $\pm 7\%$ for events selected with $n_{\text{trk}} = 0$, and amounting to less than 1% for events selected with $1 \leq n_{\text{trk}} \leq 4$. The uncertainties in the total quark-induced WW cross section and the shape of the p_{T}^{WW} distribution are taken from the MATRIX+RadISH prediction used to reweight the WW samples, amounting to 5–6%.

Because of the specific event selection of the analysis, large uncertainties are applied to minor backgrounds, where the n_{trk} modelling cannot be easily studied in data: the uncertainty in the $W\gamma$ normalisation is taken to be $\pm 100\%$, whereas uncertainties of $\pm 30\%$ are used for the normalisation of top-quark production and $WWjj$ production through vector-boson scattering (VBS) as well as gluon-induced resonant and non-resonant WW production. The numbers are informed by the size of the underlying-event correction in DY and WW events and studies on events with forward jets outside the acceptance of the ID. For the smaller background contributions from WZ and ZZ production the uncertainty is assessed by comparing the event yields predicted by POWHEG+PYTHIA8 with those predicted in SHERPA after applying the underlying-event correction described in Section 5.2.

The systematic uncertainty in the measured cross section also includes a contribution due to differences in reconstruction efficiency between elastic and dissociative photon-induced processes as well as an uncertainty due to missing spin correlations in HERWIG7, which mainly affects the $p_{\text{T}}^{e\mu}$ modelling. These uncertainties are evaluated separately by comparing the reconstruction efficiency of the elastic-only prediction with that including all production mechanisms and by comparing the reconstruction efficiency between HERWIG7 and MG5_AMC@NLO+PYTHIA8. Their combined effect is $\pm 2\%$. Uncertainties stemming from the signal modelling correction are applied to the signal prediction and are discussed in detail in Section 5.3.

8. Results

The $\gamma\gamma \rightarrow WW$ signal in proton–proton collisions is extracted using a profile likelihood fit of the estimated signal and background event yields to data. The fit uses the integrated event yields in the four kinematic regions introduced in Section 6, and the $ee + \mu\mu$ events selected as described in Section 5.3. It maximises the product of Poisson probabilities to produce the observed number of data events, N_{obs} , in each of these regions [81].

The normalisation of the backgrounds from DY and $qq \rightarrow WW$ processes are free parameters in the fit. The expected elastic $\gamma\gamma \rightarrow \ell\ell$ and $\gamma\gamma \rightarrow WW$ event yields for $n_{\text{trk}} = 0$ are multiplied by the signal modelling correction discussed in Section 5.3, which is obtained as described within the fit to preserve the experimental correlations correctly. The event yield for the $\gamma\gamma \rightarrow WW$ signal process is also multiplied by a signal strength that is a free parameter in the fit. Systematic uncertainties are included in the fit as nuisance parameters constrained by Gaussian functions. The fit can only constrain the sum of the backgrounds, since the background composition is similar in events selected with $n_{\text{trk}} = 0$ and those selected with $1 \leq n_{\text{trk}} \leq 4$. Overall, the uncertainty in the sum of their yields is dominated by the systematic uncertainties assigned to events selected with $n_{\text{trk}} = 0$. In this fit, the background-only hypothesis is expected to be rejected with a significance of 6.7 standard deviations.

Table 1 gives an overview of the number of data events compared to background and signal event yields in the different regions after the fit. The data yield in the signal region is 307, compared with 132 background events predicted by the best-fit result. The normalisations of the WW and the DY background are con-

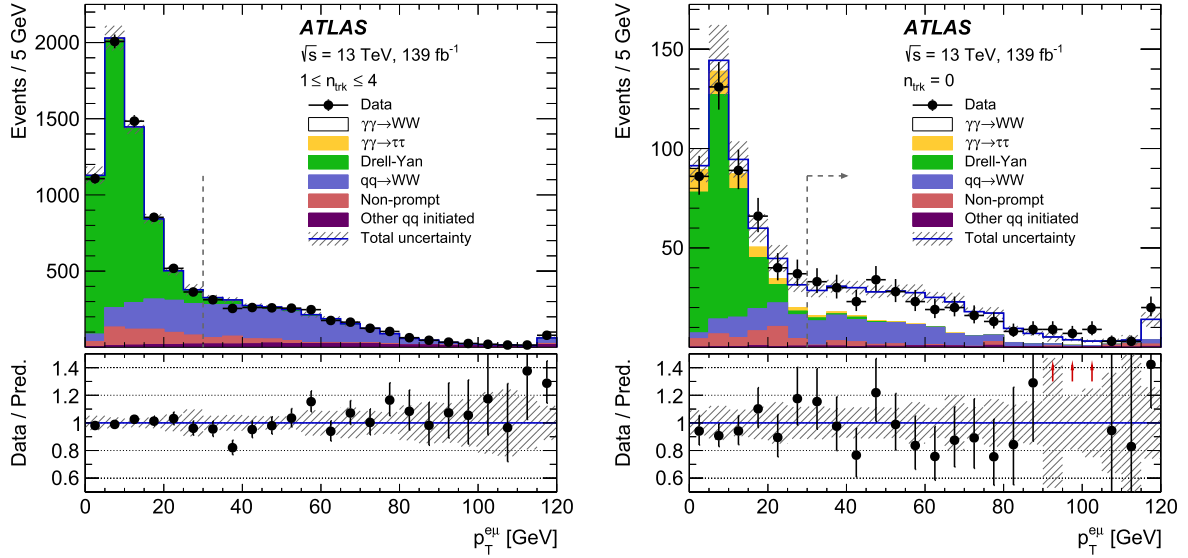


Fig. 5. The distributions of $p_T^{e\mu}$ for $1 \leq n_{\text{trk}} \leq 4$ (left) and $n_{\text{trk}} = 0$ (right) are shown. The fitted normalisation factors and nuisance parameters have been used. The yields for the likelihood fit are given by the integrals of the distributions split at $p_T^{e\mu} = 30$ GeV, as indicated by the vertical dashed lines. The $\gamma\gamma \rightarrow WW$ signal region requires a selection of $p_T^{e\mu} > 30$ GeV with $n_{\text{trk}} = 0$, as indicated by the arrow. The $qq \rightarrow WW$ component also contains a small contribution from gluon-induced WW and electroweak $WWjj$ production. Similarly, ‘other qq initiated’ includes contributions not only from WZ and ZZ diboson production but also from top-quark production and other gluon-induced processes. The total uncertainties are shown as hatched bands. The lower panels show the ratio of the data to the prediction, with the total uncertainty displayed as a hatched band. An arrow indicates that the ratio is off-scale. The last bin in both distributions includes the overflow.

strained with the help of the control regions to be $1.21^{+0.19}_{-0.23}$ (tot.) and $1.16^{+0.10}_{-0.12}$ (tot.), respectively.

By fitting the signal and background event yields in the signal and control regions, the background-only hypothesis is rejected with a significance of 8.4 standard deviations, assuming that the systematic uncertainties are Gaussian-distributed up to large values. A signal strength of $1.33^{+0.14}_{-0.14}$ (stat.) $^{+0.22}_{-0.17}$ (syst.) is measured relative to the yield of elastic $\gamma\gamma \rightarrow WW$ events predicted by HERWIG7 scaled by the signal modelling correction to account for all photon-induced production mechanisms in a phase space with no tracks associated with the interaction vertex. These results constitute the observation of photon-induced WW production in pp collisions, a process for which only evidence with significances of 3.0σ [4] and 3.6σ [6] was previously reported.

Fig. 5 shows two $p_T^{e\mu}$ distributions: on the left for events with $1 \leq n_{\text{trk}} \leq 4$ associated with the interaction vertex, and, on the right, for events with the exclusivity requirement of no tracks. The boundary between low- and high- $p_T^{e\mu}$ control and signal regions is at 30 GeV. The distributions in Fig. 5 include the fitted normalisations and nuisance parameters described above; the resulting predictions are in good agreement with the data. Fig. 6 shows the distribution of the number of reconstructed tracks for $p_T^{e\mu} > 30$ GeV.

The fiducial phase space used for the cross-section measurement is defined to be close to the acceptance of the detector. The leptons must at particle level satisfy the pseudorapidity requirement $|\eta| < 2.5$. One of the leptons is required to have a transverse momentum of at least 27 GeV, whilst the other must have $p_T > 20$ GeV. They are required to be prompt leptons from W decays. Photons in a cone of $\Delta R = 0.1$ around a lepton and not originating from the decays of hadrons are added to the four-momentum of the lepton, that is leptons are ‘‘dressed’’. Events with exactly two leptons are selected with opposite-sign and different-flavour final states. Decays of either W boson into a τ -lepton and neutrino are excluded. The invariant mass of the dilepton system is required to be $m_{\ell\ell} > 20$ GeV and its transverse momentum must be $p_T^{e\mu} > 30$ GeV. The number of charged particles, n_{ch} , with $p_T > 500$ MeV and within $|\eta| < 2.5$, excluding the selected leptons, is required to be zero.

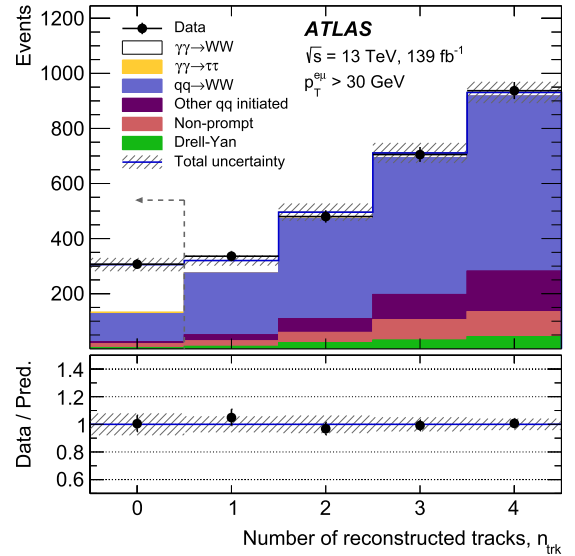


Fig. 6. The distribution of the number of tracks associated with the interaction vertex is shown. The fitted normalisation factors and nuisance parameters have been used. The $\gamma\gamma \rightarrow WW$ signal region requires a selection of $n_{\text{trk}} = 0$, as indicated by the vertical dashed line. The $qq \rightarrow WW$ component also contains a small contribution from gluon-induced WW and electroweak $WWjj$ production. Similarly, ‘other qq initiated’ includes contributions not only from WZ and ZZ diboson production but also from top-quark production and other gluon-induced processes. The total uncertainties are shown as hatched bands. The lower panel shows the ratio of the data to the prediction, with the total uncertainty displayed as a hatched band.

Without requirements on the number of reconstructed tracks, the selection efficiency after reconstruction is 75% for elastic $\gamma\gamma \rightarrow WW$ events in the fiducial region. The full selection efficiency after applying $n_{\text{trk}} = 0$ is 39%. The predicted number of signal events includes a $\sim 5\%$ contribution of leptons from $W \rightarrow \tau \nu_\tau$, $\tau \rightarrow \ell \nu_\ell \nu_\tau$, which is estimated using the MC simulation and which is removed from the measured fiducial cross section using this fractional contribution.

Table 2

The impact of different components of systematic uncertainty on the measured fiducial cross section, without taking into account correlations. The impact of each source of systematic uncertainty is computed by first performing the fit with the corresponding nuisance parameter fixed to one standard deviation up or down from the value obtained in the nominal fit, then these high and low variations are symmetrised. The impacts of several sources of systematic uncertainty are added in quadrature for each component.

Source of uncertainty	Impact [% of the fitted cross section]
Experimental	
Track reconstruction	1.1
Electron energy scale and resolution, and efficiency	0.4
Muon momentum scale and resolution, and efficiency	0.5
Misidentified leptons, systematic	1.5
Misidentified leptons, statistical	5.9
Other background, statistical	3.2
Modelling	
Pile-up modelling	1.1
Underlying-event modelling	1.4
Signal modelling	2.1
WW modelling	4.0
Other background modelling	1.7
Luminosity	1.7
Total	8.9

The observed signal strength translates into a fiducial cross section of

$$\sigma_{\text{meas}} = 3.13 \pm 0.31 (\text{stat.}) \pm 0.28 (\text{syst.}) \text{ fb}$$

for $pp(\gamma\gamma) \rightarrow p^{(*)}W^+W^-p^{(*)}$ production with $W^+W^- \rightarrow e^\pm\nu\mu^\mp\nu$. The uncertainties correspond to the statistical and systematic uncertainties, respectively. Table 2 gives an overview of the sources of systematic uncertainties, which are discussed in Section 7 and presents their effect on the measured cross section. To evaluate the impact of one source of systematic uncertainty, the fit is performed with the corresponding nuisance parameter fixed one standard deviation up or down from the value obtained in the nominal fit, then these high and low variations are symmetrised.

The data measurement can be compared with two types of predictions. The first, used in the definition of the signal strength and the calculation of the expected significance, is based on the HERWIG7 prediction for elastic $\gamma\gamma \rightarrow WW$ events scaled by the data-driven signal modelling correction to include the dissociative processes and rescattering effects as described in Section 5.3. It is found to be

$$\sigma_{\text{theo}} \times (3.59 \pm 0.15 (\text{exp.}) \pm 0.39 (\text{trans.})) = 2.34 \pm 0.27 \text{ fb},$$

where the uncertainty contains all experimental uncertainties and receives an additional component due to the transfer from the $\gamma\gamma \rightarrow \ell\ell$ to the $\gamma\gamma \rightarrow WW$ process described above. The uncertainties in the theory prediction are negligible because the scale uncertainty in the calculation of elastic production based on a photon-flux is small and partially cancels with the signal correction that is calculated with respect to the same photon-flux compared to the data. A standalone theory prediction for the fiducial cross section is computed with MG5_AMC@NLO+PYTHIA8 using the appropriate elastic or inelastic MMHT2015qed PDF sets [82] for each of the contributions by applying the fiducial requirements to all photon-induced contributions, which yields $4.3 \pm 1.0(\text{scale}) \pm 0.1(\text{PDF})$ fb. The scale uncertainty is determined by varying the factorisation scale by factors of 2 and 0.5 and symmetrising the effect. The contributions to this cross-section prediction from elastic and single-dissociative production are 16% and 81%, respectively. Double-dissociative production contributes only 3%. Using CT14qed [28] as the central PDF set yields a prediction which is 26% smaller and amounts to 3.2 fb.

The MG5_AMC@NLO+PYTHIA8 prediction does not include re-scattering effects that are expected to decrease the fiducial cross section. For elastic $\gamma\gamma \rightarrow WW$ production, a survival factor of 0.65 was estimated in Ref. [83]. In Ref. [84] a survival factor of 0.82 was calculated in a two-channel eikonal model also accounting for the helicity structure of the hard scattering process.³ Multiplying the MG5_AMC@NLO+PYTHIA8 prediction by these survival factors results in theoretical predictions of 2.8 ± 0.8 fb and 3.5 ± 1.0 fb, respectively, with the total uncertainties calculated as the quadratic sum of scale and PDF uncertainties. These predictions are in agreement with the measurement.

9. Conclusion

The photon-induced production process, $\gamma\gamma \rightarrow WW$, was studied in proton–proton collisions at $\sqrt{s} = 13$ TeV recorded with the ATLAS detector at the LHC corresponding to an integrated luminosity of 139 fb^{-1} . Events with leptonic W boson decays into $e^\pm\nu\mu^\mp\nu$ final states were selected by requiring that no tracks except those of the two charged leptons are associated with the production vertex. The background-only hypothesis is rejected with a significance of 8.4 standard deviations whereas well above 5σ was expected. This measurement constitutes the observation of photon-induced WW production in pp collisions, a process for which only evidence was previously reported. The signal strength and the cross section for the sum of elastic and dissociative production mechanisms are measured. The cross section for the $pp(\gamma\gamma) \rightarrow p^{(*)}W^+W^-p^{(*)}$ process in the decay channel $W^+W^- \rightarrow e^\pm\nu\mu^\mp\nu$ in a fiducial phase space close to the experimental acceptance is measured to be $3.13 \pm 0.31 (\text{stat.}) \pm 0.28 (\text{syst.})$ fb. This result is in agreement with the theoretical predictions and may serve as input into EFT interpretations.

Declaration of competing interest

The authors declare that they have no known competing financial interests or personal relationships that could have appeared to influence the work reported in this paper.

³ More recent calculations predict slightly lower absorption values for the dissociative processes [85,86].

Acknowledgements

We thank CERN for the very successful operation of the LHC, as well as the support staff from our institutions without whom ATLAS could not be operated efficiently.

We acknowledge the support of ANPCyT, Argentina; YerPhI, Armenia; ARC, Australia; BMWFW and FWF, Austria; ANAS, Azerbaijan; SSTC, Belarus; CNPq and FAPESP, Brazil; NSERC, NRC and CFI, Canada; CERN; ANID, Chile; CAS, MOST and NSFC, China; COLCIENCIAS, Colombia; MSMT CR, MPO CR and VSC CR, Czech Republic; DNRF and DNSRC, Denmark; IN2P3-CNRS and CEA-DRF/IRFU, France; SRNSFG, Georgia; BMBF, HGF and MPG, Germany; GSRT, Greece; RGC and Hong Kong SAR, China; ISF and Benozio Center, Israel; INFN, Italy; MEXT and JSPS, Japan; CNRST, Morocco; NWO, Netherlands; RCN, Norway; MNiSW and NCN, Poland; FCT, Portugal; MNE/IFA, Romania; MES of Russia and NRC KI, Russia Federation; JINR; MESTD, Serbia; MSSR, Slovakia; ARRS and MIZŠ, Slovenia; DST/NRF, South Africa; MICINN, Spain; SRC and Wallenberg Foundation, Sweden; SERI, SNSF and Cantons of Bern and Geneva, Switzerland; MOST, Taiwan; TAEK, Turkey; STFC, United Kingdom; DOE and NSF, United States of America. In addition, individual groups and members have received support from BCKDF, CANARIE, Compute Canada and CRC, Canada; ERC, ERDF, Horizon 2020, Marie Skłodowska-Curie Actions and COST, European Union; Investissements d'Avenir Labex, Investissements d'Avenir IDEX and ANR, France; DFG and AvH Foundation, Germany; Herakleitos, Thales and Aristeia programmes co-financed by EU-ESF and the Greek NSRF, Greece; BSF-NSF and GIF, Israel; La Caixa Banking Foundation, CERCA Programme Generalitat de Catalunya and PROMETEO and GenT Programmes Generalitat Valenciana, Spain; Göran Gustafssons Stiftelse, Sweden; The Royal Society and Leverhulme Trust, United Kingdom.

The crucial computing support from all WLCG partners is acknowledged gratefully, in particular from CERN, the ATLAS Tier-1 facilities at TRIUMF (Canada), NDGF (Denmark, Norway, Sweden), CC-IN2P3 (France), KIT/GridKA (Germany), INFN-CNAF (Italy), NL-T1 (Netherlands), PIC (Spain), ASGC (Taiwan), RAL (UK) and BNL (USA), the Tier-2 facilities worldwide and large non-WLCG resource providers. Major contributors of computing resources are listed in Ref. [87].

References

- [1] E. Chapon, C. Royon, O. Kepka, Anomalous quartic $WW\gamma\gamma$, $ZZ\gamma\gamma$, and trilinear $WW\gamma$ couplings in two-photon processes at high luminosity at the LHC, *Phys. Rev. D* 81 (2010) 074003, arXiv:0912.5161 [hep-ph].
- [2] B. Grzadkowski, M. Iskrzyński, M. Misiak, J. Rosiek, Dimension-six terms in the Standard Model Lagrangian, *J. High Energy Phys.* 10 (2010) 085, arXiv:1008.4884 [hep-ph].
- [3] O.J.P. Éboli, M.C. Gonzalez-García, S.M. Lietti, S.F. Novaes, Anomalous quartic gauge boson couplings at hadron colliders, *Phys. Rev. D* 63 (2001) 075008, arXiv:hep-ph/0009262.
- [4] ATLAS Collaboration, Measurement of exclusive $\gamma\gamma \rightarrow W^+W^-$ production and search for exclusive Higgs boson production in pp collisions at $\sqrt{s} = 8$ TeV using the ATLAS detector, *Phys. Rev. D* 94 (2016) 032011, arXiv:1607.03745 [hep-ex].
- [5] CMS Collaboration, Study of exclusive two-photon production of W^+W^- in pp collisions at $\sqrt{s} = 7$ TeV and constraints on anomalous quartic gauge couplings, *J. High Energy Phys.* 07 (2013) 116, arXiv:1305.5596 [hep-ex].
- [6] CMS Collaboration, Evidence for exclusive $\gamma\gamma \rightarrow W^+W^-$ production and constraints on anomalous quartic gauge couplings in pp collisions at $\sqrt{s} = 7$ and 8 TeV, *J. High Energy Phys.* 08 (2016) 119, arXiv:1604.04464 [hep-ex].
- [7] ATLAS Collaboration, The ATLAS experiment at the CERN Large Hadron Collider, *J. Instrum.* 3 (2008) S08003.
- [8] ATLAS Collaboration, ATLAS Insertable B-Layer Technical Design Report, ATLAS-TDR-19; CERN-LHCC-2010-013, 2010, <https://cds.cern.ch/record/1291633>.
- [9] B. Abbott, et al., Production and integration of the ATLAS Insertable B-Layer, *J. Instrum.* 13 (2018) T05008, arXiv:1803.00844 [physics.ins-det].
- [10] ATLAS Collaboration, Track Reconstruction Performance of the ATLAS Inner Detector at $\sqrt{s} = 13$ TeV, ATL-PHYS-PUB-2015-018, 2015, <https://cds.cern.ch/record/2037683>.
- [11] ATLAS Collaboration, Performance of the ATLAS trigger system in 2015, *Eur. Phys. J. C* 77 (2017) 317, arXiv:1611.09661 [hep-ex].
- [12] ATLAS Collaboration, Luminosity determination in pp collisions at $\sqrt{s} = 13$ TeV using the ATLAS detector at the LHC, ATLAS-CONF-2019-021, 2019, <https://cds.cern.ch/record/2677054>.
- [13] ATLAS Collaboration, Characterization of Interaction-Point Beam Parameters Using the pp Event-Vertex Distribution Reconstructed in the ATLAS Detector at the LHC, ATLAS-CONF-2010-027, 2010, <https://cds.cern.ch/record/1277659>.
- [14] ATLAS Collaboration, ATLAS data quality operations and performance for 2015–2018 data-taking, *J. Instrum.* 15 (2020) P04003, arXiv:1911.04632 [physics.ins-det].
- [15] G. Avoni, et al., The new LUCID-2 detector for luminosity measurement and monitoring in ATLAS, *J. Instrum.* 13 (2018) P07017.
- [16] ATLAS Collaboration, The ATLAS simulation infrastructure, *Eur. Phys. J. C* 70 (2010) 823, arXiv:1005.4568 [physics.ins-det].
- [17] S. Agostinelli, et al., GEANT4 – a simulation toolkit, *Nucl. Instrum. Methods Phys. Res., Sect. A* 506 (2003) 250.
- [18] ATLAS Collaboration, The simulation principle and performance of the ATLAS fast calorimeter simulation FastCaloSim, ATL-PHYS-PUB-2010-013, 2010, <https://cds.cern.ch/record/1300517>.
- [19] T. Sjöstrand, et al., An introduction to PYTHIA 8.2, *Comput. Phys. Commun.* 191 (2015) 159, arXiv:1410.3012 [hep-ph].
- [20] ATLAS Collaboration, The Pythia 8 A3 tune description of ATLAS minimum bias and inelastic measurements incorporating the Donnachie–Landschoff diffractive model, ATL-PHYS-PUB-2016-017, 2016, <https://cds.cern.ch/record/2206965>.
- [21] R.D. Ball, et al., Parton distributions with LHC data, *Nucl. Phys. B* 867 (2013) 244, arXiv:1207.1303 [hep-ph].
- [22] D.J. Lange, The EvtGen particle decay simulation package, *Nucl. Instrum. Methods Phys. Res., Sect. A* 462 (2001) 152.
- [23] M. Bahr, et al., Herwig++ physics and manual, *Eur. Phys. J. C* 58 (2008) 639, arXiv:0803.0883 [hep-ph].
- [24] J. Bellm, et al., Herwig 7.0/Herwig++ 3.0 release note, *Eur. Phys. J. C* 76 (2016) 196, arXiv:1512.01178 [hep-ph].
- [25] V.M. Budnev, I.F. Ginzburg, G.V. Meledin, V.G. Serbo, The two-photon particle production mechanism. Physical problems. Applications. Equivalent photon approximation, *Phys. Rep.* 15 (1975) 181.
- [26] L. Lönnblad, ThePEG: toolkit for high energy physics event generation, in: Proceedings, HERA and the LHC Workshop Series on the Implications of HERA for LHC Physics: 2006–2008, DESY, 2009, p. 733, arXiv:0903.3861 [hep-ph].
- [27] J. Alwall, et al., The automated computation of tree-level and next-to-leading order differential cross sections, and their matching to parton shower simulations, *J. High Energy Phys.* 07 (2014) 079, arXiv:1405.0301 [hep-ph].
- [28] C. Schmidt, J. Pumplin, D. Stump, C.-P. Yuan, CT14QED parton distribution functions from isolated photon production in deep inelastic scattering, *Phys. Rev. D* 93 (2016) 114015, arXiv:1509.02905 [hep-ph].
- [29] J.A.M. Vermaseren, Two-photon processes at very high energies, *Nucl. Phys. B* 229 (1983) 347.
- [30] V. Bertone, S. Carrazza, N. Hartland, J. Rojo, Illuminating the photon content of the proton within a global PDF analysis, *SciPost Phys.* 5 (2018), arXiv:1712.07053 [hep-ph].
- [31] P. Nason, A new method for combining NLO QCD with shower Monte Carlo algorithms, *J. High Energy Phys.* 11 (2004) 040, arXiv:hep-ph/0409146.
- [32] S. Frixione, P. Nason, C. Oleari, Matching NLO QCD computations with parton shower simulations: the POWHEG method, *J. High Energy Phys.* 11 (2007) 070, arXiv:0709.2092 [hep-ph].
- [33] S. Alioli, P. Nason, C. Oleari, E. Re, A general framework for implementing NLO calculations in shower Monte Carlo programs: the POWHEG BOX, *J. High Energy Phys.* 06 (2010) 043, arXiv:1002.2581 [hep-ph].
- [34] T. Melia, P. Nason, R. Röntsch, G. Zanderighi, W^+W^- , WZ and ZZ production in the POWHEG BOX, *J. High Energy Phys.* 11 (2011) 078, arXiv:1107.5051 [hep-ph].
- [35] P. Nason, G. Zanderighi, W^+W^- , WZ and ZZ production in the POWHEG-BOX-V2, *Eur. Phys. J. C* 74 (2014) 2702, arXiv:1311.1365 [hep-ph].
- [36] H.-L. Lai, et al., New parton distributions for collider physics, *Phys. Rev. D* 82 (2010) 074024, arXiv:1007.2241 [hep-ph].
- [37] ATLAS Collaboration, Measurement of the Z/γ^* boson transverse momentum distribution in pp collisions at $\sqrt{s} = 7$ TeV with the ATLAS detector, *J. High Energy Phys.* 09 (2014) 145, arXiv:1406.3660 [hep-ex].
- [38] J. Pumplin, et al., New generation of parton distributions with uncertainties from global QCD analysis, *J. High Energy Phys.* 07 (2002) 012, arXiv:hep-ph/0201195.
- [39] L.A. Harland-Lang, A.D. Martin, P. Motylinski, R.S. Thorne, Parton distributions in the LHC era: MMHT 2014 PDFs, *Eur. Phys. J. C* 75 (2015), arXiv:1412.3989 [hep-ph].
- [40] S. Höche, F. Krauss, S. Schumann, F. Siegert, QCD matrix elements and truncated showers, *J. High Energy Phys.* 05 (2009) 053, arXiv:0903.1219 [hep-ph].
- [41] E. Bothmann, et al., Event generation with Sherpa 2.2, *SciPost Phys.* 7 (2019) 034, arXiv:1905.09127 [hep-ph].

- [42] T. Gleisberg, S. Höche, Comix, a new matrix element generator, *J. High Energy Phys.* 12 (2008) 039, arXiv:0808.3674 [hep-ph].
- [43] S. Schumann, F. Krauss, A parton shower algorithm based on Catani–Seymour dipole factorisation, *J. High Energy Phys.* 03 (2008) 038, arXiv:0709.1027 [hep-ph].
- [44] S. Höche, F. Krauss, M. Schönherr, F. Siegert, A critical appraisal of NLO+PS matching methods, *J. High Energy Phys.* 09 (2012) 049, arXiv:1111.1220 [hep-ph].
- [45] S. Höche, F. Krauss, M. Schönherr, F. Siegert, QCD matrix elements + parton showers. The NLO case, *J. High Energy Phys.* 04 (2013) 027, arXiv:1207.5030 [hep-ph].
- [46] S. Catani, F. Krauss, R. Kuhn, B.R. Webber, QCD matrix elements + parton showers, *J. High Energy Phys.* 11 (2001) 063, arXiv:hep-ph/0109231.
- [47] F. Buccioni, et al., OpenLoops 2, *Eur. Phys. J. C* 79 (2019) 866, arXiv:1907.13071 [hep-ph].
- [48] F. Cascioli, P. Maierhöfer, S. Pozzorini, Scattering amplitudes with open loops, *Phys. Rev. Lett.* 108 (2012) 111601, arXiv:1111.5206 [hep-ph].
- [49] A. Denner, S. Dittmaier, L. Hofer, Collier: a fortran-based complex one-loop library in extended regularizations, *Comput. Phys. Commun.* 212 (2017) 220, arXiv:1604.06792 [hep-ph].
- [50] R.D. Ball, et al., Parton distributions for the LHC run II, *J. High Energy Phys.* 04 (2015) 040, arXiv:1410.8849 [hep-ph].
- [51] S. Frixione, P. Nason, G. Ridolfi, A positive-weight next-to-leading-order Monte Carlo for heavy flavour hadroproduction, *J. High Energy Phys.* 09 (2007) 126, arXiv:0707.3088 [hep-ph].
- [52] E. Re, Single-top Wt -channel production matched with parton showers using the POWHEG method, *Eur. Phys. J. C* 71 (2011) 1547, arXiv:1009.2450 [hep-ph].
- [53] ATLAS Collaboration, ATLAS Pythia 8 tunes to 7 TeV data, ATL-PHYS-PUB-2014-021, 2014, <https://cds.cern.ch/record/1966419>.
- [54] S. Frixione, E. Laenen, P. Motylinski, C.D. White, B.R. Webber, Single-top hadroproduction in association with a W boson, *J. High Energy Phys.* 07 (2008) 029, arXiv:0805.3067 [hep-ph].
- [55] ATLAS Collaboration, The Optimization of ATLAS Track Reconstruction in Dense Environments, ATL-PHYS-PUB-2015-006, 2015, <https://cds.cern.ch/record/2002609>.
- [56] ATLAS Collaboration, Early Inner Detector Tracking Performance in the 2015 Data at $\sqrt{s} = 13$ TeV, ATL-PHYS-PUB-2015-051, 2015, <https://cds.cern.ch/record/2110140>.
- [57] R. Frühwirth, Application of Kalman filtering to track and vertex fitting, *Nucl. Instrum. Methods Phys. Res., Sect. A* 262 (1987) 444.
- [58] ATLAS Collaboration, Electron reconstruction and identification in the ATLAS experiment using the 2015 and 2016 LHC proton–proton collision data at $\sqrt{s} = 13$ TeV, *Eur. Phys. J. C* 79 (2019) 639, arXiv:1902.04655 [hep-ex].
- [59] ATLAS Collaboration, Electron and photon performance measurements with the ATLAS detector using the 2015–2017 LHC proton–proton collision data, *J. Instrum.* 14 (2019) P12006, arXiv:1908.00005 [hep-ex].
- [60] ATLAS Collaboration, Muon reconstruction performance of the ATLAS detector in proton–proton collision data at $\sqrt{s} = 13$ TeV, *Eur. Phys. J. C* 76 (2016) 292, arXiv:1603.05598 [hep-ex].
- [61] ATLAS Collaboration, Performance of electron and photon triggers in ATLAS during LHC Run 2, *Eur. Phys. J. C* 80 (2020) 47, arXiv:1909.00761 [hep-ex].
- [62] ATLAS Collaboration, Performance of the ATLAS muon triggers in Run 2, arXiv:2004.13447 [hep-ex], 2020.
- [63] ATLAS Collaboration, Vertex Reconstruction Performance of the ATLAS Detector at $\sqrt{s} = 13$ TeV, ATL-PHYS-PUB-2015-026, 2015, <https://cds.cern.ch/record/2037717>.
- [64] S. Kallweit, E. Re, L. Rottoli, M. Wiesemann, Accurate single- and double-differential resummation of colour-singlet processes with MATRIX+RadISH: W^+W^- production at the LHC, arXiv:2004.07720 [hep-ph], 2020.
- [65] M. Grazzini, S. Kallweit, M. Wiesemann, Fully differential NNLO computations with MATRIX, *Eur. Phys. J. C* 78 (2018) 537, arXiv:1711.06631 [hep-ph].
- [66] M. Grazzini, S. Kallweit, S. Pozzorini, D. Rathlev, M. Wiesemann, W^+W^- production at the LHC: fiducial cross sections and distributions in NNLO QCD, *J. High Energy Phys.* 08 (2016) 140, arXiv:1605.02716 [hep-ph].
- [67] T. Gehrmann, et al., W^+W^- production at hadron colliders in next to next to leading order QCD, *Phys. Rev. Lett.* 113 (2014) 212001, arXiv:1408.5243 [hep-ph].
- [68] W. Bizon, P.F. Monni, E. Re, L. Rottoli, P. Torrielli, Momentum-space resummation for transverse observables and the Higgs p_\perp at $N^3\text{LL}+\text{NNLO}$, *J. High Energy Phys.* 02 (2018) 108, arXiv:1705.09127 [hep-ph].
- [69] P.F. Monni, E. Re, P. Torrielli, Higgs transverse-momentum resummation in direct space, *Phys. Rev. Lett.* 116 (2016) 242001, arXiv:1604.02191 [hep-ph].
- [70] T. Gehrmann, A. von Manteuffel, L. Tancredi, The two-loop helicity amplitudes for $q\bar{q} \rightarrow V_1 V_2 \rightarrow 4$ leptons, *J. High Energy Phys.* 09 (2015) 128, arXiv:1503.04812 [hep-ph].
- [71] S. Catani, M. Grazzini, An NNLO subtraction formalism in hadron collisions and its application to Higgs boson production at the LHC, *Phys. Rev. Lett.* 98 (2007) 222002, arXiv:hep-ph/0703012 [hep-ph].
- [72] S. Catani, L. Cieri, D. de Florian, G. Ferrera, M. Grazzini, Vector boson production at hadron colliders: hard-collinear coefficients at the NNLO, *Eur. Phys. J. C* 72 (2012) 2195, arXiv:1209.0158 [hep-ph].
- [73] ATLAS Collaboration, Measurement of distributions sensitive to the underlying event in inclusive Z boson production in pp collisions at $\sqrt{s} = 13$ TeV with the ATLAS detector, *Eur. Phys. J. C* 79 (2019) 666, arXiv:1905.09752 [hep-ex].
- [74] ATLAS Collaboration, Measurement of charged-particle distributions sensitive to the underlying event in $\sqrt{s} = 13$ TeV proton–proton collisions with the ATLAS detector at the LHC, *J. High Energy Phys.* 03 (2017) 157, arXiv:1701.05390 [hep-ex].
- [75] ATLAS Collaboration, Measurement of event-shape observables in $Z \rightarrow \ell^+ \ell^-$ events in pp collisions at $\sqrt{s} = 7$ TeV with the ATLAS detector at the LHC, *Eur. Phys. J. C* 76 (2016) 375, arXiv:1602.08980 [hep-ex].
- [76] ATLAS Collaboration, Measurement of distributions sensitive to the underlying event in inclusive Z -boson production in pp collisions at $\sqrt{s} = 7$ TeV with the ATLAS detector, *Eur. Phys. J. C* 74 (2014) 3195, arXiv:1409.3433 [hep-ex].
- [77] ATLAS Collaboration, Measurement of the exclusive $\gamma\gamma \rightarrow \mu^+ \mu^-$ process in proton–proton collisions at $\sqrt{s} = 13$ TeV with the ATLAS detector, *Phys. Lett. B* 777 (2018) 303, arXiv:1708.04053 [hep-ex].
- [78] G. D’Agostini, A multidimensional unfolding method based on Bayes’ theorem, *Nucl. Instrum. Methods Phys. Res., Sect. A* (ISSN 0168-9002) 362 (1995) 487.
- [79] G. D’Agostini, Improved iterative Bayesian unfolding, arXiv:1010.0632 [physics.data-an], 2010.
- [80] ATLAS Collaboration, Charged-particle distributions in $\sqrt{s} = 13$ TeV pp interactions measured with the ATLAS detector at the LHC, *Phys. Lett. B* 758 (2016) 67, arXiv:1602.01633 [hep-ex].
- [81] K. Cranmer, G. Lewis, L. Moneta, A. Shibata, W. Verkerke, HistFactory: a tool for creating statistical models for use with RooFit and RooStats, CERN-OPEN-2012-016, 2012, <https://cds.cern.ch/record/1456844>.
- [82] L. Harland-Lang, A. Martin, R. Nathvani, R. Thorne, Ad Lucem: QED parton distribution functions in the MMHT framework, *Eur. Phys. J. C* 79 (2019) 811, arXiv:1907.02750 [hep-ph].
- [83] M. Dyndal, L. Schoeffel, The role of finite-size effects on the spectrum of equivalent photons in proton–proton collisions at the LHC, *Phys. Lett. B* 741 (2015) 66, arXiv:1410.2983 [hep-ph].
- [84] L. Harland-Lang, V. Khoze, M. Ryskin, Exclusive physics at the LHC with SuperChic 2, *Eur. Phys. J. C* 76 (2016) 9, arXiv:1508.02718 [hep-ph].
- [85] L. Harland-Lang, V. Khoze, M. Ryskin, The photon PDF in events with rapidity gaps, *Eur. Phys. J. C* 76 (2016) 255, arXiv:1601.03772 [hep-ph].
- [86] L. Harland-Lang, M. Tasevsky, V. Khoze, M. Ryskin, A new approach to modelling elastic and inelastic photon-initiated production at the LHC: SuperChic 4, *Eur. Phys. J. C* 80 (2020) 925, arXiv:2007.12704 [hep-ph].
- [87] ATLAS Collaboration, ATLAS computing acknowledgements, ATL-SOFT-PUB-2020-001, <https://cds.cern.ch/record/2717821>.

The ATLAS Collaboration

G. Aad¹⁰², B. Abbott¹²⁸, D.C. Abbott¹⁰³, A. Abed Abud³⁶, K. Abeling⁵³, D.K. Abhayasinghe⁹⁴, S.H. Abidi¹⁶⁷, O.S. AbouZeid⁴⁰, N.L. Abraham¹⁵⁶, H. Abramowicz¹⁶¹, H. Abreu¹⁶⁰, Y. Abulaiti⁶, B.S. Acharya^{67a,67b,o}, B. Achkar⁵³, L. Adam¹⁰⁰, C. Adam Bourdarios⁵, L. Adamczyk^{84a}, L. Adamek¹⁶⁷, J. Adelman¹²¹, A. Adiguzel^{12c,ad}, S. Adorni⁵⁴, T. Adye¹⁴³, A.A. Affolder¹⁴⁵, Y. Afik¹⁶⁰, C. Agapopoulou⁶⁵, M.N. Agarar³⁸, A. Aggarwal¹¹⁹, C. Agheorghiesei^{27c}, J.A. Aguilar-Saavedra^{139f,139a,ac}, A. Ahmad³⁶, F. Ahmadov⁸⁰, W.S. Ahmed¹⁰⁴, X. Ai¹⁸, G. Aielli^{74a,74b}, S. Akatsuka⁸⁶, M. Akbiyik¹⁰⁰, T.P.A. Åkesson⁹⁷, E. Akilli⁵⁴, A.V. Akimov¹¹¹, K. Al Houry⁶⁵, G.L. Alberghi^{23b,23a}, J. Albert¹⁷⁶, M.J. Alconada Verzini¹⁶¹, S. Alderweireldt³⁶, M. Aleksa³⁶, I.N. Aleksandrov⁸⁰, C. Alexa^{27b}, T. Alexopoulos¹⁰, A. Alfonsi¹²⁰, F. Alfonsi^{23b,23a}, M. Alhroob¹²⁸, B. Ali¹⁴¹, S. Ali¹⁵⁸, M. Aliev¹⁶⁶, G. Alimonti^{69a}, C. Allaire³⁶, B.M.M. Allbrooke¹⁵⁶, B.W. Allen¹³¹, P.P. Allport²¹, A. Aloisio^{70a,70b}, F. Alonso⁸⁹, C. Alpigiani¹⁴⁸,

E. Alunno Camelia ^{74a,74b}, M. Alvarez Estevez ⁹⁹, M.G. Alviggi ^{70a,70b}, Y. Amaral Coutinho ^{81b},
A. Ambler ¹⁰⁴, L. Ambroz ¹³⁴, C. Amelung ³⁶, D. Amidei ¹⁰⁶, S.P. Amor Dos Santos ^{139a}, S. Amoroso ⁴⁶,
C.S. Amrouche ⁵⁴, F. An ⁷⁹, C. Anastopoulos ¹⁴⁹, N. Andari ¹⁴⁴, T. Andeen ¹¹, J.K. Anders ²⁰,
S.Y. Andrean ^{45a,45b}, A. Andreazza ^{69a,69b}, V. Andrei ^{61a}, C.R. Anelli ¹⁷⁶, S. Angelidakis ⁹, A. Angerami ³⁹,
A.V. Anisenkov ^{122b,122a}, A. Annovi ^{72a}, C. Antel ⁵⁴, M.T. Anthony ¹⁴⁹, E. Antipov ¹²⁹, M. Antonelli ⁵¹,
D.J.A. Antrim ¹⁸, F. Anulli ^{73a}, M. Aoki ⁸², J.A. Aparisi Pozo ¹⁷⁴, M.A. Aparo ¹⁵⁶, L. Aperio Bella ⁴⁶,
N. Aranzabal ³⁶, V. Araujo Ferraz ^{81a}, R. Araujo Pereira ^{81b}, C. Arcangeletti ⁵¹, A.T.H. Arce ⁴⁹, J-F. Arguin ¹¹⁰,
S. Argyropoulos ⁵², J.-H. Arling ⁴⁶, A.J. Armbruster ³⁶, A. Armstrong ¹⁷¹, O. Arnaez ¹⁶⁷, H. Arnold ¹²⁰,
Z.P. Arrubarrena Tame ¹¹⁴, G. Artoni ¹³⁴, H. Asada ¹¹⁷, K. Asai ¹²⁶, S. Asai ¹⁶³, T. Asawatavonvanich ¹⁶⁵,
N. Asbah ⁵⁹, E.M. Asimakopoulou ¹⁷², L. Asquith ¹⁵⁶, J. Assahsah ^{35e}, K. Assamagan ²⁹, R. Astalos ^{28a},
R.J. Atkin ^{33a}, M. Atkinson ¹⁷³, N.B. Atlay ¹⁹, H. Atmani ⁶⁵, P.A. Atmasiddha ¹⁰⁶, K. Augsten ¹⁴¹,
V.A. Austrup ¹⁸², G. Avolio ³⁶, M.K. Ayoub ^{15a}, G. Azeulos ^{110,ak}, D. Babal ^{28a}, H. Bachacou ¹⁴⁴,
K. Bachas ¹⁶², F. Backman ^{45a,45b}, P. Bagnaia ^{73a,73b}, M. Bahmani ⁸⁵, H. Bahrasemani ¹⁵², A.J. Bailey ¹⁷⁴,
V.R. Bailey ¹⁷³, J.T. Baines ¹⁴³, C. Bakalis ¹⁰, O.K. Baker ¹⁸³, P.J. Bakker ¹²⁰, E. Bakos ¹⁶, D. Bakshi Gupta ⁸,
S. Balaji ¹⁵⁷, R. Balasubramanian ¹²⁰, E.M. Baldin ^{122b,122a}, P. Balek ¹⁸⁰, F. Balli ¹⁴⁴, W.K. Balunas ¹³⁴,
J. Balz ¹⁰⁰, E. Banas ⁸⁵, M. Bandieramonte ¹³⁸, A. Bandyopadhyay ¹⁹, Sw. Banerjee ^{181,j}, L. Barak ¹⁶¹,
W.M. Barbe ³⁸, E.L. Barberio ¹⁰⁵, D. Barberis ^{55b,55a}, M. Barbero ¹⁰², G. Barbour ⁹⁵, T. Barillari ¹¹⁵,
M.-S. Barisits ³⁶, J. Barkeloo ¹³¹, T. Barklow ¹⁵³, R. Barnea ¹⁶⁰, B.M. Barnett ¹⁴³, R.M. Barnett ¹⁸,
Z. Barnovska-Blenessy ^{60a}, A. Baroncelli ^{60a}, G. Barone ²⁹, A.J. Barr ¹³⁴, L. Barranco Navarro ^{45a,45b},
F. Barreiro ⁹⁹, J. Barreiro Guimarães da Costa ^{15a}, U. Barron ¹⁶¹, S. Barsov ¹³⁷, F. Bartels ^{61a},
R. Bartoldus ¹⁵³, G. Bartolini ¹⁰², A.E. Barton ⁹⁰, P. Bartos ^{28a}, A. Basalaev ⁴⁶, A. Basan ¹⁰⁰, A. Bassalat ^{65,ah},
M.J. Basso ¹⁶⁷, R.L. Bates ⁵⁷, S. Batlamous ^{35f}, J.R. Batley ³², B. Batool ¹⁵¹, M. Battaglia ¹⁴⁵, M. Bauce ^{73a,73b},
F. Bauer ^{144,*}, P. Bauer ²⁴, H.S. Bawa ³¹, A. Bayirli ^{12c}, J.B. Beacham ⁴⁹, T. Beau ¹³⁵, P.H. Beauchemin ¹⁷⁰,
F. Becherer ⁵², P. Bechtle ²⁴, H.C. Beck ⁵³, H.P. Beck ^{20,q}, K. Becker ¹⁷⁸, C. Becot ⁴⁶, A. Beddall ^{12d},
A.J. Beddall ^{12a}, V.A. Bednyakov ⁸⁰, M. Bedognetti ¹²⁰, C.P. Bee ¹⁵⁵, T.A. Beermann ¹⁸², M. Begalli ^{81b},
M. Begel ²⁹, A. Behera ¹⁵⁵, J.K. Behr ⁴⁶, F. Beisiegel ²⁴, M. Belfkir ⁵, A.S. Bell ⁹⁵, G. Bella ¹⁶¹,
L. Bellagamba ^{23b}, A. Bellerive ³⁴, P. Bellos ⁹, K. Beloborodov ^{122b,122a}, K. Belotskiy ¹¹², N.L. Belyaev ¹¹²,
D. Benchekroun ^{35a}, N. Benekos ¹⁰, Y. Benhammou ¹⁶¹, D.P. Benjamin ⁶, M. Benoit ²⁹, J.R. Bensinger ²⁶,
S. Bentvelsen ¹²⁰, L. Beresford ¹³⁴, M. Beretta ⁵¹, D. Berge ¹⁹, E. Bergeaas Kuutmann ¹⁷², N. Berger ⁵,
B. Bergmann ¹⁴¹, L.J. Bergsten ²⁶, J. Beringer ¹⁸, S. Berlendis ⁷, G. Bernardi ¹³⁵, C. Bernius ¹⁵³,
F.U. Bernlochner ²⁴, T. Berry ⁹⁴, P. Berta ¹⁰⁰, A. Berthold ⁴⁸, I.A. Bertram ⁹⁰, O. Bessidskaia Bylund ¹⁸²,
N. Besson ¹⁴⁴, S. Bethke ¹¹⁵, A. Betti ⁴², A.J. Bevan ⁹³, J. Beyer ¹¹⁵, S. Bhatta ¹⁵⁵, D.S. Bhattacharya ¹⁷⁷,
P. Bhattarai ²⁶, V.S. Bhopatkar ⁶, R. Bi ¹³⁸, R.M. Bianchi ¹³⁸, O. Biebel ¹¹⁴, D. Biedermann ¹⁹, R. Bielski ³⁶,
K. Bierwagen ¹⁰⁰, N.V. Biesuz ^{72a,72b}, M. Biglietti ^{75a}, T.R.V. Billoud ¹⁴¹, M. Bindi ⁵³, A. Bingul ^{12d},
C. Bini ^{73a,73b}, S. Biondi ^{23b,23a}, C.J. Birch-sykes ¹⁰¹, M. Birman ¹⁸⁰, T. Bisanz ³⁶, J.P. Biswal ³, D. Biswas ^{181,j},
A. Bitadze ¹⁰¹, C. Bittrich ⁴⁸, K. Bjørke ¹³³, T. Blazek ^{28a}, I. Bloch ⁴⁶, C. Blocker ²⁶, A. Blue ⁵⁷,
U. Blumenschein ⁹³, G.J. Bobbink ¹²⁰, V.S. Bobrovnikov ^{122b,122a}, S.S. Bocchetta ⁹⁷, D. Bogavac ¹⁴,
A.G. Bogdanchikov ^{122b,122a}, C. Boehm ^{45a}, V. Boisvert ⁹⁴, P. Bokan ^{172,53}, T. Bold ^{84a}, A.E. Bolz ^{61b},
M. Bomben ¹³⁵, M. Bona ⁹³, J.S. Bonilla ¹³¹, M. Boonekamp ¹⁴⁴, C.D. Booth ⁹⁴, A.G. Borbély ⁵⁷,
H.M. Borecka-Bielska ⁹¹, L.S. Borgna ⁹⁵, A. Borisov ¹²³, G. Borissov ⁹⁰, D. Bortoletto ¹³⁴, D. Boscherini ^{23b},
M. Bosman ¹⁴, J.D. Bossio Sola ¹⁰⁴, K. Bouaouda ^{35a}, J. Boudreau ¹³⁸, E.V. Bouhova-Thacker ⁹⁰,
D. Boumediene ³⁸, A. Boveia ¹²⁷, J. Boyd ³⁶, D. Boye ^{33c}, I.R. Boyko ⁸⁰, A.J. Bozson ⁹⁴, J. Bracinik ²¹,
N. Brahimi ^{60d,60c}, G. Brandt ¹⁸², O. Brandt ³², F. Braren ⁴⁶, B. Brau ¹⁰³, J.E. Brau ¹³¹,
W.D. Breaden Madden ⁵⁷, K. Brendlinger ⁴⁶, R. Brenner ¹⁶⁰, L. Brenner ³⁶, R. Brenner ¹⁷², S. Bressler ¹⁸⁰,
B. Brickwedde ¹⁰⁰, D.L. Briglin ²¹, D. Britton ⁵⁷, D. Britzger ¹¹⁵, I. Brock ²⁴, R. Brock ¹⁰⁷, G. Brooijmans ³⁹,
W.K. Brooks ^{146d}, E. Brost ²⁹, P.A. Bruckman de Renstrom ⁸⁵, B. Brüers ⁴⁶, D. Bruncko ^{28b}, A. Bruni ^{23b},
G. Bruni ^{23b}, M. Bruschi ^{23b}, N. Bruscino ^{73a,73b}, L. Bryngemark ¹⁵³, T. Buanes ¹⁷, Q. Buat ¹⁵⁵,
P. Buchholz ¹⁵¹, A.G. Buckley ⁵⁷, I.A. Budagov ⁸⁰, M.K. Bugge ¹³³, O. Bulekov ¹¹², B.A. Bullard ⁵⁹,
T.J. Burch ¹²¹, S. Burdin ⁹¹, C.D. Burgard ¹²⁰, A.M. Burger ¹²⁹, B. Burghgrave ⁸, J.T.P. Burr ⁴⁶, C.D. Burton ¹¹,
J.C. Burzynski ¹⁰³, V. Büscher ¹⁰⁰, E. Buschmann ⁵³, P.J. Bussey ⁵⁷, J.M. Butler ²⁵, C.M. Buttar ⁵⁷,
J.M. Butterworth ⁹⁵, P. Butti ³⁶, W. Buttinger ¹⁴³, C.J. Buxo Vazquez ¹⁰⁷, A. Buzatu ¹⁵⁸,
A.R. Buzykaev ^{122b,122a}, G. Cabras ^{23b,23a}, S. Cabrera Urbán ¹⁷⁴, D. Caforio ⁵⁶, H. Cai ¹³⁸, V.M.M. Cairo ¹⁵³,
O. Cakir ^{4a}, N. Calace ³⁶, P. Calafiura ¹⁸, G. Calderini ¹³⁵, P. Calfayan ⁶⁶, G. Callea ⁵⁷, L.P. Caloba ^{81b},

A. Caltabiano^{74a,74b}, S. Calvente Lopez⁹⁹, D. Calvet³⁸, S. Calvet³⁸, T.P. Calvet¹⁰², M. Calvetti^{72a,72b}, R. Camacho Toro¹³⁵, S. Camarda³⁶, D. Camarero Munoz⁹⁹, P. Camarri^{74a,74b}, M.T. Camerlingo^{75a,75b}, D. Cameron¹³³, C. Camincher³⁶, S. Campana³⁶, M. Campanelli⁹⁵, A. Camplani⁴⁰, V. Canale^{70a,70b}, A. Canesse¹⁰⁴, M. Cano Bret⁷⁸, J. Cantero¹²⁹, T. Cao¹⁶¹, Y. Cao¹⁷³, M. Capua^{41b,41a}, R. Cardarelli^{74a}, F. Cardillo¹⁷⁴, G. Carducci^{41b,41a}, I. Carli¹⁴², T. Carli³⁶, G. Carlino^{70a}, B.T. Carlson¹³⁸, E.M. Carlson^{176,168a}, L. Carminati^{69a,69b}, R.M.D. Carney¹⁵³, S. Caron¹¹⁹, E. Carquin^{146d}, S. Carrá⁴⁶, G. Carratta^{23b,23a}, J.W.S. Carter¹⁶⁷, T.M. Carter⁵⁰, M.P. Casado^{14,g}, A.F. Casha¹⁶⁷, E.G. Castiglia¹⁸³, F.L. Castillo¹⁷⁴, L. Castillo Garcia¹⁴, V. Castillo Gimenez¹⁷⁴, N.F. Castro^{139a,139e}, A. Catinaccio³⁶, J.R. Catmore¹³³, A. Cattai³⁶, V. Cavaliere²⁹, V. Cavasinni^{72a,72b}, E. Celebi^{12b}, F. Celli¹³⁴, K. Cerny¹³⁰, A.S. Cerqueira^{81a}, A. Cerri¹⁵⁶, L. Cerrito^{74a,74b}, F. Cerutti¹⁸, A. Cervelli^{23b,23a}, S.A. Cetin^{12b}, Z. Chadi^{35a}, D. Chakraborty¹²¹, J. Chan¹⁸¹, W.S. Chan¹²⁰, W.Y. Chan⁹¹, J.D. Chapman³², B. Chargeishvili^{159b}, D.G. Charlton²¹, T.P. Charman⁹³, M. Chatterjee²⁰, C.C. Chau³⁴, S. Che¹²⁷, S. Chekanov⁶, S.V. Chekulaev^{168a}, G.A. Chelkov^{80,af}, B. Chen⁷⁹, C. Chen^{60a}, C.H. Chen⁷⁹, H. Chen^{15c}, H. Chen²⁹, J. Chen^{60a}, J. Chen³⁹, J. Chen²⁶, S. Chen¹³⁶, S.J. Chen^{15c}, X. Chen^{15b}, Y. Chen^{60a}, Y.-H. Chen⁴⁶, H.C. Cheng^{63a}, H.J. Cheng^{15a}, A. Cheplakov⁸⁰, E. Cheremushkina¹²³, R. Cherkaoui El Moursli^{35f}, E. Cheu⁷, K. Cheung⁶⁴, T.J.A. Chevaléras¹⁴⁴, L. Chevalier¹⁴⁴, V. Chiarella⁵¹, G. Chiarelli^{72a}, G. Chiodini^{68a}, A.S. Chisholm²¹, A. Chitan^{27b}, I. Chiu¹⁶³, Y.H. Chiu¹⁷⁶, M.V. Chizhov⁸⁰, K. Choi¹¹, A.R. Chomont^{73a,73b}, Y. Chou¹⁰³, Y.S. Chow¹²⁰, L.D. Christopher^{33e}, M.C. Chu^{63a}, X. Chu^{15a,15d}, J. Chudoba¹⁴⁰, J.J. Chwastowski⁸⁵, L. Chytka¹³⁰, D. Cieri¹¹⁵, K.M. Ciesla⁸⁵, V. Cindro⁹², I.A. Cioară^{27b}, A. Ciocio¹⁸, F. Ciotto^{70a,70b}, Z.H. Citron^{180,k}, M. Citterio^{69a}, D.A. Ciubotaru^{27b}, B.M. Ciungu¹⁶⁷, A. Clark⁵⁴, P.J. Clark⁵⁰, S.E. Clawson¹⁰¹, C. Clement^{45a,45b}, L. Clissa^{23b,23a}, Y. Coadou¹⁰², M. Cobal^{67a,67c}, A. Coccaro^{55b}, J. Cochran⁷⁹, R. Coelho Lopes De Sa¹⁰³, H. Cohen¹⁶¹, A.E.C. Coimbra³⁶, B. Cole³⁹, A.P. Colijn¹²⁰, J. Collot⁵⁸, P. Conde Muiño^{139a,139h}, S.H. Connell^{33c}, I.A. Connelly⁵⁷, S. Constantinescu^{27b}, F. Conventi^{70a,al}, A.M. Cooper-Sarkar¹³⁴, F. Cormier¹⁷⁵, K.J.R. Cormier¹⁶⁷, L.D. Corpe⁹⁵, M. Corradi^{73a,73b}, E.E. Corrigan⁹⁷, F. Corriveau^{104,aa}, M.J. Costa¹⁷⁴, F. Costanza⁵, D. Costanzo¹⁴⁹, G. Cowan⁹⁴, J.W. Cowley³², J. Crane¹⁰¹, K. Cranmer¹²⁵, R.A. Creager¹³⁶, S. Crépe-Renaudin⁵⁸, F. Crescioli¹³⁵, M. Cristinziani²⁴, V. Croft¹⁷⁰, G. Crosetti^{41b,41a}, A. Cueto⁵, T. Cuhadar Donszelmann¹⁷¹, H. Cui^{15a,15d}, A.R. Cukierman¹⁵³, W.R. Cunningham⁵⁷, S. Czekierda⁸⁵, P. Czodrowski³⁶, M.M. Czurylo^{61b}, M.J. Da Cunha Sargedas De Sousa^{60b}, J.V. Da Fonseca Pinto^{81b}, C. Da Via¹⁰¹, W. Dabrowski^{84a}, F. Dachs³⁶, T. Dado⁴⁷, S. Dahbi^{33e}, T. Dai¹⁰⁶, C. Dallapiccola¹⁰³, M. Dam⁴⁰, G. D'amen²⁹, V. D'Amico^{75a,75b}, J. Damp¹⁰⁰, J.R. Dandoy¹³⁶, M.F. Daneri³⁰, M. Danninger¹⁵², V. Dao³⁶, G. Darbo^{55b}, O. Dartsis⁵, A. Dattagupta¹³¹, T. Daubney⁴⁶, S. D'Auria^{69a,69b}, C. David^{168b}, T. Davidek¹⁴², D.R. Davis⁴⁹, I. Dawson¹⁴⁹, K. De⁸, R. De Asmundis^{70a}, M. De Beurs¹²⁰, S. De Castro^{23b,23a}, N. De Groot¹¹⁹, P. de Jong¹²⁰, H. De la Torre¹⁰⁷, A. De Maria^{15c}, D. De Pedis^{73a}, A. De Salvo^{73a}, U. De Sanctis^{74a,74b}, M. De Santis^{74a,74b}, A. De Santo¹⁵⁶, J.B. De Vivie De Regie⁶⁵, D.V. Dedovich⁸⁰, A.M. Deiana⁴², J. Del Peso⁹⁹, Y. Delabat Diaz⁴⁶, D. Delgove⁶⁵, F. Deliot¹⁴⁴, C.M. Delitzsch⁷, M. Della Pietra^{70a,70b}, D. Della Volpe⁵⁴, A. Dell'Acqua³⁶, L. Dell'Asta^{74a,74b}, M. Delmastro⁵, C. Delporte⁶⁵, P.A. Delsart⁵⁸, S. Demers¹⁸³, M. Demichev⁸⁰, G. Demontigny¹¹⁰, S.P. Denisov¹²³, L. D'Eramo¹²¹, D. Derendarz⁸⁵, J.E. Derkaoui^{35e}, F. Derue¹³⁵, P. Dervan⁹¹, K. Desch²⁴, K. Dette¹⁶⁷, C. Deutsch²⁴, M.R. Devesa³⁰, P.O. Deviveiros³⁶, F.A. Di Bello^{73a,73b}, A. Di Ciaccio^{74a,74b}, L. Di Ciaccio⁵, W.K. Di Clemente¹³⁶, C. Di Donato^{70a,70b}, A. Di Girolamo³⁶, G. Di Gregorio^{72a,72b}, A. Di Luca^{76a,76b}, B. Di Micco^{75a,75b}, R. Di Nardo^{75a,75b}, K.F. Di Petrillo⁵⁹, R. Di Sipio¹⁶⁷, C. Diaconu¹⁰², F.A. Dias¹²⁰, T. Dias Do Vale^{139a}, M.A. Diaz^{146a}, F.G. Diaz Capriles²⁴, J. Dickinson¹⁸, M. Didenko¹⁶⁶, E.B. Diehl¹⁰⁶, J. Dietrich¹⁹, S. Díez Cornell⁴⁶, C. Diez Pardos¹⁵¹, A. Dimitrievska¹⁸, W. Ding^{15b}, J. Dingfelder²⁴, S.J. Dittmeier^{61b}, F. Dittus³⁶, F. Djama¹⁰², T. Djobava^{159b}, J.I. Djuvsland¹⁷, M.A.B. Do Vale¹⁴⁷, M. Dobre^{27b}, D. Dodsworth²⁶, C. Doglioni⁹⁷, J. Dolejsi¹⁴², Z. Dolezal¹⁴², M. Donadelli^{81c}, B. Dong^{60c}, J. Donini³⁸, A. D'onofrio^{15c}, M. D'Onofrio⁹¹, J. Dopke¹⁴³, A. Doria^{70a}, M.T. Dova⁸⁹, A.T. Doyle⁵⁷, E. Drechsler¹⁵², E. Dreyer¹⁵², T. Dreyer⁵³, A.S. Drobac¹⁷⁰, D. Du^{60b}, T.A. du Pree¹²⁰, Y. Duan^{60d}, F. Dubinin¹¹¹, M. Dubovsky^{28a}, A. Dubreuil⁵⁴, E. Duchovni¹⁸⁰, G. Duckeck¹¹⁴, O.A. Ducu^{36,27b}, D. Duda¹¹⁵, A. Dudarev³⁶, A.C. Dudder¹⁰⁰, E.M. Duffield¹⁸, M. D'uffizi¹⁰¹, L. Duflot⁶⁵, M. Dührssen³⁶, C. Dülsen¹⁸², M. Dumancic¹⁸⁰, A.E. Dumitriu^{27b}, M. Dunford^{61a}, S. Dungs⁴⁷, A. Duperrin¹⁰², H. Duran Yildiz^{4a}, M. Düren⁵⁶, A. Durglishvili^{159b}, D. Duschinger⁴⁸, B. Dutta⁴⁶, D. Duvnjak¹, G.I. Dyckes¹³⁶, M. Dyndal³⁶, S. Dysch¹⁰¹, B.S. Dziedzic⁸⁵, M.G. Eggleston⁴⁹, T. Eifert⁸, G. Eigen¹⁷,

K. Einsweiler¹⁸, T. Ekelof¹⁷², H. El Jarrari^{35f}, V. Ellajosyula¹⁷², M. Ellert¹⁷², F. Ellinghaus¹⁸²,
 A.A. Elliot⁹³, N. Ellis³⁶, J. Elmsheuser²⁹, M. Elsing³⁶, D. Emeliyanov¹⁴³, A. Emerman³⁹, Y. Enari¹⁶³,
 M.B. Epland⁴⁹, J. Erdmann⁴⁷, A. Ereditato²⁰, P.A. Erland⁸⁵, M. Errenst¹⁸², M. Escalier⁶⁵, C. Escobar¹⁷⁴,
 O. Estrada Pastor¹⁷⁴, E. Etzion¹⁶¹, G. Evans^{139a}, H. Evans⁶⁶, M.O. Evans¹⁵⁶, A. Ezhilov¹³⁷, F. Fabbri⁵⁷,
 L. Fabbri^{23b,23a}, V. Fabiani¹¹⁹, G. Facini¹⁷⁸, R.M. Fakhruddinov¹²³, S. Falciano^{73a}, P.J. Falke²⁴, S. Falke³⁶,
 J. Faltova¹⁴², Y. Fang^{15a}, Y. Fang^{15a}, G. Fanourakis⁴⁴, M. Fanti^{69a,69b}, M. Faraj^{67a,67c}, A. Farbin⁸,
 A. Farilla^{75a}, E.M. Farina^{71a,71b}, T. Farooque¹⁰⁷, S.M. Farrington⁵⁰, P. Farthouat³⁶, F. Fassi^{35f},
 P. Fassnacht³⁶, D. Fassouliotis⁹, M. Faucci Giannelli⁵⁰, W.J. Fawcett³², L. Fayard⁶⁵, O.L. Fedin^{137,p},
 W. Fedorko¹⁷⁵, A. Fehr²⁰, M. Feickert¹⁷³, L. Feligioni¹⁰², A. Fell¹⁴⁹, C. Feng^{60b}, M. Feng⁴⁹,
 M.J. Fenton¹⁷¹, A.B. Fenyuk¹²³, S.W. Ferguson⁴³, J. Ferrando⁴⁶, A. Ferrari¹⁷², P. Ferrari¹²⁰, R. Ferrari^{71a},
 D.E. Ferreira de Lima^{61b}, A. Ferrer¹⁷⁴, D. Ferrere⁵⁴, C. Ferretti¹⁰⁶, F. Fiedler¹⁰⁰, A. Filipčič⁹²,
 F. Filthaut¹¹⁹, K.D. Finelli²⁵, M.C.N. Fiolhais^{139a,139c,a}, L. Fiorini¹⁷⁴, F. Fischer¹¹⁴, J. Fischer¹⁰⁰,
 W.C. Fisher¹⁰⁷, T. Fitschen²¹, I. Fleck¹⁵¹, P. Fleischmann¹⁰⁶, T. Flick¹⁸², B.M. Flierl¹¹⁴, L. Flores¹³⁶,
 L.R. Flores Castillo^{63a}, F.M. Follega^{76a,76b}, N. Fomin¹⁷, J.H. Foo¹⁶⁷, G.T. Forcolin^{76a,76b}, B.C. Forland⁶⁶,
 A. Formica¹⁴⁴, F.A. Förster¹⁴, A.C. Forti¹⁰¹, E. Fortin¹⁰², M.G. Foti¹³⁴, D. Fournier⁶⁵, H. Fox⁹⁰,
 P. Francavilla^{72a,72b}, S. Francescato^{73a,73b}, M. Franchini^{23b,23a}, S. Franchino^{61a}, D. Francis³⁶, L. Franco⁵,
 L. Franconi²⁰, M. Franklin⁵⁹, G. Frattari^{73a,73b}, A.N. Fray⁹³, P.M. Freeman²¹, B. Freund¹¹⁰,
 W.S. Freund^{81b}, E.M. Freundlich⁴⁷, D.C. Frizzell¹²⁸, D. Froidevaux³⁶, J.A. Frost¹³⁴, M. Fujimoto¹²⁶,
 C. Fukunaga¹⁶⁴, E. Fullana Torregrosa¹⁷⁴, T. Fusayasu¹¹⁶, J. Fuster¹⁷⁴, A. Gabrielli^{23b,23a}, A. Gabrielli³⁶,
 S. Gadatsch⁵⁴, P. Gadow¹¹⁵, G. Gagliardi^{55b,55a}, L.G. Gagnon¹¹⁰, G.E. Gallardo¹³⁴, E.J. Gallas¹³⁴,
 B.J. Gallop¹⁴³, R. Gamboa Goni⁹³, K.K. Gan¹²⁷, S. Ganguly¹⁸⁰, J. Gao^{60a}, Y. Gao⁵⁰, Y.S. Gao^{31,m},
 F.M. Garay Walls^{146a}, C. García¹⁷⁴, J.E. García Navarro¹⁷⁴, J.A. García Pascual^{15a}, C. Garcia-Argos⁵²,
 M. Garcia-Sciveres¹⁸, R.W. Gardner³⁷, N. Garelli¹⁵³, S. Gargiulo⁵², C.A. Garner¹⁶⁷, V. Garonne¹³³,
 S.J. Gasirowski¹⁴⁸, P. Gaspar^{81b}, A. Gaudiello^{55b,55a}, G. Gaudio^{71a}, P. Gauzzi^{73a,73b}, I.L. Gavrilenko¹¹¹,
 A. Gavriluk¹²⁴, C. Gay¹⁷⁵, G. Gaycken⁴⁶, E.N. Gazis¹⁰, A.A. Geanta^{27b}, C.M. Gee¹⁴⁵, C.N.P. Gee¹⁴³,
 J. Geisen⁹⁷, M. Geisen¹⁰⁰, C. Gemme^{55b}, M.H. Genest⁵⁸, C. Geng¹⁰⁶, S. Gentile^{73a,73b}, S. George⁹⁴,
 T. Geralis⁴⁴, L.O. Gerlach⁵³, P. Gessinger-Befurt¹⁰⁰, G. Gessner⁴⁷, M. Ghasemi Bostanabad¹⁷⁶,
 M. Ghneimat¹⁵¹, A. Ghosh⁶⁵, A. Ghosh⁷⁸, B. Giacobbe^{23b}, S. Giagu^{73a,73b}, N. Giangiacomi¹⁶⁷,
 P. Giannetti^{72a}, A. Giannini^{70a,70b}, G. Giannini¹⁴, S.M. Gibson⁹⁴, M. Gignac¹⁴⁵, D.T. Gil^{84b}, B.J. Gilbert³⁹,
 D. Gillberg³⁴, G. Gilles¹⁸², N.E.K. Gillwald⁴⁶, D.M. Gingrich^{3,ak}, M.P. Giordani^{67a,67c}, P.F. Giraud¹⁴⁴,
 G. Giugliarelli^{67a,67c}, D. Giugni^{69a}, F. Giuli^{74a,74b}, S. Gkaitatzis¹⁶², I. Gkialas^{9,h}, E.L. Gkougkousis¹⁴,
 P. Gkoutoumis¹⁰, L.K. Gladilin¹¹³, C. Glasman⁹⁹, J. Glatzer¹⁴, P.C.F. Glaysheer⁴⁶, A. Glazov⁴⁶,
 G.R. Gledhill¹³¹, I. Gnesi^{41b,c}, M. Goblirsch-Kolb²⁶, D. Godin¹¹⁰, S. Goldfarb¹⁰⁵, T. Golling⁵⁴,
 D. Golubkov¹²³, A. Gomes^{139a,139b}, R. Goncalves Gama⁵³, R. Gonçalves^{139a,139c}, G. Gonella¹³¹,
 L. Gonella²¹, A. Gongadze⁸⁰, F. Gonnella²¹, J.L. Gonski³⁹, S. González de la Hoz¹⁷⁴,
 S. Gonzalez Fernandez¹⁴, R. Gonzalez Lopez⁹¹, C. Gonzalez Renteria¹⁸, R. Gonzalez Suarez¹⁷²,
 S. Gonzalez-Sevilla⁵⁴, G.R. Gonzalvo Rodriguez¹⁷⁴, L. Goossens³⁶, N.A. Gorasia²¹, P.A. Gorbounov¹²⁴,
 H.A. Gordon²⁹, B. Gorini³⁶, E. Gorini^{68a,68b}, A. Gorišek⁹², A.T. Goshaw⁴⁹, M.I. Gostkin⁸⁰,
 C.A. Gottardo¹¹⁹, M. Gouighri^{35b}, A.G. Goussiou¹⁴⁸, N. Govender^{33c}, C. Goy⁵, I. Grabowska-Bold^{84a},
 E.C. Graham⁹¹, J. Gramling¹⁷¹, E. Gramstad¹³³, S. Grancagnolo¹⁹, M. Grandi¹⁵⁶, V. Gratchev¹³⁷,
 P.M. Gravila^{27f}, F.G. Gravili^{68a,68b}, C. Gray⁵⁷, H.M. Gray¹⁸, C. Grefe²⁴, K. Gregersen⁹⁷, I.M. Gregor⁴⁶,
 P. Grenier¹⁵³, K. Grevtsov⁴⁶, C. Grieco¹⁴, N.A. Grieser¹²⁸, A.A. Grillo¹⁴⁵, K. Grimm^{31,l}, S. Grinstein^{14,w},
 J.-F. Grivaz⁶⁵, S. Groh¹⁰⁰, E. Gross¹⁸⁰, J. Grosse-Knetter⁵³, Z.J. Grout⁹⁵, C. Grud¹⁰⁶, A. Grummer¹¹⁸,
 J.C. Grundy¹³⁴, L. Guan¹⁰⁶, W. Guan¹⁸¹, C. Gubbels¹⁷⁵, J. Guenther⁷⁷, A. Guerguichon⁶⁵,
 J.G.R. Guerrero Rojas¹⁷⁴, F. Guescini¹¹⁵, D. Guest⁷⁷, R. Gugel¹⁰⁰, A. Guida⁴⁶, T. Guillemin⁵,
 S. Guindon³⁶, J. Guo^{60c}, W. Guo¹⁰⁶, Y. Guo^{60a}, Z. Guo¹⁰², R. Gupta⁴⁶, S. Gurbuz^{12c}, G. Gustavino¹²⁸,
 M. Guth⁵², P. Gutierrez¹²⁸, C. Gutsche⁹⁵, C. Guyot¹⁴⁴, C. Gwenlan¹³⁴, C.B. Gwilliam⁹¹,
 E.S. Haaland¹³³, A. Haas¹²⁵, C. Haber¹⁸, H.K. Hadavand⁸, A. Hadeef¹⁰⁰, M. Haleem¹⁷⁷, J. Haley¹²⁹,
 J.J. Hall¹⁴⁹, G. Halladjian¹⁰⁷, G.D. Hallewell¹⁰², K. Hamano¹⁷⁶, H. Hamdaoui^{35f}, M. Hamer²⁴,
 G.N. Hamity⁵⁰, K. Han^{60a}, L. Han^{15c}, L. Han^{60a}, S. Han¹⁸, Y.F. Han¹⁶⁷, K. Hanagaki^{82,u}, M. Hance¹⁴⁵,
 D.M. Handl¹¹⁴, M.D. Hank³⁷, R. Hankache¹³⁵, E. Hansen⁹⁷, J.B. Hansen⁴⁰, J.D. Hansen⁴⁰, M.C. Hansen²⁴,
 P.H. Hansen⁴⁰, E.C. Hanson¹⁰¹, K. Hara¹⁶⁹, T. Harenberg¹⁸², S. Harkusha¹⁰⁸, P.F. Harrison¹⁷⁸,
 N.M. Hartman¹⁵³, N.M. Hartmann¹¹⁴, Y. Hasegawa¹⁵⁰, A. Hasib⁵⁰, S. Hassani¹⁴⁴, S. Haug²⁰,

R. Hauser¹⁰⁷, M. Havranek¹⁴¹, C.M. Hawkes²¹, R.J. Hawkins³⁶, S. Hayashida¹¹⁷, D. Hayden¹⁰⁷, C. Hayes¹⁰⁶, R.L. Hayes¹⁷⁵, C.P. Hays¹³⁴, J.M. Hays⁹³, H.S. Hayward⁹¹, S.J. Haywood¹⁴³, F. He^{60a}, Y. He¹⁶⁵, M.P. Heath⁵⁰, V. Hedberg⁹⁷, A.L. Heggelund¹³³, N.D. Hehir⁹³, C. Heidegger⁵², K.K. Heidegger⁵², W.D. Heidorn⁷⁹, J. Heilman³⁴, S. Heim⁴⁶, T. Heim¹⁸, B. Heinemann^{46,ai}, J.G. Heinlein¹³⁶, J.J. Heinrich¹³¹, L. Heinrich³⁶, J. Hejbal¹⁴⁰, L. Helary⁴⁶, A. Held¹²⁵, S. Hellesund¹³³, C.M. Helling¹⁴⁵, S. Hellman^{45a,45b}, C. Helsens³⁶, R.C.W. Henderson⁹⁰, L. Henkelmann³², A.M. Henriques Correia³⁶, H. Herde²⁶, Y. Hernández Jiménez^{33e}, H. Herr¹⁰⁰, M.G. Herrmann¹¹⁴, T. Herrmann⁴⁸, G. Herten⁵², R. Hertenberger¹¹⁴, L. Hervas³⁶, G.G. Hesketh⁹⁵, N.P. Hessey^{168a}, H. Hibi⁸³, S. Higashino⁸², E. Higón-Rodríguez¹⁷⁴, K. Hildebrand³⁷, J.C. Hill³², K.K. Hill²⁹, K.H. Hiller⁴⁶, S.J. Hillier²¹, M. Hils⁴⁸, I. Hinchliffe¹⁸, F. Hinterkeuser²⁴, M. Hirose¹³², S. Hirose¹⁶⁹, D. Hirschbuehl¹⁸², B. Hiti⁹², O. Hladik¹⁴⁰, J. Hobbs¹⁵⁵, R. Hobincu^{27e}, N. Hod¹⁸⁰, M.C. Hodgkinson¹⁴⁹, A. Hoecker³⁶, D. Hohn⁵², D. Hohov⁶⁵, T. Holm²⁴, T.R. Holmes³⁷, M. Holzbock¹¹⁵, L.B.A.H. Hommels³², T.M. Hong¹³⁸, J.C. Honig⁵², A. Hönle¹¹⁵, B.H. Hooberman¹⁷³, W.H. Hopkins⁶, Y. Horii¹¹⁷, P. Horn⁴⁸, L.A. Horyn³⁷, S. Hou¹⁵⁸, A. Hoummada^{35a}, J. Howarth⁵⁷, J. Hoya⁸⁹, M. Hrabovsky¹³⁰, J. Hrivnac⁶⁵, A. Hrynevich¹⁰⁹, T. Hryn'ova⁵, P.J. Hsu⁶⁴, S.-C. Hsu¹⁴⁸, Q. Hu³⁹, S. Hu^{60c}, Y.F. Hu^{15a,15d,am}, D.P. Huang⁹⁵, X. Huang^{15c}, Y. Huang^{60a}, Y. Huang^{15a}, Z. Hubacek¹⁴¹, F. Hubaut¹⁰², M. Huebner²⁴, F. Huetting²⁴, T.B. Huffman¹³⁴, M. Huhtinen³⁶, R. Hulsken⁵⁸, R.F.H. Hunter³⁴, N. Huseynov^{80,ab}, J. Huston¹⁰⁷, J. Huth⁵⁹, R. Hyneman¹⁵³, S. Hyrych^{28a}, G. Iacobucci⁵⁴, G. Iakovidis²⁹, I. Ibragimov¹⁵¹, L. Iconomidou-Fayard⁶⁵, P. Iengo³⁶, R. Ignazzi⁴⁰, R. Iguchi¹⁶³, T. Iizawa⁵⁴, Y. Ikegami⁸², M. Ikeno⁸², N. Ilic^{119,167,aa}, F. Iltzsche⁴⁸, H. Imam^{35a}, G. Introzzi^{71a,71b}, M. Iodice^{75a}, K. Iordanidou^{168a}, V. Ippolito^{73a,73b}, M.F. Isacson¹⁷², M. Ishino¹⁶³, W. Islam¹²⁹, C. Issever^{19,46}, S. Istin¹⁶⁰, J.M. Iturbe Ponce^{63a}, R. Iuppa^{76a,76b}, A. Ivina¹⁸⁰, J.M. Izen⁴³, V. Izzo^{70a}, P. Jacka¹⁴⁰, P. Jackson¹, R.M. Jacobs⁴⁶, B.P. Jaeger¹⁵², V. Jain², G. Jäkel¹⁸², K.B. Jakobi¹⁰⁰, K. Jakobs⁵², T. Jakoubek¹⁸⁰, J. Jamieson⁵⁷, K.W. Janas^{84a}, R. Jansky⁵⁴, M. Janus⁵³, P.A. Janus^{84a}, G. Jarlskog⁹⁷, A.E. Jaspán⁹¹, N. Javadov^{80,ab}, T. Javůrek³⁶, M. Javurkova¹⁰³, F. Jeanneau¹⁴⁴, L. Jeanty¹³¹, J. Jejelava^{159a}, P. Jenni^{52,d}, N. Jeong⁴⁶, S. Jézéquel⁵, J. Jia¹⁵⁵, Z. Jia^{15c}, H. Jiang⁷⁹, Y. Jiang^{60a}, Z. Jiang¹⁵³, S. Jiggins⁵², F.A. Jimenez Morales³⁸, J. Jimenez Pena¹¹⁵, S. Jin^{15c}, A. Jinaru^{27b}, O. Jinnouchi¹⁶⁵, H. Jivan^{33e}, P. Johansson¹⁴⁹, K.A. Johns⁷, C.A. Johnson⁶⁶, E. Jones¹⁷⁸, R.W.L. Jones⁹⁰, S.D. Jones¹⁵⁶, T.J. Jones⁹¹, J. Jovicevic³⁶, X. Ju¹⁸, J.J. Jungeburth¹¹⁵, A. Juste Rozas^{14,w}, A. Kaczmarska⁸⁵, M. Kado^{73a,73b}, H. Kagan¹²⁷, M. Kagan¹⁵³, A. Kahn³⁹, C. Kahra¹⁰⁰, T. Kaji¹⁷⁹, E. Kajomovitz¹⁶⁰, C.W. Kalderon²⁹, A. Kaluza¹⁰⁰, A. Kamenshchikov¹²³, M. Kaneda¹⁶³, N.J. Kang¹⁴⁵, S. Kang⁷⁹, Y. Kano¹¹⁷, J. Kanzaki⁸², L.S. Kaplan¹⁸¹, D. Kar^{33e}, K. Karava¹³⁴, M.J. Kareem^{168b}, I. Karkanas¹⁶², S.N. Karpov⁸⁰, Z.M. Karpova⁸⁰, V. Kartvelishvili⁹⁰, A.N. Karyukhin¹²³, E. Kasimi¹⁶², A. Kastanas^{45a,45b}, C. Kato^{60d}, J. Katzy⁴⁶, K. Kawade¹⁵⁰, K. Kawagoe⁸⁸, T. Kawaguchi¹¹⁷, T. Kawamoto¹⁴⁴, G. Kawamura⁵³, E.F. Kay¹⁷⁶, F.I. Kaya¹⁷⁰, S. Kazakos¹⁴, V.F. Kazanin^{122b,122a}, J.M. Keaveney^{33a}, R. Keeler¹⁷⁶, J.S. Keller³⁴, E. Kellermann⁹⁷, D. Kelsey¹⁵⁶, J.J. Kempster²¹, J. Kendrick²¹, K.E. Kennedy³⁹, O. Kepka¹⁴⁰, S. Kersten¹⁸², B.P. Kerševan⁹², S. Ketabchi Haghghat¹⁶⁷, F. Khalil-Zada¹³, M. Khandoga¹⁴⁴, A. Khanov¹²⁹, A.G. Kharlamov^{122b,122a}, T. Kharlamova^{122b,122a}, E.E. Khoda¹⁷⁵, T.J. Khoo⁷⁷, G. Khorauli¹⁷⁷, E. Khramov⁸⁰, J. Khubua^{159b}, S. Kido⁸³, M. Kiehn³⁶, E. Kim¹⁶⁵, Y.K. Kim³⁷, N. Kimura⁹⁵, A. Kirchhoff⁵³, D. Kirchmeier⁴⁸, J. Kirk¹⁴³, A.E. Kiryunin¹¹⁵, T. Kishimoto¹⁶³, D.P. Kisliuk¹⁶⁷, V. Kitali⁴⁶, C. Kitsaki¹⁰, O. Kivernyk²⁴, T. Klapdor-Kleingrothaus⁵², M. Klassen^{61a}, C. Klein³⁴, M.H. Klein¹⁰⁶, M. Klein⁹¹, U. Klein⁹¹, K. Kleinknecht¹⁰⁰, P. Klimek³⁶, A. Klimentov²⁹, F. Klimpel³⁶, T. Klingl²⁴, T. Klioutchnikova³⁶, F.F. Klitzner¹¹⁴, P. Kluit¹²⁰, S. Kluth¹¹⁵, E. Kneringer⁷⁷, E.B.F.G. Knoop¹⁰², A. Knue⁵², D. Kobayashi⁸⁸, M. Kobel⁴⁸, M. Kocian¹⁵³, T. Kodama¹⁶³, P. Kodys¹⁴², D.M. Koeck¹⁵⁶, P.T. Koenig²⁴, T. Koffas³⁴, N.M. Köhler³⁶, M. Kolb¹⁴⁴, I. Koletsou⁵, T. Komarek¹³⁰, T. Kondo⁸², K. Köneke⁵², A.X.Y. Kong¹, A.C. König¹¹⁹, T. Kono¹²⁶, V. Konstantinides⁹⁵, N. Konstantinidis⁹⁵, B. Konya⁹⁷, R. Kopeliansky⁶⁶, S. Koperny^{84a}, K. Korcyl⁸⁵, K. Kordas¹⁶², G. Koren¹⁶¹, A. Korn⁹⁵, I. Korolkov¹⁴, E.V. Korolkova¹⁴⁹, N. Korotkova¹¹³, O. Kortner¹¹⁵, S. Kortner¹¹⁵, V.V. Kostyukhin^{149,166}, A. Kotskechagia⁶⁵, A. Kotwal⁴⁹, A. Koulouris¹⁰, A. Kourkoumeli-Charalampidi^{71a,71b}, C. Kourkoumelis⁹, E. Kourlitis⁶, V. Kouskoura²⁹, R. Kowalewski¹⁷⁶, W. Kozanecki¹⁰¹, A.S. Kozhin¹²³, V.A. Kramarenko¹¹³, G. Kramberger⁹², D. Krasnopevtsev^{60a}, M.W. Krasny¹³⁵, A. Krasznahorkay³⁶, D. Krauss¹¹⁵, J.A. Kremer¹⁰⁰, J. Kretzschmar⁹¹, K. Kreul¹⁹, P. Krieger¹⁶⁷, F. Krieter¹¹⁴, S. Krishnamurthy¹⁰³, A. Krishnan^{61b}, M. Krivos¹⁴², K. Krizka¹⁸, K. Kroeninger⁴⁷, H. Kroha¹¹⁵, J. Kroll¹⁴⁰, J. Kroll¹³⁶, K.S. Krowpman¹⁰⁷, U. Kruchonak⁸⁰, H. Krüger²⁴,

N. Krumnack⁷⁹, M.C. Kruse⁴⁹, J.A. Krzysiak⁸⁵, A. Kubota¹⁶⁵, O. Kuchinskaia¹⁶⁶, S. Kuday^{4b}, D. Kuechler⁴⁶, J.T. Kuechler⁴⁶, S. Kuehn³⁶, T. Kuhl⁴⁶, V. Kukhtin⁸⁰, Y. Kulchitsky^{108,ae}, S. Kuleshov^{146b}, Y.P. Kulinich¹⁷³, M. Kuna⁵⁸, A. Kupco¹⁴⁰, T. Kupfer⁴⁷, O. Kuprash⁵², H. Kurashige⁸³, L.L. Kurchaninov^{168a}, Y.A. Kurochkin¹⁰⁸, A. Kurova¹¹², M.G. Kurth^{15a,15d}, E.S. Kuwertz³⁶, M. Kuze¹⁶⁵, A.K. Kvam¹⁴⁸, J. Kvita¹³⁰, T. Kwan¹⁰⁴, C. Lacasta¹⁷⁴, F. Lacava^{73a,73b}, D.P.J. Lack¹⁰¹, H. Lacker¹⁹, D. Lacour¹³⁵, E. Ladygin⁸⁰, R. Lafaye⁵, B. Laforge¹³⁵, T. Lagouri^{146c}, S. Lai⁵³, I.K. Lakomic^{84a}, J.E. Lambert¹²⁸, S. Lammers⁶⁶, W. Lampl⁷, C. Lampoudis¹⁶², E. Lançon²⁹, U. Landgraf⁵², M.P.J. Landon⁹³, V.S. Lang⁵², J.C. Lange⁵³, R.J. Langenberg¹⁰³, A.J. Lankford¹⁷¹, F. Lanni²⁹, K. Lantzsch²⁴, A. Lanza^{71a}, A. Lapertosa^{55b,55a}, J.F. Laporte¹⁴⁴, T. Lari^{69a}, F. Lasagni Manghi^{23b,23a}, M. Lassnig³⁶, V. Latonova¹⁴⁰, T.S. Lau^{63a}, A. Laudrain¹⁰⁰, A. Laurier³⁴, M. Lavorgna^{70a,70b}, S.D. Lawlor⁹⁴, M. Lazzaroni^{69a,69b}, B. Le¹⁰¹, E. Le Guirriec¹⁰², A. Lebedev⁷⁹, M. LeBlanc⁷, T. LeCompte⁶, F. Ledroit-Guillon⁵⁸, A.C.A. Lee⁹⁵, C.A. Lee²⁹, G.R. Lee¹⁷, L. Lee⁵⁹, S.C. Lee¹⁵⁸, S. Lee⁷⁹, B. Lefebvre^{168a}, H.P. Lefebvre⁹⁴, M. Lefebvre¹⁷⁶, C. Leggett¹⁸, K. Lehmann¹⁵², N. Lehmann²⁰, G. Lehmann Miotto³⁶, W.A. Leight⁴⁶, A. Leisos^{162,v}, M.A.L. Leite^{81c}, C.E. Leitgeb¹¹⁴, R. Leitner¹⁴², K.J.C. Leney⁴², T. Lenz²⁴, S. Leone^{72a}, C. Leonidopoulos⁵⁰, A. Leopold¹³⁵, C. Leroy¹¹⁰, R. Les¹⁰⁷, C.G. Lester³², M. Levchenko¹³⁷, J. Levêque⁵, D. Levin¹⁰⁶, L.J. Levinson¹⁸⁰, D.J. Lewis²¹, B. Li^{15b}, B. Li¹⁰⁶, C-Q. Li^{60c,60d}, F. Li^{60c}, H. Li^{60a}, H. Li^{60b}, J. Li^{60c}, K. Li¹⁴⁸, L. Li^{60c}, M. Li^{15a,15d}, Q.Y. Li^{60a}, S. Li^{60d,60c,b}, X. Li⁴⁶, Y. Li⁴⁶, Z. Li^{60b}, Z. Li¹³⁴, Z. Li¹⁰⁴, Z. Li⁹¹, Z. Liang^{15a}, M. Liberatore⁴⁶, B. Liberti^{74a}, K. Lie^{63c}, S. Lim²⁹, C.Y. Lin³², K. Lin¹⁰⁷, R.A. Linck⁶⁶, R.E. Lindley⁷, J.H. Lindon²¹, A. Linss⁴⁶, A.L. Lioni⁵⁴, E. Lipeles¹³⁶, A. Lipniacka¹⁷, T.M. Liss^{173,qj}, A. Lister¹⁷⁵, J.D. Little⁸, B. Liu⁷⁹, B.X. Liu¹⁵², H.B. Liu²⁹, J.B. Liu^{60a}, J.K.K. Liu³⁷, K. Liu^{60d,60c}, M. Liu^{60a}, M.Y. Liu^{60a}, P. Liu^{15a}, X. Liu^{60a}, Y. Liu⁴⁶, Y. Liu^{15a,15d}, Y.L. Liu¹⁰⁶, Y.W. Liu^{60a}, M. Livan^{71a,71b}, A. Lleres⁵⁸, J. Llorente Merino¹⁵², S.L. Lloyd⁹³, C.Y. Lo^{63b}, E.M. Lobodzinska⁴⁶, P. Loch⁷, S. Loffredo^{74a,74b}, T. Lohse¹⁹, K. Lohwasser¹⁴⁹, M. Lokajicek¹⁴⁰, J.D. Long¹⁷³, R.E. Long⁹⁰, I. Longarini^{73a,73b}, L. Longo³⁶, I. Lopez Paz¹⁰¹, A. Lopez Solis¹⁴⁹, J. Lorenz¹¹⁴, N. Lorenzo Martinez⁵, A.M. Lory¹¹⁴, A. Lösle⁵², X. Lou^{45a,45b}, X. Lou^{15a}, A. Lounis⁶⁵, J. Love⁶, P.A. Love⁹⁰, J.J. Lozano Bahilo¹⁷⁴, M. Lu^{60a}, Y.J. Lu⁶⁴, H.J. Lubatti¹⁴⁸, C. Luci^{73a,73b}, F.L. Lucio Alves^{15c}, A. Lucotte⁵⁸, F. Luehring⁶⁶, I. Luise¹⁵⁵, L. Luminari^{73a}, B. Lund-Jensen¹⁵⁴, N.A. Luongo¹³¹, M.S. Lutz¹⁶¹, D. Lynn²⁹, H. Lyons⁹¹, R. Lysak¹⁴⁰, E. Lytken⁹⁷, F. Lyu^{15a}, V. Lyubushkin⁸⁰, T. Lyubushkina⁸⁰, H. Ma²⁹, L.L. Ma^{60b}, Y. Ma⁹⁵, D.M. Mac Donell¹⁷⁶, G. Maccarrone⁵¹, C.M. Macdonald¹⁴⁹, J.C. MacDonald¹⁴⁹, J. Machado Miguens¹³⁶, R. Madar³⁸, W.F. Mader⁴⁸, M. Madugoda Ralalage Don¹²⁹, N. Madysa⁴⁸, J. Maeda⁸³, T. Maeno²⁹, M. Maerker⁴⁸, V. Magerl⁵², N. Magini⁷⁹, J. Magro^{67a,67c,r}, D.J. Mahon³⁹, C. Maidantchik^{81b}, A. Maio^{139a,139b,139d}, K. Maj^{84a}, O. Majersky^{28a}, S. Majewski¹³¹, Y. Makida⁸², N. Makovec⁶⁵, B. Malaescu¹³⁵, Pa. Malecki⁸⁵, V.P. Maleev¹³⁷, F. Malek⁵⁸, D. Malito^{41b,41a}, U. Mallik⁷⁸, C. Malone³², S. Maltezos¹⁰, S. Malyukov⁸⁰, J. Mamuzic¹⁷⁴, G. Mancini⁵¹, J.P. Mandalia⁹³, I. Mandić⁹², L. Manhaes de Andrade Filho^{81a}, I.M. Maniatis¹⁶², J. Manjarres Ramos⁴⁸, K.H. Mankinen⁹⁷, A. Mann¹¹⁴, A. Manousos⁷⁷, B. Mansoulie¹⁴⁴, I. Manthos¹⁶², S. Manzoni¹²⁰, A. Marantis¹⁶², G. Marceca³⁰, L. Marchese¹³⁴, G. Marchiori¹³⁵, M. Marcisovsky¹⁴⁰, L. Marcoccia^{74a,74b}, C. Marcon⁹⁷, M. Marjanovic¹²⁸, Z. Marshall¹⁸, M.U.F. Martensson¹⁷², S. Marti-Garcia¹⁷⁴, C.B. Martin¹²⁷, T.A. Martin¹⁷⁸, V.J. Martin⁵⁰, B. Martin dit Latour¹⁷, L. Martinelli^{75a,75b}, M. Martinez^{14,w}, P. Martinez Agullo¹⁷⁴, V.I. Martinez Outschoorn¹⁰³, S. Martin-Haugh¹⁴³, V.S. Martoiu^{27b}, A.C. Martyniuk⁹⁵, A. Marzin³⁶, S.R. Maschek¹¹⁵, L. Masetti¹⁰⁰, T. Mashimo¹⁶³, R. Mashinistov¹¹¹, J. Masik¹⁰¹, A.L. Maslennikov^{122b,122a}, L. Massa^{23b,23a}, P. Massarotti^{70a,70b}, P. Mastrandrea^{72a,72b}, A. Mastroberardino^{41b,41a}, T. Masubuchi¹⁶³, D. Matakias²⁹, A. Matic¹¹⁴, N. Matsuzawa¹⁶³, P. Mättig²⁴, J. Maurer^{27b}, B. Maček⁹², D.A. Maximov^{122b,122a}, R. Mazini¹⁵⁸, I. Maznas¹⁶², S.M. Mazza¹⁴⁵, J.P. Mc Gowan¹⁰⁴, S.P. Mc Kee¹⁰⁶, T.G. McCarthy¹¹⁵, W.P. McCormack¹⁸, E.F. McDonald¹⁰⁵, A.E. McDougall¹²⁰, J.A. MCFayden¹⁸, G. Mchedlidze^{159b}, M.A. McKay⁴², K.D. McLean¹⁷⁶, S.J. McMahon¹⁴³, P.C. McNamara¹⁰⁵, C.J. McNicol¹⁷⁸, R.A. McPherson^{176,aa}, J.E. Mdhlluli^{33e}, Z.A. Meadows¹⁰³, S. Meehan³⁶, T. Megy³⁸, S. Mehlhase¹¹⁴, A. Mehta⁹¹, B. Meirose⁴³, D. Melini¹⁶⁰, B.R. Mellado Garcia^{33e}, J.D. Mellenthin⁵³, M. Melo^{28a}, F. Meloni⁴⁶, A. Melzer²⁴, E.D. Mendes Gouveia^{139a,139e}, A.M. Mendes Jacques Da Costa²¹, H.Y. Meng¹⁶⁷, L. Meng³⁶, X.T. Meng¹⁰⁶, S. Menke¹¹⁵, E. Meoni^{41b,41a}, S. Mergelmeyer¹⁹, S.A.M. Merkt¹³⁸, C. Merlassino¹³⁴, P. Mermod⁵⁴, L. Merola^{70a,70b}, C. Meroni^{69a}, G. Merz¹⁰⁶, O. Meshkov^{113,111}, J.K.R. Meshreki¹⁵¹, J. Metcalfe⁶, A.S. Mete⁶, C. Meyer⁶⁶, J-P. Meyer¹⁴⁴, M. Michetti¹⁹, R.P. Middleton¹⁴³, L. Mijović⁵⁰, G. Mikenberg¹⁸⁰, M. Mikestikova¹⁴⁰, M. Mikuž⁹², H. Mildner¹⁴⁹, A. Milic¹⁶⁷, C.D. Milke⁴²,

D.W. Miller³⁷, L.S. Miller³⁴, A. Milov¹⁸⁰, D.A. Milstead^{45a,45b}, A.A. Minaenko¹²³, I.A. Minashvili^{159b}, L. Mince⁵⁷, A.I. Mincer¹²⁵, B. Mindur^{84a}, M. Mineev⁸⁰, Y. Minegishi¹⁶³, Y. Mino⁸⁶, L.M. Mir¹⁴, M. Mironova¹³⁴, T. Mitani¹⁷⁹, J. Mitrevski¹¹⁴, V.A. Mitsou¹⁷⁴, M. Mittal^{60c}, O. Miu¹⁶⁷, A. Miucci²⁰, P.S. Miyagawa⁹³, A. Mizukami⁸², J.U. Mjörnmark⁹⁷, T. Mkrtchyan^{61a}, M. Mlynarikova¹²¹, T. Moa^{45a,45b}, S. Mobius⁵³, K. Mochizuki¹¹⁰, P. Moder⁴⁶, P. Mogg¹¹⁴, S. Mohapatra³⁹, R. Moles-Valls²⁴, K. Mönig⁴⁶, E. Monnier¹⁰², A. Montalbano¹⁵², J. Montejo Berlingen³⁶, M. Montella⁹⁵, F. Monticelli⁸⁹, S. Monzani^{69a}, N. Morange⁶⁵, A.L. Moreira De Carvalho^{139a}, D. Moreno^{22a}, M. Moreno Llácer¹⁷⁴, C. Moreno Martinez¹⁴, P. Morettini^{55b}, M. Morgenstern¹⁶⁰, S. Morgenstern⁴⁸, D. Mori¹⁵², M. Morii⁵⁹, M. Morinaga¹⁷⁹, V. Morisbak¹³³, A.K. Morley³⁶, G. Mornacchi³⁶, A.P. Morris⁹⁵, L. Morvaj³⁶, P. Moschovakos³⁶, B. Moser¹²⁰, M. Mosidze^{159b}, T. Moskalets¹⁴⁴, P. Moskvitina¹¹⁹, J. Moss^{31,n}, E.J.W. Moyse¹⁰³, S. Muanza¹⁰², J. Mueller¹³⁸, R.S.P. Mueller¹¹⁴, D. Muenstermann⁹⁰, G.A. Mullier⁹⁷, D.P. Mungo^{69a,69b}, J.L. Munoz Martinez¹⁴, F.J. Munoz Sanchez¹⁰¹, P. Murin^{28b}, W.J. Murray^{178,143}, A. Murrone^{69a,69b}, J.M. Muse¹²⁸, M. Muškinja¹⁸, C. Mwewa^{33a}, A.G. Myagkov^{123,af}, A.A. Myers¹³⁸, G. Myers⁶⁶, J. Myers¹³¹, M. Myska¹⁴¹, B.P. Nachman¹⁸, O. Nackenhorst⁴⁷, A. Nag Nag⁴⁸, K. Nagai¹³⁴, K. Nagano⁸², Y. Nagasaka⁶², J.L. Nagle²⁹, E. Nagy¹⁰², A.M. Nairz³⁶, Y. Nakahama¹¹⁷, K. Nakamura⁸², T. Nakamura¹⁶³, H. Nanjo¹³², F. Napolitano^{61a}, R.F. Naranjo Garcia⁴⁶, R. Narayan⁴², I. Naryshkin¹³⁷, M. Naseri³⁴, T. Naumann⁴⁶, G. Navarro^{22a}, P.Y. Nechaeva¹¹¹, F. Nechansky⁴⁶, T.J. Neep²¹, A. Negri^{71a,71b}, M. Negrini^{23b}, C. Nellist¹¹⁹, C. Nelson¹⁰⁴, M.E. Nelson^{45a,45b}, S. Nemecek¹⁴⁰, M. Nessi^{36,f}, M.S. Neubauer¹⁷³, F. Neuhaus¹⁰⁰, M. Neumann¹⁸², R. Newhouse¹⁷⁵, P.R. Newman²¹, C.W. Ng¹³⁸, Y.S. Ng¹⁹, Y.W.Y. Ng¹⁷¹, B. Ngair^{35f}, H.D.N. Nguyen¹⁰², T. Nguyen Manh¹¹⁰, E. Nibigira³⁸, R.B. Nickerson¹³⁴, R. Nicolaidou¹⁴⁴, D.S. Nielsen⁴⁰, J. Nielsen¹⁴⁵, M. Niemeyer⁵³, N. Nikiforou¹¹, V. Nikolaenko^{123,af}, I. Nikolic-Audit¹³⁵, K. Nikolopoulos²¹, P. Nilsson²⁹, H.R. Nindhito⁵⁴, A. Nisati^{73a}, N. Nishu^{60c}, R. Nisius¹¹⁵, I. Nitsche⁴⁷, T. Nitta¹⁷⁹, T. Nobe¹⁶³, D.L. Noel³², Y. Noguchi⁸⁶, I. Nomidis¹³⁵, M.A. Nomura²⁹, M. Nordberg³⁶, J. Novak⁹², T. Novak⁹², O. Novgorodova⁴⁸, R. Novotny¹¹⁸, L. Nozka¹³⁰, K. Ntekas¹⁷¹, E. Nurse⁹⁵, F.G. Oakham^{34,ak}, J. Ocariz¹³⁵, A. Ochi⁸³, I. Ochoa^{139a}, J.P. Ochoa-Ricoux^{146a}, K. O'Connor²⁶, S. Oda⁸⁸, S. Odaka⁸², S. Oerdek⁵³, A. Ogrodnik^{84a}, A. Oh¹⁰¹, C.C. Ohm¹⁵⁴, H. Oide¹⁶⁵, R. Oishi¹⁶³, M.L. Ojeda¹⁶⁷, H. Okawa¹⁶⁹, Y. Okazaki⁸⁶, M.W. O'Keefe⁹¹, Y. Okumura¹⁶³, A. Olariu^{27b}, L.F. Oleiro Seabra^{139a}, S.A. Olivares Pino^{146a}, D. Oliveira Damazio²⁹, J.L. Oliver¹, M.J.R. Olsson¹⁷¹, A. Olszewski⁸⁵, J. Olszowska⁸⁵, Ö.O. Öncel²⁴, D.C. O'Neil¹⁵², A.P. O'Neill¹³⁴, A. Onofre^{139a,139e}, P.U.E. Onyisi¹¹, H. Oppen¹³³, R.G. Oreamuno Madriz¹²¹, M.J. Oreglia³⁷, G.E. Orellana⁸⁹, D. Orestano^{75a,75b}, N. Orlando¹⁴, R.S. Orr¹⁶⁷, V. O'Shea⁵⁷, R. Ospanov^{60a}, G. Otero y Garzon³⁰, H. Otono⁸⁸, P.S. Ott^{61a}, G.J. Ottino¹⁸, M. Ouchrif^{35e}, J. Ouellette²⁹, F. Ould-Saada¹³³, A. Ouraou^{144,*}, Q. Ouyang^{15a}, M. Owen⁵⁷, R.E. Owen¹⁴³, V.E. Ozcan^{12c}, N. Ozturk⁸, J. Pacalt¹³⁰, H.A. Pacey³², K. Pachal⁴⁹, A. Pacheco Pages¹⁴, C. Padilla Aranda¹⁴, S. Pagan Griso¹⁸, G. Palacino⁶⁶, S. Palazzo⁵⁰, S. Palestini³⁶, M. Palka^{84b}, P. Palni^{84a}, C.E. Pandini⁵⁴, J.G. Panduro Vazquez⁹⁴, P. Pani⁴⁶, G. Panizzo^{67a,67c}, L. Paolozzi⁵⁴, C. Papadatos¹¹⁰, K. Papageorgiou^{9,h}, S. Parajuli⁴², A. Paramonov⁶, C. Paraskevopoulos¹⁰, D. Paredes Hernandez^{63b}, S.R. Paredes Saenz¹³⁴, B. Parida¹⁸⁰, T.H. Park¹⁶⁷, A.J. Parker³¹, M.A. Parker³², F. Parodi^{55b,55a}, E.W. Parrish¹²¹, J.A. Parsons³⁹, U. Parzefall⁵², L. Pascual Dominguez¹³⁵, V.R. Pascuzzi¹⁸, J.M.P. Pasner¹⁴⁵, F. Pasquali¹²⁰, E. Pasqualucci^{73a}, S. Passaggio^{55b}, F. Pastore⁹⁴, P. Pasuwan^{45a,45b}, S. Pataria¹⁰⁰, J.R. Pater¹⁰¹, A. Pathak^{181,j}, J. Patton⁹¹, T. Pauly³⁶, J. Pearkes¹⁵³, M. Pedersen¹³³, L. Pedraza Diaz¹¹⁹, R. Pedro^{139a}, T. Peiffer⁵³, S.V. Peleganchuk^{122b,122a}, O. Penc¹⁴⁰, C. Peng^{63b}, H. Peng^{60a}, B.S. Peralva^{81a}, M.M. Perego⁶⁵, A.P. Pereira Peixoto^{139a}, L. Pereira Sanchez^{45a,45b}, D.V. Perepelitsa²⁹, E. Perez Codina^{168a}, L. Perini^{69a,69b}, H. Pernegger³⁶, S. Perrella³⁶, A. Perrevoort¹²⁰, K. Peters⁴⁶, R.F.Y. Peters¹⁰¹, B.A. Petersen³⁶, T.C. Petersen⁴⁰, E. Petit¹⁰², V. Petousis¹⁴¹, C. Petridou¹⁶², F. Petrucci^{75a,75b}, M. Pettee¹⁸³, N.E. Pettersson¹⁰³, K. Petukhova¹⁴², A. Peyaud¹⁴⁴, R. Pezoa^{146d}, L. Pezzotti^{71a,71b}, T. Pham¹⁰⁵, P.W. Phillips¹⁴³, M.W. Phipps¹⁷³, G. Piacquadio¹⁵⁵, E. Pianori¹⁸, A. Picazio¹⁰³, R.H. Pickles¹⁰¹, R. Piegaia³⁰, D. Pietreanu^{27b}, J.E. Pilcher³⁷, A.D. Pilkington¹⁰¹, M. Pinamonti^{67a,67c}, J.L. Pinfold³, C. Pitman Donaldson⁹⁵, M. Pitt¹⁶¹, L. Pizzimento^{74a,74b}, A. Pizzini¹²⁰, M.-A. Pleier²⁹, V. Plesanovs⁵², V. Pleskot¹⁴², E. Plotnikova⁸⁰, P. Podberczko^{122b,122a}, R. Poettgen⁹⁷, R. Poggi⁵⁴, L. Poggioli¹³⁵, I. Pogrebnyak¹⁰⁷, D. Pohl²⁴, I. Pokharel⁵³, G. Polesello^{71a}, A. Poley^{152,168a}, A. Policicchio^{73a,73b}, R. Polifka¹⁴², A. Polini^{23b}, C.S. Pollard⁴⁶, V. Polychronakos²⁹, D. Ponomarenko¹¹², L. Pontecorvo³⁶, S. Popa^{27a}, G.A. Popeneciu^{27d}, L. Portales⁵, D.M. Portillo Quintero⁵⁸, S. Pospisil¹⁴¹,

K. Potamianos⁴⁶, I.N. Potrap⁸⁰, C.J. Potter³², H. Potti¹¹, T. Poulsen⁹⁷, J. Poveda¹⁷⁴, T.D. Powell¹⁴⁹,
 G. Pownall⁴⁶, M.E. Pozo Astigarraga³⁶, A. Prades Ibanez¹⁷⁴, P. Pralavorio¹⁰², M.M. Prapa⁴⁴, S. Prell⁷⁹,
 D. Price¹⁰¹, M. Primavera^{68a}, M.L. Proffitt¹⁴⁸, N. Proklova¹¹², K. Prokofiev^{63c}, F. Prokoshin⁸⁰,
 S. Protopopescu²⁹, J. Proudfoot⁶, M. Przybycien^{84a}, D. Pudzha¹³⁷, A. Puri¹⁷³, P. Puzo⁶⁵,
 D. Pyatiizbyantseva¹¹², J. Qian¹⁰⁶, Y. Qin¹⁰¹, A. Quadt⁵³, M. Queitsch-Maitland³⁶, G. Rabanal Bolanos⁵⁹,
 M. Racko^{28a}, F. Ragusa^{69a,69b}, G. Rahal⁹⁸, J.A. Raine⁵⁴, S. Rajagopalan²⁹, A. Ramirez Morales⁹³,
 K. Ran^{15a,15d}, D.F. Rassloff^{61a}, D.M. Rauch⁴⁶, F. Rauscher¹¹⁴, S. Rave¹⁰⁰, B. Ravina⁵⁷, I. Ravinovich¹⁸⁰,
 J.H. Rawling¹⁰¹, M. Raymond³⁶, A.L. Read¹³³, N.P. Readioff¹⁴⁹, M. Reale^{68a,68b}, D.M. Rebuffi^{71a,71b},
 G. Redlinger²⁹, K. Reeves⁴³, D. Reikher¹⁶¹, A. Reiss¹⁰⁰, A. Rej¹⁵¹, C. Rembser³⁶, A. Renardi⁴⁶,
 M. Renda^{27b}, M.B. Rendel¹¹⁵, A.G. Rennie⁵⁷, S. Resconi^{69a}, E.D. Resseguie¹⁸, S. Rettie⁹⁵, B. Reynolds¹²⁷,
 E. Reynolds²¹, O.L. Rezanova^{122b,122a}, P. Reznicek¹⁴², E. Ricci^{76a,76b}, R. Richter¹¹⁵, S. Richter⁴⁶,
 E. Richter-Was^{84b}, M. Ridel¹³⁵, P. Rieck¹¹⁵, O. Rifki⁴⁶, M. Rijssenbeek¹⁵⁵, A. Rimoldi^{71a,71b},
 M. Rimoldi⁴⁶, L. Rinaldi^{23b}, T.T. Rinn¹⁷³, G. Ripellino¹⁵⁴, I. Riu¹⁴, P. Rivadeneira⁴⁶,
 J.C. Rivera Vergara¹⁷⁶, F. Rizatdinova¹²⁹, E. Rizvi⁹³, C. Rizzi³⁶, S.H. Robertson^{104,aa}, M. Robin⁴⁶,
 D. Robinson³², C.M. Robles Gajardo^{146d}, M. Robles Manzano¹⁰⁰, A. Robson⁵⁷, A. Rocchi^{74a,74b},
 C. Roda^{72a,72b}, S. Rodriguez Bosca¹⁷⁴, A. Rodriguez Rodriguez⁵², A.M. Rodríguez Vera^{168b}, S. Roe³⁶,
 J. Roggel¹⁸², O. Røhne¹³³, R. Röhrig¹¹⁵, R.A. Rojas^{146d}, B. Roland⁵², C.P.A. Roland⁶⁶, J. Roloff²⁹,
 A. Romaniouk¹¹², M. Romano^{23b,23a}, N. Rompotis⁹¹, M. Ronzani¹²⁵, L. Roos¹³⁵, S. Rosati^{73a},
 G. Rosin¹⁰³, B.J. Rosser¹³⁶, E. Rossi⁴⁶, E. Rossi^{75a,75b}, E. Rossi^{70a,70b}, L.P. Rossi^{55b}, L. Rossini⁴⁶,
 R. Rosten¹⁴, M. Rotaru^{27b}, B. Rottler⁵², D. Rousseau⁶⁵, G. Rovelli^{71a,71b}, A. Roy¹¹, D. Roy^{33e},
 A. Rozanov¹⁰², Y. Rozen¹⁶⁰, X. Ruan^{33e}, T.A. Ruggeri¹, F. Rühr⁵², A. Ruiz-Martinez¹⁷⁴, A. Rummler³⁶,
 Z. Rurikova⁵², N.A. Rusakovich⁸⁰, H.L. Russell¹⁰⁴, L. Rustige^{38,47}, J.P. Rutherford⁷, E.M. Rüttinger¹⁴⁹,
 M. Rybar¹⁴², G. Rybkin⁶⁵, E.B. Rye¹³³, A. Ryzhov¹²³, J.A. Sabater Iglesias⁴⁶, P. Sabatini¹⁷⁴,
 L. Sabetta^{73a,73b}, S. Sacerdoti⁶⁵, H.F-W. Sadrozinski¹⁴⁵, R. Sadykov⁸⁰, F. Safai Tehrani^{73a},
 B. Safarzadeh Samani¹⁵⁶, M. Safdari¹⁵³, P. Saha¹²¹, S. Saha¹⁰⁴, M. Sahinsoy¹¹⁵, A. Sahu¹⁸²,
 M. Saimpert³⁶, M. Saito¹⁶³, T. Saito¹⁶³, H. Sakamoto¹⁶³, D. Salamani⁵⁴, G. Salamanna^{75a,75b},
 A. Salnikov¹⁵³, J. Salt¹⁷⁴, A. Salvador Salas¹⁴, D. Salvatore^{41b,41a}, F. Salvatore¹⁵⁶, A. Salvucci^{63a},
 A. Salzburger³⁶, J. Samarati³⁶, D. Sammel⁵², D. Sampsonidis¹⁶², D. Sampsonidou^{60d,60c}, J. Sánchez¹⁷⁴,
 A. Sanchez Pineda^{67a,36,67c}, H. Sandaker¹³³, C.O. Sander⁴⁶, I.G. Sanderswood⁹⁰, M. Sandhoff¹⁸²,
 C. Sandoval^{22b}, D.P.C. Sankey¹⁴³, M. Sannino^{55b,55a}, Y. Sano¹¹⁷, A. Sansoni⁵¹, C. Santoni³⁸,
 H. Santos^{139a,139b}, S.N. Santpur¹⁸, A. Santra¹⁷⁴, K.A. Saoucha¹⁴⁹, A. Saponov⁸⁰, J.G. Saraiva^{139a,139d},
 O. Sasaki⁸², K. Sato¹⁶⁹, F. Sauerburger⁵², E. Sauvan⁵, P. Savard^{167,ak}, R. Sawada¹⁶³, C. Sawyer¹⁴³,
 L. Sawyer⁹⁶, I. Sayago Galvan¹⁷⁴, C. Sbarra^{23b}, A. Sbrizzi^{67a,67c}, T. Scanlon⁹⁵, J. Schaarschmidt¹⁴⁸,
 P. Schacht¹¹⁵, D. Schaefer³⁷, L. Schaefer¹³⁶, U. Schäfer¹⁰⁰, A.C. Schaffer⁶⁵, D. Schaile¹¹⁴,
 R.D. Schamberger¹⁵⁵, E. Schanet¹¹⁴, C. Scharf¹⁹, N. Scharmberg¹⁰¹, V.A. Schegelsky¹³⁷, D. Scheirich¹⁴²,
 F. Schenck¹⁹, M. Schernau¹⁷¹, C. Schiavi^{55b,55a}, L.K. Schildgen²⁴, Z.M. Schillaci²⁶, E.J. Schioppa^{68a,68b},
 M. Schioppa^{41b,41a}, K.E. Schleicher⁵², S. Schlenker³⁶, K.R. Schmidt-Sommerfeld¹¹⁵, K. Schmieden¹⁰⁰,
 C. Schmitt¹⁰⁰, S. Schmitt⁴⁶, L. Schoeffel¹⁴⁴, A. Schoening^{61b}, P.G. Scholer⁵², E. Schopf¹³⁴, M. Schott¹⁰⁰,
 J.F.P. Schouwenberg¹¹⁹, J. Schovancova³⁶, S. Schramm⁵⁴, F. Schroeder¹⁸², A. Schulte¹⁰⁰,
 H-C. Schultz-Coulon^{61a}, M. Schumacher⁵², B.A. Schumm¹⁴⁵, Ph. Schune¹⁴⁴, A. Schwartzman¹⁵³,
 T.A. Schwarz¹⁰⁶, Ph. Schwemling¹⁴⁴, R. Schwienhorst¹⁰⁷, A. Sciandra¹⁴⁵, G. Sciolla²⁶, F. Scuri^{72a},
 F. Scutti¹⁰⁵, L.M. Scyboz¹¹⁵, C.D. Sebastiani⁹¹, K. Sedlaczek⁴⁷, P. Seema¹⁹, S.C. Seidel¹¹⁸, A. Seiden¹⁴⁵,
 B.D. Seidlitz²⁹, T. Seiss³⁷, C. Seitz⁴⁶, J.M. Seixas^{81b}, G. Sekhniadze^{70a}, S.J. Sekula⁴²,
 N. Semprini-Cesari^{23b,23a}, S. Sen⁴⁹, C. Serfon²⁹, L. Serin⁶⁵, L. Serkin^{67a,67b}, M. Sessa^{60a}, H. Severini¹²⁸,
 S. Sevova¹⁵³, F. Sforza^{55b,55a}, A. Sfyrla⁵⁴, E. Shabalina⁵³, J.D. Shahinian¹³⁶, N.W. Shaikh^{45a,45b},
 D. Shaked Renous¹⁸⁰, L.Y. Shan^{15a}, M. Shapiro¹⁸, A. Sharma³⁶, A.S. Sharma¹, P.B. Shatalov¹²⁴,
 K. Shaw¹⁵⁶, S.M. Shaw¹⁰¹, M. Shehade¹⁸⁰, Y. Shen¹²⁸, A.D. Sherman²⁵, P. Sherwood⁹⁵, L. Shi⁹⁵,
 C.O. Shimmin¹⁸³, Y. Shimogama¹⁷⁹, M. Shimojima¹¹⁶, J.D. Shinner⁹⁴, I.P.J. Shipsey¹³⁴, S. Shirabe¹⁶⁵,
 M. Shiyakova^{80,y}, J. Shlomi¹⁸⁰, A. Shmeleva¹¹¹, M.J. Shochet³⁷, J. Shojaii¹⁰⁵, D.R. Shope¹⁵⁴,
 S. Shrestha¹²⁷, E.M. Shrif^{33e}, M.J. Shroff¹⁷⁶, E. Shulga¹⁸⁰, P. Sicho¹⁴⁰, A.M. Sickles¹⁷³,
 E. Sideras Haddad^{33e}, O. Sidiropoulou³⁶, A. Sidoti^{23b,23a}, F. Siegert⁴⁸, Dj. Sijacki¹⁶, M.Jr. Silva¹⁸¹,
 M.V. Silva Oliveira³⁶, S.B. Silverstein^{45a}, S. Simion⁶⁵, R. Simoniello¹⁰⁰, C.J. Simpson-allsoy²¹,
 S. Simsek^{12b}, P. Sinervo¹⁶⁷, V. Sinetckii¹¹³, S. Singh¹⁵², S. Sinha^{33e}, M. Sioli^{23b,23a}, I. Siral¹³¹,

S.Yu. Sivoklokov¹¹³, J. Sjölin^{45a,45b}, A. Skaf⁵³, E. Skorda⁹⁷, P. Skubic¹²⁸, M. Slawinska⁸⁵, K. Sliwa¹⁷⁰, V. Smakhtin¹⁸⁰, B.H. Smart¹⁴³, J. Smiesko^{28b}, N. Smirnov¹¹², S.Yu. Smirnov¹¹², Y. Smirnov¹¹², L.N. Smirnova^{113,s}, O. Smirnova⁹⁷, E.A. Smith³⁷, H.A. Smith¹³⁴, M. Smizanska⁹⁰, K. Smolek¹⁴¹, A. Smykiewicz⁸⁵, A.A. Snesev¹¹¹, H.L. Snoek¹²⁰, I.M. Snyder¹³¹, S. Snyder²⁹, R. Sobie^{176,aa}, A. Soffer¹⁶¹, A. Søgaard⁵⁰, F. Sohns⁵³, C.A. Solans Sanchez³⁶, E.Yu. Soldatov¹¹², U. Soldevila¹⁷⁴, A.A. Solodkov¹²³, A. Soloshenko⁸⁰, O.V. Solovyanov¹²³, V. Solovyev¹³⁷, P. Sommer¹⁴⁹, H. Son¹⁷⁰, A. Sonay¹⁴, W. Song¹⁴³, W.Y. Song^{168b}, A. Sopczak¹⁴¹, A.L. Sopio⁹⁵, F. Sopkova^{28b}, S. Sottocornola^{71a,71b}, R. Soualah^{67a,67c}, A.M. Soukharev^{122b,122a}, D. South⁴⁶, S. Spagnolo^{68a,68b}, M. Spalla¹¹⁵, M. Spangenberg¹⁷⁸, F. Spanò⁹⁴, D. Sperlich⁵², T.M. Spieker^{61a}, G. Spigo³⁶, M. Spina¹⁵⁶, D.P. Spiteri⁵⁷, M. Spousta¹⁴², A. Stabile^{69a,69b}, B.L. Stamas¹²¹, R. Stamen^{61a}, M. Stamenkovic¹²⁰, A. Stampekiš²¹, E. Stanecka⁸⁵, B. Stanislaus¹³⁴, M.M. Stanitzki⁴⁶, M. Stankaityte¹³⁴, B. Stapf¹²⁰, E.A. Starchenko¹²³, G.H. Stark¹⁴⁵, J. Stark⁵⁸, P. Staroba¹⁴⁰, P. Starovoitov^{61a}, S. Stärz¹⁰⁴, R. Staszewski⁸⁵, G. Stavropoulos⁴⁴, M. Stegler⁴⁶, P. Steinberg²⁹, A.L. Steinhebel¹³¹, B. Stelzer^{152,168a}, H.J. Stelzer¹³⁸, O. Stelzer-Chilton^{168a}, H. Stenzel⁵⁶, T.J. Stevenson¹⁵⁶, G.A. Stewart³⁶, M.C. Stockton³⁶, G. Stoica^{27b}, M. Stolarski^{139a}, S. Stonjek¹¹⁵, A. Straessner⁴⁸, J. Strandberg¹⁵⁴, S. Strandberg^{45a,45b}, M. Strauss¹²⁸, T. Strebler¹⁰², P. Strizenec^{28b}, R. Ströhmer¹⁷⁷, D.M. Strom¹³¹, R. Stroynowski⁴², A. Strubig^{45a,45b}, S.A. Stucci²⁹, B. Stugu¹⁷, J. Stupak¹²⁸, N.A. Styles⁴⁶, D. Su¹⁵³, W. Su^{60d,148,60c}, X. Su^{60a}, N.B. Suarez¹³⁸, V.V. Sulin¹¹¹, M.J. Sullivan⁹¹, D.M.S. Sultan⁵⁴, S. Sultansoy^{4c}, T. Sumida⁸⁶, S. Sun¹⁰⁶, X. Sun¹⁰¹, C.J.E. Suster¹⁵⁷, M.R. Sutton¹⁵⁶, S. Suzuki⁸², M. Svatos¹⁴⁰, M. Swiatlowski^{168a}, S.P. Swift², T. Swirski¹⁷⁷, A. Sydorenko¹⁰⁰, I. Sykora^{28a}, M. Sykora¹⁴², T. Sykora¹⁴², D. Ta¹⁰⁰, K. Tackmann^{46,x}, J. Taenzer¹⁶¹, A. Taffard¹⁷¹, R. Tafirout^{168a}, E. Tagiev¹²³, R.H.M. Taibah¹³⁵, R. Takashima⁸⁷, K. Takeda⁸³, T. Takeshita¹⁵⁰, E.P. Takeva⁵⁰, Y. Takubo⁸², M. Talby¹⁰², A.A. Talyshev^{122b,122a}, K.C. Tam^{63b}, N.M. Tamir¹⁶¹, J. Tanaka¹⁶³, R. Tanaka⁶⁵, S. Tapia Araya¹⁷³, S. Tapprogge¹⁰⁰, A. Tarek Abouelfadl Mohamed¹⁰⁷, S. Tarem¹⁶⁰, K. Tariq^{60b}, G. Tarna^{27b,e}, G.F. Tartarelli^{69a}, P. Tas¹⁴², M. Tasevsky¹⁴⁰, E. Tassi^{41b,41a}, G. Tateno¹⁶³, A. Tavares Delgado^{139a}, Y. Tayalati^{35f}, A.J. Taylor⁵⁰, G.N. Taylor¹⁰⁵, W. Taylor^{168b}, H. Teagle⁹¹, A.S. Tee⁹⁰, R. Teixeira De Lima¹⁵³, P. Teixeira-Dias⁹⁴, H. Ten Kate³⁶, J.J. Teoh¹²⁰, K. Terashi¹⁶³, J. Terron⁹⁹, S. Terzo¹⁴, M. Testa⁵¹, R.J. Teuscher^{167,aa}, N. Themistokleous⁵⁰, T. Theveneaux-Pelzer¹⁹, D.W. Thomas⁹⁴, J.P. Thomas²¹, E.A. Thompson⁴⁶, P.D. Thompson²¹, E. Thomson¹³⁶, E.J. Thorpe⁹³, V.O. Tikhomirov^{111,ag}, Yu.A. Tikhonov^{122b,122a}, S. Timoshenko¹¹², P. Tipton¹⁸³, S. Tisserant¹⁰², K. Todome^{23b,23a}, S. Todorova-Nova¹⁴², S. Todt⁴⁸, J. Tojo⁸⁸, S. Tokár^{28a}, K. Tokushuku⁸², E. Tolley¹²⁷, R. Tombs³², K.G. Tomiwa^{33e}, M. Tomoto^{82,117}, L. Tompkins¹⁵³, P. Tornambe¹⁰³, E. Torrence¹³¹, H. Torres⁴⁸, E. Torró Pastor¹⁷⁴, M. Toscani³⁰, C. Toscirì¹³⁴, J. Toth^{102,z}, D.R. Tovey¹⁴⁹, A. Traet¹⁷, C.J. Treado¹²⁵, T. Trefzger¹⁷⁷, F. Tresoldi¹⁵⁶, A. Tricoli²⁹, I.M. Trigger^{168a}, S. Trincz-Duvoid¹³⁵, D.A. Trischuk¹⁷⁵, W. Trischuk¹⁶⁷, B. Trocmé⁵⁸, A. Trofymov⁶⁵, C. Troncon^{69a}, F. Trovato¹⁵⁶, L. Truong^{33c}, M. Trzebinski⁸⁵, A. Trzupek⁸⁵, F. Tsai⁴⁶, P.V. Tsiarehka^{108,ae}, A. Tsirigotis^{162,v}, V. Tsiskaridze¹⁵⁵, E.G. Tskhadadze^{159a}, M. Tsopoulou¹⁶², I.I. Tsukerman¹²⁴, V. Tsulaia¹⁸, S. Tsuno⁸², D. Tsybychev¹⁵⁵, Y. Tu^{63b}, A. Tudorache^{27b}, V. Tudorache^{27b}, A.N. Tuna³⁶, S. Turchikhin⁸⁰, D. Turgeman¹⁸⁰, I. Turk Cakir^{4b,t}, R.J. Turner²¹, R. Turra^{69a}, P.M. Tuts³⁹, S. Tzamarias¹⁶², E. Tzovara¹⁰⁰, K. Uchida¹⁶³, F. Ukegawa¹⁶⁹, G. Unal³⁶, M. Unal¹¹, A. Undrus²⁹, G. Unel¹⁷¹, F.C. Ungaro¹⁰⁵, Y. Unno⁸², K. Uno¹⁶³, J. Urban^{28b}, P. Urquijo¹⁰⁵, G. Usai⁸, Z. Uysal^{12d}, V. Vacek¹⁴¹, B. Vachon¹⁰⁴, K.O.H. Vadla¹³³, T. Vafeiadis³⁶, A. Vaidya⁹⁵, C. Valderanis¹¹⁴, E. Valdes Santurio^{45a,45b}, M. Valente^{168a}, S. Valentinetti^{23b,23a}, A. Valero¹⁷⁴, L. Valéry⁴⁶, R.A. Vallance²¹, A. Vallier³⁶, J.A. Valls Ferrer¹⁷⁴, T.R. Van Daalen¹⁴, P. Van Gemmeren⁶, S. Van Stroud⁹⁵, I. Van Vulpen¹²⁰, M. Vanadia^{74a,74b}, W. Vandelli³⁶, M. Vandenbroucke¹⁴⁴, E.R. Vandewall¹²⁹, D. Vannicola^{73a,73b}, R. Vari^{73a}, E.W. Varnes⁷, C. Varni^{55b,55a}, T. Varol¹⁵⁸, D. Varouchas⁶⁵, K.E. Varvell¹⁵⁷, M.E. Vasile^{27b}, G.A. Vasquez¹⁷⁶, F. Vazeille³⁸, D. Vazquez Furelos¹⁴, T. Vazquez Schroeder³⁶, J. Veatch⁵³, V. Vecchio¹⁰¹, M.J. Veen¹²⁰, L.M. Veloce¹⁶⁷, F. Veloso^{139a,139c}, S. Veneziano^{73a}, A. Ventura^{68a,68b}, A. Verbytskyi¹¹⁵, V. Vercesi^{71a}, M. Verducci^{72a,72b}, C.M. Vergel Infante⁷⁹, C. Vergis²⁴, W. Verkerke¹²⁰, A.T. Vermeulen¹²⁰, J.C. Vermeulen¹²⁰, C. Vernieri¹⁵³, P.J. Verschuur⁹⁴, M.C. Vetterli^{152,ak}, N. Viaux Maira^{146d}, T. Vickey¹⁴⁹, O.E. Vickey Boeriu¹⁴⁹, G.H.A. Viehhauser¹³⁴, L. Vignani^{61b}, M. Villa^{23b,23a}, M. Villaplana Perez¹⁷⁴, E.M. Villhauer⁵⁰, E. Vilucchi⁵¹, M.G. Vincker³⁴, G.S. Virdee²¹, A. Vishwakarma⁵⁰, C. Vittori^{23b,23a}, I. Vivarelli¹⁵⁶, M. Vogel¹⁸², P. Vokac¹⁴¹, J. Von Ahnen⁴⁶, S.E. von Buddenbrock^{33e}, E. Von Toerne²⁴, V. Vorobel¹⁴²,

K. Vorobev¹¹², M. Vos¹⁷⁴, J.H. Vosseveld⁹¹, M. Vozak¹⁰¹, N. Vranjes¹⁶, M. Vranjes Milosavljevic¹⁶, V. Vrba^{141,*}, M. Vreeswijk¹²⁰, N.K. Vu¹⁰², R. Vuillermet³⁶, I. Vukotic³⁷, S. Wada¹⁶⁹, P. Wagner²⁴, W. Wagner¹⁸², J. Wagner-Kuhr¹¹⁴, S. Wahdan¹⁸², H. Wahlberg⁸⁹, R. Wakasa¹⁶⁹, V.M. Walbrecht¹¹⁵, J. Walder¹⁴³, R. Walker¹¹⁴, S.D. Walker⁹⁴, W. Walkowiak¹⁵¹, V. Wallangen^{45a,45b}, A.M. Wang⁵⁹, A.Z. Wang¹⁸¹, C. Wang^{60a}, C. Wang^{60c}, H. Wang¹⁸, H. Wang³, J. Wang^{63a}, P. Wang⁴², Q. Wang¹²⁸, R.-J. Wang¹⁰⁰, R. Wang^{60a}, R. Wang⁶, S.M. Wang¹⁵⁸, W.T. Wang^{60a}, W. Wang^{15c}, W.X. Wang^{60a}, Y. Wang^{60a}, Z. Wang¹⁰⁶, C. Wanotayaroj⁴⁶, A. Warburton¹⁰⁴, C.P. Ward³², R.J. Ward²¹, N. Warrack⁵⁷, A.T. Watson²¹, M.F. Watson²¹, G. Watts¹⁴⁸, B.M. Waugh⁹⁵, A.F. Webb¹¹, C. Weber²⁹, M.S. Weber²⁰, S.A. Weber³⁴, S.M. Weber^{61a}, Y. Wei¹³⁴, A.R. Weidberg¹³⁴, J. Weingarten⁴⁷, M. Weirich¹⁰⁰, C. Weiser⁵², P.S. Wells³⁶, T. Wenaus²⁹, B. Wendland⁴⁷, T. Wengler³⁶, S. Wenig³⁶, N. Vermes²⁴, M. Wessels^{61a}, T.D. Weston²⁰, K. Whalen¹³¹, A.M. Wharton⁹⁰, A.S. White¹⁰⁶, A. White⁸, M.J. White¹, D. Whiteson¹⁷¹, B.W. Whitmore⁹⁰, W. Wiedenmann¹⁸¹, C. Wiel⁴⁸, M. Wielers¹⁴³, N. Wieseotte¹⁰⁰, C. Wiglesworth⁴⁰, L.A.M. Wiik-Fuchs⁵², H.G. Wilkens³⁶, L.J. Wilkins⁹⁴, D.M. Williams³⁹, H.H. Williams¹³⁶, S. Williams³², S. Willocq¹⁰³, P.J. Windischhofer¹³⁴, I. Wingerter-Seez⁵, E. Winkels¹⁵⁶, F. Winklmeier¹³¹, B.T. Winter⁵², M. Wittgen¹⁵³, M. Wobisch⁹⁶, A. Wolf¹⁰⁰, R. Wölker¹³⁴, J. Wollrath⁵², M.W. Wolter⁸⁵, H. Wolters^{139a,139c}, V.W.S. Wong¹⁷⁵, A.F. Wongel⁴⁶, N.L. Woods¹⁴⁵, S.D. Worm⁴⁶, B.K. Wosiek⁸⁵, K.W. Woźniak⁸⁵, K. Wraight⁵⁷, S.L. Wu¹⁸¹, X. Wu⁵⁴, Y. Wu^{60a}, J. Wuerzinger¹³⁴, T.R. Wyatt¹⁰¹, B.M. Wynne⁵⁰, S. Xella⁴⁰, J. Xiang^{63c}, X. Xiao¹⁰⁶, X. Xie^{60a}, I. Xiotidis¹⁵⁶, D. Xu^{15a}, H. Xu^{60a}, H. Xu^{60a}, L. Xu²⁹, R. Xu¹³⁶, T. Xu¹⁴⁴, W. Xu¹⁰⁶, Y. Xu^{15b}, Z. Xu^{60b}, Z. Xu¹⁵³, B. Yabsley¹⁵⁷, S. Yacoob^{33a}, D.P. Yallup⁹⁵, N. Yamaguchi⁸⁸, Y. Yamaguchi¹⁶⁵, A. Yamamoto⁸², M. Yamatani¹⁶³, T. Yamazaki¹⁶³, Y. Yamazaki⁸³, J. Yan^{60c}, Z. Yan²⁵, H.J. Yang^{60c,60d}, H.T. Yang¹⁸, S. Yang^{60a}, T. Yang^{63c}, X. Yang^{60a}, X. Yang^{60b,58}, Y. Yang¹⁶³, Z. Yang^{106,60a}, W.-M. Yao¹⁸, Y.C. Yap⁴⁶, H. Ye^{15c}, J. Ye⁴², S. Ye²⁹, I. Yeletsikh⁸⁰, M.R. Yexley⁹⁰, E. Yigitbasi²⁵, P. Yin³⁹, K. Yorita¹⁷⁹, K. Yoshihara⁷⁹, C.J.S. Young³⁶, C. Young¹⁵³, J. Yu⁷⁹, R. Yuan^{60b,i}, X. Yue^{61a}, M. Zaazoua^{35f}, B. Zabinski⁸⁵, G. Zacharis¹⁰, E. Zaffaroni⁵⁴, J. Zahreddine¹³⁵, A.M. Zaitsev^{123,af}, T. Zakareishvili^{159b}, N. Zakharchuk³⁴, S. Zambito³⁶, D. Zanzi³⁶, S.V. Zeiřner⁴⁷, C. Zeitnitz¹⁸², G. Zemaityte¹³⁴, J.C. Zeng¹⁷³, O. Zenin¹²³, T. Ženiř^{28a}, D. Zerwas⁶⁵, M. Zgubič¹³⁴, B. Zhang^{15c}, D.F. Zhang^{15b}, G. Zhang^{15b}, J. Zhang⁶, K. Zhang^{15a}, L. Zhang^{15c}, L. Zhang^{60a}, M. Zhang¹⁷³, R. Zhang¹⁸¹, S. Zhang¹⁰⁶, X. Zhang^{60c}, X. Zhang^{60b}, Y. Zhang^{15a,15d}, Z. Zhang^{63a}, Z. Zhang⁶⁵, P. Zhao⁴⁹, Y. Zhao¹⁴⁵, Z. Zhao^{60a}, A. Zhemchugov⁸⁰, Z. Zheng¹⁰⁶, D. Zhong¹⁷³, B. Zhou¹⁰⁶, C. Zhou¹⁸¹, H. Zhou⁷, M. Zhou¹⁵⁵, N. Zhou^{60c}, Y. Zhou⁷, C.G. Zhu^{60b}, C. Zhu^{15a,15d}, H.L. Zhu^{60a}, H. Zhu^{15a}, J. Zhu¹⁰⁶, Y. Zhu^{60a}, X. Zhuang^{15a}, K. Zhukov¹¹¹, V. Zhulanov^{122b,122a}, D. Zieminska⁶⁶, N.I. Zimine⁸⁰, S. Zimmermann^{52,*}, Z. Zinonos¹¹⁵, M. Ziolkowski¹⁵¹, L. Živković¹⁶, G. Zobernig¹⁸¹, A. Zoccoli^{23b,23a}, K. Zoch⁵³, T.G. Zorbas¹⁴⁹, R. Zou³⁷, L. Zwalinski³⁶

¹ Department of Physics, University of Adelaide, Adelaide, Australia

² Physics Department, SUNY Albany, Albany NY, United States of America

³ Department of Physics, University of Alberta, Edmonton AB, Canada

⁴ (a) Department of Physics, Ankara University, Ankara; (b) Istanbul Aydın University, Application and Research Center for Advanced Studies, Istanbul; (c) Division of Physics, TOBB University of Economics and Technology, Ankara, Turkey

⁵ LAPP, Université Grenoble Alpes, Université Savoie Mont Blanc, CNRS/IN2P3, Annecy, France

⁶ High Energy Physics Division, Argonne National Laboratory, Argonne IL, United States of America

⁷ Department of Physics, University of Arizona, Tucson AZ, United States of America

⁸ Department of Physics, University of Texas at Arlington, Arlington TX, United States of America

⁹ Physics Department, National and Kapodistrian University of Athens, Athens, Greece

¹⁰ Physics Department, National Technical University of Athens, Zografou, Greece

¹¹ Department of Physics, University of Texas at Austin, Austin TX, United States of America

¹² (a) Bahcesehir University, Faculty of Engineering and Natural Sciences, Istanbul; (b) Istanbul Bilgi University, Faculty of Engineering and Natural Sciences, Istanbul; (c) Department of Physics, Bogaziçi University, Istanbul; (d) Department of Physics Engineering, Gaziantep University, Gaziantep, Turkey

¹³ Institute of Physics, Azerbaijan Academy of Sciences, Baku, Azerbaijan

¹⁴ Institut de Física d'Altes Energies (IFAE), Barcelona Institute of Science and Technology, Barcelona, Spain

¹⁵ (a) Institute of High Energy Physics, Chinese Academy of Sciences, Beijing; (b) Physics Department, Tsinghua University, Beijing; (c) Department of Physics, Nanjing University, Nanjing;

(d) University of Chinese Academy of Science (UCAS), Beijing, China

¹⁶ Institute of Physics, University of Belgrade, Belgrade, Serbia

¹⁷ Department for Physics and Technology, University of Bergen, Bergen, Norway

¹⁸ Physics Division, Lawrence Berkeley National Laboratory and University of California, Berkeley CA, United States of America

¹⁹ Institut für Physik, Humboldt Universität zu Berlin, Berlin, Germany

²⁰ Albert Einstein Center for Fundamental Physics and Laboratory for High Energy Physics, University of Bern, Bern, Switzerland

²¹ School of Physics and Astronomy, University of Birmingham, Birmingham, United Kingdom

²² (a) Facultad de Ciencias y Centro de Investigaciones, Universidad Antonio Nariño, Bogotá; (b) Departamento de Física, Universidad Nacional de Colombia, Bogotá, Colombia

²³ (a) INFN Bologna and Università di Bologna, Dipartimento di Fisica; (b) INFN Sezione di Bologna, Italy

²⁴ Physikalisches Institut, Universität Bonn, Bonn, Germany

²⁵ Department of Physics, Boston University, Boston MA, United States of America

²⁶ Department of Physics, Brandeis University, Waltham MA, United States of America

- 27 ^(a) Transilvania University of Brasov, Brasov; ^(b) Horia Hulubei National Institute of Physics and Nuclear Engineering, Bucharest; ^(c) Department of Physics, Alexandru Ioan Cuza University of Iasi, Iasi; ^(d) National Institute for Research and Development of Isotopic and Molecular Technologies, Physics Department, Cluj-Napoca; ^(e) University Politehnica Bucharest, Bucharest; ^(f) West University in Timisoara, Timisoara, Romania
- 28 ^(a) Faculty of Mathematics, Physics and Informatics, Comenius University, Bratislava; ^(b) Department of Subnuclear Physics, Institute of Experimental Physics of the Slovak Academy of Sciences, Kosice, Slovak Republic
- 29 Physics Department, Brookhaven National Laboratory, Upton NY, United States of America
- 30 Departamento de Física, Universidad de Buenos Aires, Buenos Aires, Argentina
- 31 California State University, CA, United States of America
- 32 Cavendish Laboratory, University of Cambridge, Cambridge, United Kingdom
- 33 ^(a) Department of Physics, University of Cape Town, Cape Town; ^(b) iThema Labs, Western Cape; ^(c) Department of Mechanical Engineering Science, University of Johannesburg, Johannesburg; ^(d) University of South Africa, Department of Physics, Pretoria; ^(e) School of Physics, University of the Witwatersrand, Johannesburg, South Africa
- 34 Department of Physics, Carleton University, Ottawa ON, Canada
- 35 ^(a) Faculté des Sciences Ain Chock, Réseau Universitaire de Physique des Hautes Energies – Université Hassan II, Casablanca; ^(b) Faculté des Sciences, Université Ibn-Tofail, Kénitra; ^(c) Faculté des Sciences Semlalia, Université Cadi Ayyad, LPHEA, Marrakech; ^(d) Moroccan Foundation for Advanced Science Innovation and Research (MASRI), Rabat; ^(e) LPMR, Faculté des Sciences, Université Mohamed Premier, Oujda; ^(f) Faculté des sciences, Université Mohammed V, Rabat, Morocco
- 36 CERN, Geneva, Switzerland
- 37 Enrico Fermi Institute, University of Chicago, Chicago IL, United States of America
- 38 LPC, Université Clermont Auvergne, CNRS/IN2P3, Clermont-Ferrand, France
- 39 Nevis Laboratory, Columbia University, Irvington NY, United States of America
- 40 Niels Bohr Institute, University of Copenhagen, Copenhagen, Denmark
- 41 ^(a) Dipartimento di Fisica, Università della Calabria, Rende; ^(b) INFN Gruppo Collegato di Cosenza, Laboratori Nazionali di Frascati, Italy
- 42 Physics Department, Southern Methodist University, Dallas TX, United States of America
- 43 Physics Department, University of Texas at Dallas, Richardson TX, United States of America
- 44 National Centre for Scientific Research “Demokritos”, Agia Paraskevi, Greece
- 45 ^(a) Department of Physics, Stockholm University; ^(b) Oskar Klein Centre, Stockholm, Sweden
- 46 Deutsches Elektronen-Synchrotron DESY, Hamburg and Zeuthen, Germany
- 47 Lehrstuhl für Experimentelle Physik IV, Technische Universität Dortmund, Dortmund, Germany
- 48 Institut für Kern- und Teilchenphysik, Technische Universität Dresden, Dresden, Germany
- 49 Department of Physics, Duke University, Durham NC, United States of America
- 50 SUPA – School of Physics and Astronomy, University of Edinburgh, Edinburgh, United Kingdom
- 51 INFN e Laboratori Nazionali di Frascati, Frascati, Italy
- 52 Physikalisches Institut, Albert-Ludwigs-Universität Freiburg, Freiburg, Germany
- 53 II. Physikalisches Institut, Georg-August-Universität Göttingen, Göttingen, Germany
- 54 Département de Physique Nucléaire et Corpusculaire, Université de Genève, Genève, Switzerland
- 55 ^(a) Dipartimento di Fisica, Università di Genova, Genova; ^(b) INFN Sezione di Genova, Italy
- 56 II. Physikalisches Institut, Justus-Liebig-Universität Giessen, Giessen, Germany
- 57 SUPA – School of Physics and Astronomy, University of Glasgow, Glasgow, United Kingdom
- 58 LPSC, Université Grenoble Alpes, CNRS/IN2P3, Grenoble INP, Grenoble, France
- 59 Laboratory for Particle Physics and Cosmology, Harvard University, Cambridge MA, United States of America
- 60 ^(a) Department of Modern Physics and State Key Laboratory of Particle Detection and Electronics, University of Science and Technology of China, Hefei; ^(b) Institute of Frontier and Interdisciplinary Science and Key Laboratory of Particle Physics and Particle Irradiation (MOE), Shandong University, Qingdao; ^(c) School of Physics and Astronomy, Shanghai Jiao Tong University, Key Laboratory for Particle Astrophysics and Cosmology (MOE), SKLPPC, Shanghai; ^(d) Tsung-Dao Lee Institute, Shanghai, China
- 61 ^(a) Kirchhoff-Institut für Physik, Ruprecht-Karls-Universität Heidelberg, Heidelberg; ^(b) Physikalisches Institut, Ruprecht-Karls-Universität Heidelberg, Heidelberg, Germany
- 62 Faculty of Applied Information Science, Hiroshima Institute of Technology, Hiroshima, Japan
- 63 ^(a) Department of Physics, Chinese University of Hong Kong, Shatin, N.T., Hong Kong; ^(b) Department of Physics, University of Hong Kong, Hong Kong; ^(c) Department of Physics and Institute for Advanced Study, Hong Kong University of Science and Technology, Clear Water Bay, Kowloon, Hong Kong, China
- 64 Department of Physics, National Tsing Hua University, Hsinchu, Taiwan
- 65 IJCLab, Université Paris-Saclay, CNRS/IN2P3, 91405, Orsay, France
- 66 Department of Physics, Indiana University, Bloomington IN, United States of America
- 67 ^(a) INFN Gruppo Collegato di Udine, Sezione di Trieste, Udine; ^(b) ICTP, Trieste; ^(c) Dipartimento Politecnico di Ingegneria e Architettura, Università di Udine, Udine, Italy
- 68 ^(a) INFN Sezione di Lecce; ^(b) Dipartimento di Matematica e Fisica, Università del Salento, Lecce, Italy
- 69 ^(a) INFN Sezione di Milano; ^(b) Dipartimento di Fisica, Università di Milano, Milano, Italy
- 70 ^(a) INFN Sezione di Napoli; ^(b) Dipartimento di Fisica, Università di Napoli, Napoli, Italy
- 71 ^(a) INFN Sezione di Pavia; ^(b) Dipartimento di Fisica, Università di Pavia, Pavia, Italy
- 72 ^(a) INFN Sezione di Pisa; ^(b) Dipartimento di Fisica E. Fermi, Università di Pisa, Pisa, Italy
- 73 ^(a) INFN Sezione di Roma; ^(b) Dipartimento di Fisica, Sapienza Università di Roma, Roma, Italy
- 74 ^(a) INFN Sezione di Roma Tor Vergata; ^(b) Dipartimento di Fisica, Università di Roma Tor Vergata, Roma, Italy
- 75 ^(a) INFN Sezione di Roma Tre; ^(b) Dipartimento di Matematica e Fisica, Università Roma Tre, Roma, Italy
- 76 ^(a) INFN-TIFPA; ^(b) Università degli Studi di Trento, Trento, Italy
- 77 Institut für Astro- und Teilchenphysik, Leopold-Franzens-Universität, Innsbruck, Austria
- 78 University of Iowa, Iowa City IA, United States of America
- 79 Department of Physics and Astronomy, Iowa State University, Ames IA, United States of America
- 80 Joint Institute for Nuclear Research, Dubna, Russia
- 81 ^(a) Departamento de Engenharia Elétrica, Universidade Federal de Juiz de Fora (UFJF), Juiz de Fora; ^(b) Universidade Federal do Rio De Janeiro COPPE/EE/IF, Rio de Janeiro; ^(c) Instituto de Física, Universidade de São Paulo, São Paulo, Brazil
- 82 KEK, High Energy Accelerator Research Organization, Tsukuba, Japan
- 83 Graduate School of Science, Kobe University, Kobe, Japan
- 84 ^(a) AGH University of Science and Technology, Faculty of Physics and Applied Computer Science, Krakow; ^(b) Marian Smoluchowski Institute of Physics, Jagiellonian University, Krakow, Poland
- 85 Institute of Nuclear Physics Polish Academy of Sciences, Krakow, Poland
- 86 Faculty of Science, Kyoto University, Kyoto, Japan
- 87 Kyoto University of Education, Kyoto, Japan
- 88 Research Center for Advanced Particle Physics and Department of Physics, Kyushu University, Fukuoka, Japan
- 89 Instituto de Física La Plata, Universidad Nacional de La Plata and CONICET, La Plata, Argentina
- 90 Physics Department, Lancaster University, Lancaster, United Kingdom
- 91 Oliver Lodge Laboratory, University of Liverpool, Liverpool, United Kingdom
- 92 Department of Experimental Particle Physics, Jožef Stefan Institute and Department of Physics, University of Ljubljana, Ljubljana, Slovenia
- 93 School of Physics and Astronomy, Queen Mary University of London, London, United Kingdom
- 94 Department of Physics, Royal Holloway University of London, Egham, United Kingdom
- 95 Department of Physics and Astronomy, University College London, London, United Kingdom

- ⁹⁶ Louisiana Tech University, Ruston LA, United States of America
- ⁹⁷ Fysiska institutionen, Lunds universitet, Lund, Sweden
- ⁹⁸ Centre de Calcul de l'Institut National de Physique Nucléaire et de Physique des Particules (IN2P3), Villeurbanne, France
- ⁹⁹ Departamento de Física Teórica C-15 and CIAFF, Universidad Autónoma de Madrid, Madrid, Spain
- ¹⁰⁰ Institut für Physik, Universität Mainz, Mainz, Germany
- ¹⁰¹ School of Physics and Astronomy, University of Manchester, Manchester, United Kingdom
- ¹⁰² CPPM, Aix-Marseille Université, CNRS/IN2P3, Marseille, France
- ¹⁰³ Department of Physics, University of Massachusetts, Amherst MA, United States of America
- ¹⁰⁴ Department of Physics, McGill University, Montreal QC, Canada
- ¹⁰⁵ School of Physics, University of Melbourne, Victoria, Australia
- ¹⁰⁶ Department of Physics, University of Michigan, Ann Arbor MI, United States of America
- ¹⁰⁷ Department of Physics and Astronomy, Michigan State University, East Lansing MI, United States of America
- ¹⁰⁸ B.I. Stepanov Institute of Physics, National Academy of Sciences of Belarus, Minsk, Belarus
- ¹⁰⁹ Research Institute for Nuclear Problems of Byelorussian State University, Minsk, Belarus
- ¹¹⁰ Group of Particle Physics, University of Montreal, Montreal QC, Canada
- ¹¹¹ P.N. Lebedev Physical Institute of the Russian Academy of Sciences, Moscow, Russia
- ¹¹² National Research Nuclear University MEPhI, Moscow, Russia
- ¹¹³ D.V. Skobeltsyn Institute of Nuclear Physics, M.V. Lomonosov Moscow State University, Moscow, Russia
- ¹¹⁴ Fakultät für Physik, Ludwig-Maximilians-Universität München, München, Germany
- ¹¹⁵ Max-Planck-Institut für Physik (Werner-Heisenberg-Institut), München, Germany
- ¹¹⁶ Nagasaki Institute of Applied Science, Nagasaki, Japan
- ¹¹⁷ Graduate School of Science and Kobayashi-Maskawa Institute, Nagoya University, Nagoya, Japan
- ¹¹⁸ Department of Physics and Astronomy, University of New Mexico, Albuquerque NM, United States of America
- ¹¹⁹ Institute for Mathematics, Astrophysics and Particle Physics, Radboud University/Nikhef, Nijmegen, Netherlands
- ¹²⁰ Nikhef National Institute for Subatomic Physics and University of Amsterdam, Amsterdam, Netherlands
- ¹²¹ Department of Physics, Northern Illinois University, DeKalb IL, United States of America
- ¹²² ^(a) Budker Institute of Nuclear Physics and NSU, SB RAS, Novosibirsk; ^(b) Novosibirsk State University Novosibirsk, Russia
- ¹²³ Institute for High Energy Physics of the National Research Centre Kurchatov Institute, Protvino, Russia
- ¹²⁴ Institute for Theoretical and Experimental Physics named by A.I. Alikhanov of National Research Centre "Kurchatov Institute", Moscow, Russia
- ¹²⁵ Department of Physics, New York University, New York NY, United States of America
- ¹²⁶ Ochanomizu University, Otsuka, Bunkyo-ku, Tokyo, Japan
- ¹²⁷ Ohio State University, Columbus OH, United States of America
- ¹²⁸ Homer L. Dodge Department of Physics and Astronomy, University of Oklahoma, Norman OK, United States of America
- ¹²⁹ Department of Physics, Oklahoma State University, Stillwater OK, United States of America
- ¹³⁰ Palacký University, RCPTM, Joint Laboratory of Optics, Olomouc, Czech Republic
- ¹³¹ Institute for Fundamental Science, University of Oregon, Eugene, OR, United States of America
- ¹³² Graduate School of Science, Osaka University, Osaka, Japan
- ¹³³ Department of Physics, University of Oslo, Oslo, Norway
- ¹³⁴ Department of Physics, Oxford University, Oxford, United Kingdom
- ¹³⁵ LPNHE, Sorbonne Université, Université de Paris, CNRS/IN2P3, Paris, France
- ¹³⁶ Department of Physics, University of Pennsylvania, Philadelphia PA, United States of America
- ¹³⁷ Konstantinov Nuclear Physics Institute of National Research Centre "Kurchatov Institute", PNPI, St. Petersburg, Russia
- ¹³⁸ Department of Physics and Astronomy, University of Pittsburgh, Pittsburgh PA, United States of America
- ¹³⁹ ^(a) Laboratório de Instrumentação e Física Experimental de Partículas – LIP, Lisboa; ^(b) Departamento de Física, Faculdade de Ciências, Universidade de Lisboa, Lisboa; ^(c) Departamento de Física, Universidade de Coimbra, Coimbra; ^(d) Centro de Física Nuclear da Universidade de Lisboa, Lisboa; ^(e) Departamento de Física, Universidade do Minho, Braga; ^(f) Departamento de Física Teórica y del Cosmos, Universidad de Granada, Granada (Spain); ^(g) Dep Física and CEFITEC of Faculdade de Ciências e Tecnologia, Universidade Nova de Lisboa, Caparica; ^(h) Instituto Superior Técnico, Universidade de Lisboa, Lisboa, Portugal
- ¹⁴⁰ Institute of Physics of the Czech Academy of Sciences, Prague, Czech Republic
- ¹⁴¹ Czech Technical University in Prague, Prague, Czech Republic
- ¹⁴² Charles University, Faculty of Mathematics and Physics, Prague, Czech Republic
- ¹⁴³ Particle Physics Department, Rutherford Appleton Laboratory, Didcot, United Kingdom
- ¹⁴⁴ IRFU, CEA, Université Paris-Saclay, Gif-sur-Yvette, France
- ¹⁴⁵ Santa Cruz Institute for Particle Physics, University of California Santa Cruz, Santa Cruz CA, United States of America
- ¹⁴⁶ ^(a) Departamento de Física, Pontificia Universidad Católica de Chile, Santiago; ^(b) Universidad Andres Bello, Department of Physics, Santiago; ^(c) Instituto de Alta Investigación, Universidad de Tarapacá; ^(d) Departamento de Física, Universidad Técnica Federico Santa María, Valparaíso, Chile
- ¹⁴⁷ Universidade Federal de São João del Rei (UFJSJ), São João del Rei, Brazil
- ¹⁴⁸ Department of Physics, University of Washington, Seattle WA, United States of America
- ¹⁴⁹ Department of Physics and Astronomy, University of Sheffield, Sheffield, United Kingdom
- ¹⁵⁰ Department of Physics, Shinshu University, Nagano, Japan
- ¹⁵¹ Department Physik, Universität Siegen, Siegen, Germany
- ¹⁵² Department of Physics, Simon Fraser University, Burnaby BC, Canada
- ¹⁵³ SLAC National Accelerator Laboratory, Stanford CA, United States of America
- ¹⁵⁴ Physics Department, Royal Institute of Technology, Stockholm, Sweden
- ¹⁵⁵ Departments of Physics and Astronomy, Stony Brook University, Stony Brook NY, United States of America
- ¹⁵⁶ Department of Physics and Astronomy, University of Sussex, Brighton, United Kingdom
- ¹⁵⁷ School of Physics, University of Sydney, Sydney, Australia
- ¹⁵⁸ Institute of Physics, Academia Sinica, Taipei, Taiwan
- ¹⁵⁹ ^(a) E. Andronikashvili Institute of Physics, Iv. Javakishvili Tbilisi State University, Tbilisi; ^(b) High Energy Physics Institute, Tbilisi State University, Tbilisi, Georgia
- ¹⁶⁰ Department of Physics, Technion, Israel Institute of Technology, Haifa, Israel
- ¹⁶¹ Raymond and Beverly Sackler School of Physics and Astronomy, Tel Aviv University, Tel Aviv, Israel
- ¹⁶² Department of Physics, Aristotle University of Thessaloniki, Thessaloniki, Greece
- ¹⁶³ International Center for Elementary Particle Physics and Department of Physics, University of Tokyo, Tokyo, Japan
- ¹⁶⁴ Graduate School of Science and Technology, Tokyo Metropolitan University, Tokyo, Japan
- ¹⁶⁵ Department of Physics, Tokyo Institute of Technology, Tokyo, Japan
- ¹⁶⁶ Tomsk State University, Tomsk, Russia
- ¹⁶⁷ Department of Physics, University of Toronto, Toronto ON, Canada
- ¹⁶⁸ ^(a) TRIUMF, Vancouver BC; ^(b) Department of Physics and Astronomy, York University, Toronto ON, Canada
- ¹⁶⁹ Division of Physics and Tomonaga Center for the History of the Universe, Faculty of Pure and Applied Sciences, University of Tsukuba, Tsukuba, Japan
- ¹⁷⁰ Department of Physics and Astronomy, Tufts University, Medford MA, United States of America
- ¹⁷¹ Department of Physics and Astronomy, University of California Irvine, Irvine CA, United States of America

- ¹⁷² Department of Physics and Astronomy, University of Uppsala, Uppsala, Sweden
¹⁷³ Department of Physics, University of Illinois, Urbana IL, United States of America
¹⁷⁴ Instituto de Física Corpuscular (IFIC), Centro Mixto Universidad de Valencia – CSIC, Valencia, Spain
¹⁷⁵ Department of Physics, University of British Columbia, Vancouver BC, Canada
¹⁷⁶ Department of Physics and Astronomy, University of Victoria, Victoria BC, Canada
¹⁷⁷ Fakultät für Physik und Astronomie, Julius-Maximilians-Universität Würzburg, Würzburg, Germany
¹⁷⁸ Department of Physics, University of Warwick, Coventry, United Kingdom
¹⁷⁹ Waseda University, Tokyo, Japan
¹⁸⁰ Department of Particle Physics and Astrophysics, Weizmann Institute of Science, Rehovot, Israel
¹⁸¹ Department of Physics, University of Wisconsin, Madison WI, United States of America
¹⁸² Fakultät für Mathematik und Naturwissenschaften, Fachgruppe Physik, Bergische Universität Wuppertal, Wuppertal, Germany
¹⁸³ Department of Physics, Yale University, New Haven CT, United States of America

- ^a Also at Borough of Manhattan Community College, City University of New York, New York NY, United States of America.
^b Also at Center for High Energy Physics, Peking University, China.
^c Also at Centro Studi e Ricerche Enrico Fermi, Italy.
^d Also at CERN, Geneva, Switzerland.
^e Also at CPPM, Aix-Marseille Université, CNRS/IN2P3, Marseille, France.
^f Also at Département de Physique Nucléaire et Corpusculaire, Université de Genève, Genève, Switzerland.
^g Also at Departament de Física de la Universitat Autònoma de Barcelona, Barcelona, Spain.
^h Also at Department of Financial and Management Engineering, University of the Aegean, Chios, Greece.
ⁱ Also at Department of Physics and Astronomy, Michigan State University, East Lansing MI, United States of America.
^j Also at Department of Physics and Astronomy, University of Louisville, Louisville, KY, United States of America.
^k Also at Department of Physics, Ben Gurion University of the Negev, Beer Sheva, Israel.
^l Also at Department of Physics, California State University, East Bay, United States of America.
^m Also at Department of Physics, California State University, Fresno, United States of America.
ⁿ Also at Department of Physics, California State University, Sacramento, United States of America.
^o Also at Department of Physics, King's College London, London, United Kingdom.
^p Also at Department of Physics, St. Petersburg State Polytechnical University, St. Petersburg, Russia.
^q Also at Department of Physics, University of Fribourg, Fribourg, Switzerland.
^r Also at Dipartimento di Matematica, Informatica e Fisica, Università di Udine, Udine, Italy.
^s Also at Faculty of Physics, M.V. Lomonosov Moscow State University, Moscow, Russia.
^t Also at Giresun University, Faculty of Engineering, Giresun, Turkey.
^u Also at Graduate School of Science, Osaka University, Osaka, Japan.
^v Also at Hellenic Open University, Patras, Greece.
^w Also at Institutio Catalana de Recerca i Estudis Avancats, ICREA, Barcelona, Spain.
^x Also at Institut für Experimentalphysik, Universität Hamburg, Hamburg, Germany.
^y Also at Institute for Nuclear Research and Nuclear Energy (INRNE) of the Bulgarian Academy of Sciences, Sofia, Bulgaria.
^z Also at Institute for Particle and Nuclear Physics, Wigner Research Centre for Physics, Budapest, Hungary.
^{aa} Also at Institute of Particle Physics (IPP), Canada.
^{ab} Also at Institute of Physics, Azerbaijan Academy of Sciences, Baku, Azerbaijan.
^{ac} Also at Instituto de Física Teórica, IFT-UAM/CSIC, Madrid, Spain.
^{ad} Also at Istanbul University, Dept. of Physics, Istanbul, Turkey.
^{ae} Also at Joint Institute for Nuclear Research, Dubna, Russia.
^{af} Also at Moscow Institute of Physics and Technology State University, Dolgoprudny, Russia.
^{ag} Also at National Research Nuclear University MEPhI, Moscow, Russia.
^{ah} Also at Physics Department, An-Najah National University, Nablus, Palestine.
^{ai} Also at Physikalisches Institut, Albert-Ludwigs-Universität Freiburg, Freiburg, Germany.
^{aj} Also at The City College of New York, New York NY, United States of America.
^{ak} Also at TRIUMF, Vancouver BC, Canada.
^{al} Also at Università di Napoli Parthenope, Napoli, Italy.
^{am} Also at University of Chinese Academy of Sciences (UCAS), Beijing, China.
* Deceased.